nagra.

Arbeitsbericht NAB 20-09

TBO Trüllikon-1-1: Data Report

Dossier VII Hydraulic Packer Testing

June 2021

R. Schwarz, L. Schlickenrieder, H.R. Müller,
S. Köhler, A. Pechstein & T. Vogt

National Cooperative
for the Disposal of
Radioactive Waste

Hardstrasse 73
P.O. Box 280
5430 Wettingen
Switzerland
Tel. +41 56 437 11 11

www.nagra.ch

nagra.

Arbeitsbericht NAB 20-09

TBO Trüllikon-1-1: Data Report

Dossier VII Hydraulic Packer Testing

June 2021

R. Schwarz[1], L. Schlickenrieder[1], H.R. Müller[1], S. Köhler[2], A. Pechstein[2] & T. Vogt[2]

[1] CSD Ingenieure AG
[2] Nagra

Keywords:
TRU1-1, Zürich Nordost, TBO, deep drilling campaign, hydrogeology, hydraulic packer tests, hydraulic conductivity, hydraulic head

National Cooperative for the Disposal of Radioactive Waste

Hardstrasse 73
P.O. Box 280
5430 Wettingen
Switzerland
Tel. +41 56 437 11 11

www.nagra.ch

Nagra Arbeitsberichte ("Working Reports") present the results of work in progress that have not necessarily been subject to a comprehensive review. They are intended to provide rapid dissemination of current information.

This NAB aims at reporting drilling results at an early stage. Additional borehole-specific data will be published elsewhere.

In the event of inconsistencies between dossiers of this NAB, the dossier addressing the specific topic takes priority. In the event of discrepancies between Nagra reports, the chronologically later report is generally considered to be correct. Data sets and interpretations laid out in this NAB may be revised in subsequent reports. The reasoning leading to these revisions will be detailed there.

This Dossier was prepared by a project team consisting of:
R. Schwarz (QC of test analysis, QC of test reports, writing)
L. Schlickenrieder (writing)
H.R. Müller (writing)
S. Köhler (project management, conceptualisation, review)
A. Pechstein (project management, conceptualisation)
T. Vogt (project management, conceptualisation)

The present report is based on the detailed reports about the performance and analysis of the hydraulic packer tests and fluid logging, as well as on the mobilisation reports about test equipment. These detailed reports and mobilisation reports were written by the testing companies INTERA Inc. for the hydraulic packer tests (R. Beauheim, R. Roberts (Hydro-Resolutions LLC), T. Cavalera and C. Yu) and Solexperts AG / Terratec Geophysical Services GmbH & Co. KG for fluid logging (G. Mühlebach).

Editorial work and Graphics: P. Blaser and M. Unger

The Dossier has greatly benefitted from technical discussions with, and reviews by, external and internal experts. Their input and work are very much appreciated.

Table of Contents

List of Tables

List of Figures

1 Introduction

1.1 Context

To provide input for site selection and the safety case for deep geological repositories for radioactive waste, Nagra has drilled a series of deep boreholes in Northern Switzerland. The aim of the drilling campaign is to characterise the deep underground of the three remaining siting regions located at the edge of the Northern Alpine Molasse Basin (Fig. 1-1).

In this report, we present the results from the Trüllikon-1-1 borehole.

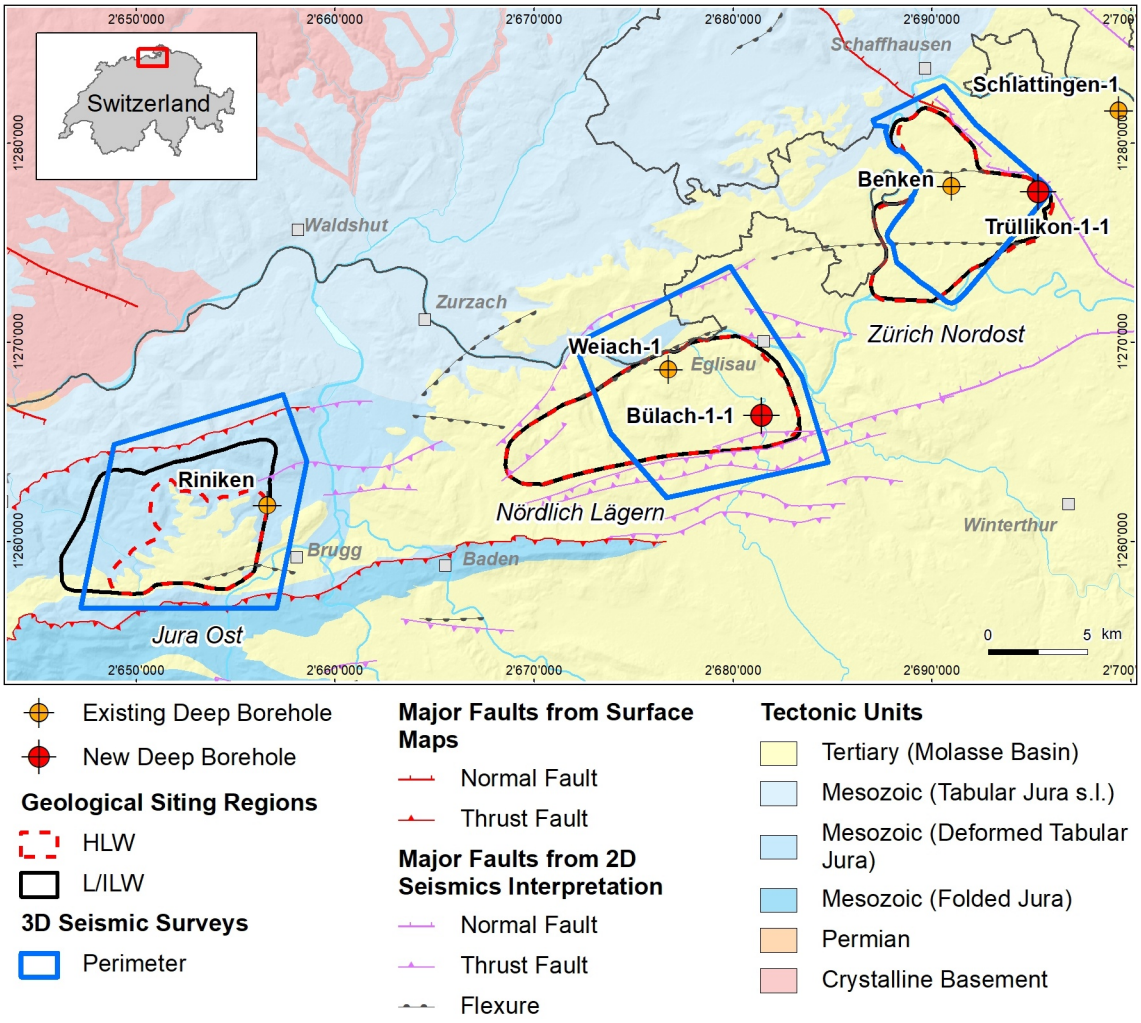

Fig. 1-1: Tectonic overview map with the three siting regions under investigation

1.2 Location and specifications of the borehole

The Trüllikon-1-1 (TRU1-1) exploratory borehole is the second borehole drilled within the framework of the TBO project. The drill site is located in the eastern part of the Zürich Nordost siting region (Fig. 1-2). The vertical borehole reached a final depth of 1'310 m (MD)[1]. The borehole specifications are provided in Tab. 1-1.

Tab. 1-1: General information about the TRU1-1 borehole

Siting region	Zürich Nordost
Municipality	Trüllikon (Canton Zurich / ZH), Switzerland
Drill site	Trüllikon-1 (TRU1)
Borehole	Trüllikon-1-1 (TRU1-1)
Coordinates	LV95: 2'695'372.648 / 1'277'548.076
Elevation	Ground level = top of rig cellar: 475.07 m above sea level (asl)
Borehole depth	1'310.0 m measured depth (MD) below ground level (bgl)
Drilling period	15. August 2019 – 5. April 2020 (spud date to end of rig release)
Drilling company	PR Marriott Drilling Ltd.
Drilling rig	Rig-16 Drillmec HH102
Drilling fluid	Water-based mud with various amounts of different components such as[2]: 46 – 712 m: Pure-Bore® 712 – 1'161 m: Potassium silicate 1'161 – 1'310 m: Sodium chloride & polymers

The lithostratigraphic profile and the casing scheme are shown in Fig. 1-3. The comparison of the core versus log depth[3] of the main lithostratigraphic boundaries in the TRU1-1 borehole is shown in Tab. 1-2.

[1] Measured depth (MD) refers to the position along the borehole trajectory, starting at ground level, which for this borehole is the top of the rig cellar. For a perfectly vertical borehole, MD below ground level (bgl) and true vertical depth (TVD) are the same. In all Dossiers depth refers to MD unless stated otherwise.

[2] For detailed information see Dossier I.

[3] Core depth refers to the depth marked on the drill cores. Log depth results from the depth observed during geophysical wireline logging. Note that the petrophysical logs have not been shifted to core depth, hence log depth differs from core depth.

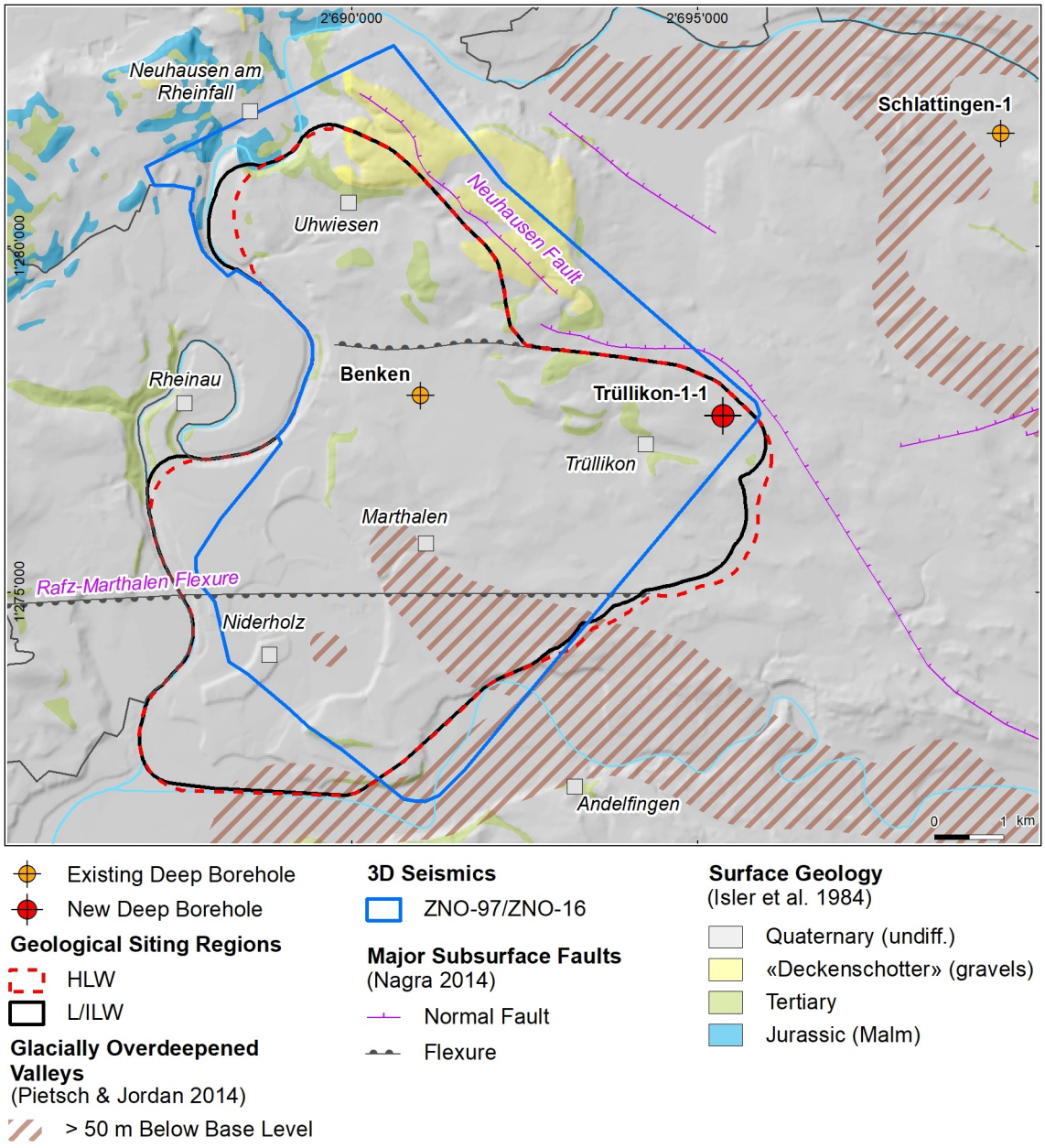

Fig. 1-2: Overview map of the investigation area in the Zürich Nordost siting region with the location of the TRU1-1 borehole in relation to the boreholes Benken and Schlattingen

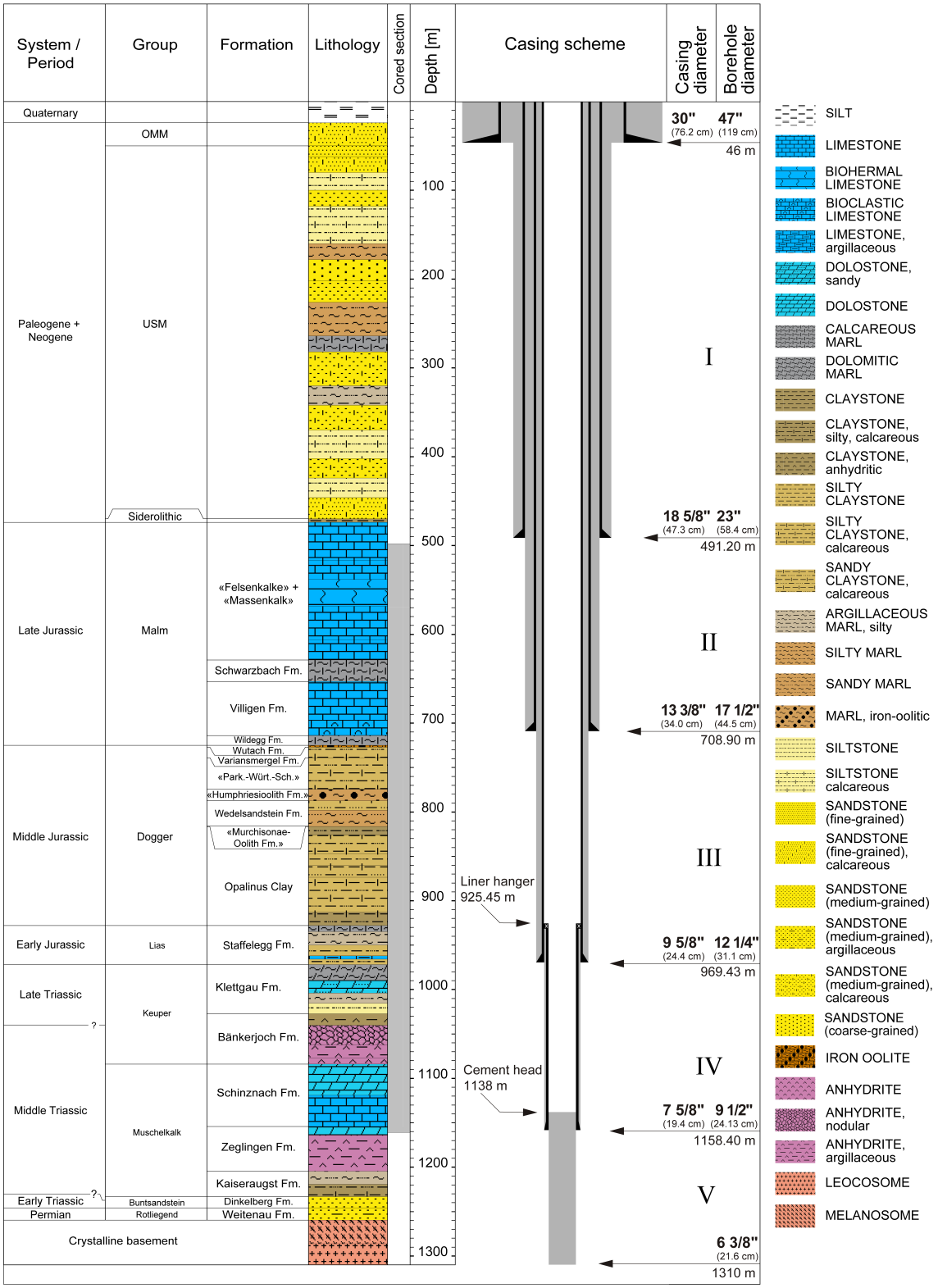

Fig. 1-3: Lithostratigraphic profile and casing scheme for the TRU1-1 borehole[4]

[4] For detailed information see Dossier I and III.

Tab. 1-2: Core and log depth for the main lithostratigraphic boundaries in the TRU1-1 borehole[5]

System / Period	Group	Formation	Core depth in m (MD)	Log depth in m (MD)	
Quaternary				**24.0**	—
Paleogene + Neogene	OMM			50.0	—
	USM			470.0	—
	Siderolithic			**474.0**	—
Jurassic	Malm	«Felsenkalke» + «Massenkalk»	628.87	628.75	—
		Schwarzbach Formation	653.29	653.15	—
		Villigen Formation	714.00	714.00	—
		Wildegg Formation	724.85	725.03	—
	Dogger	Wutach Formation	727.13	727.27	—
		Variansmergel Formation	738.97	739.06	—
		«Parkinsoni-Württembergica-Schichten»	774.55	774.66	—
		«Humphriesioolith Formation»	787.50	787.55	—
		Wedelsandstein Formation	815.51	815.50	—
		«Murchisonae-Oolith Formation»	816.42	816.43	—
		Opalinus Clay	927.91	927.87	—
	Lias	Staffelegg Formation	**971.68**	**971.55**	—
Triassic	Keuper	Klettgau Formation	1027.22	1027.44	—
		Bänkerjoch Formation	1084.01	1084.22	—
	Muschelkalk	Schinznach Formation	1154.25	1154.43	—
		Zeglingen Formation	1204.5		—
		Kaiseraugst Formation	1233.2		—
	Buntsandstein	Dinkelberg Formation	**1246.1**		—
Permian	Rotliegend	Weitenau Formation	**1259.7**		—
		Crystalline Basement	1310.0	final depth	

[5] For details regarding lithostratigraphic boundaries see Dossier III; for details about depth shifts (core goniometry) see Dossier V.

1.3 Documentation structure for the TRU1-1 borehole

NAB 20-09 documents the majority of the investigations carried out in the TRU1-1 borehole, including laboratory investigations on core material. The NAB comprises a series of stand-alone dossiers addressing individual topics and a final dossier with a summary composite plot (Tab. 1-3).

This documentation aims at early publication of the data collected in the TRU1-1 borehole. It includes most of the data available approximately one year after completion of the borehole. Some analyses are still ongoing (e.g. diffusion experiments, analysis of veins, hydrochemical interpretation of water samples) and results will be published in separate reports.

The current borehole report will provide an important basis for the integration of datasets from different boreholes. The integration and interpretation of the results in the wider geological context will be documented later in separate geoscientific reports.

Tab. 1-3: List of dossiers included in NAB 20-09

Black indicates the dossier at hand.

Dossier	Title	Authors
I	TBO Trüllikon-1-1: Drilling	M. Ammen & P.-J. Palten
II	TBO Trüllikon-1-1: Core Photography	D. Kaehr & M. Gysi
III	TBO Trüllikon-1-1: Lithostratigraphy	M. Schwarz, P. Jordan, P. Schürch, H. Naef, T. Ibele, R. Felber & M. Gysi
IV	TBO Trüllikon-1-1: Microfacies, Bio- and Chemostratigraphic Analyses	S. Wohlwend, H.R. Bläsi, S. Feist-Burkhardt, B. Hostettler, U. Menkveld-Gfeller, V. Dietze & G. Deplazes
V	TBO Trüllikon-1-1: Structural Geology	A. Ebert, S. Cioldi, L. Gregorczyk, S. Rust, D. Böhni & M. Gysi
VI	TBO Trüllikon-1-1: Wireline Logging and Microhydraulic Fracturing	J. Gonus, E. Bailey, J. Desroches & R. Garrard
VII	TBO Trüllikon-1-1: Hydraulic Packer Testing	R. Schwarz, L. Schlickenrieder, H.R. Müller, S. Köhler, A. Pechstein & T. Vogt
VIII	TBO Trüllikon-1-1: Rock Properties, Porewater Characterisation and Natural Tracer Profiles	L. Aschwanden, L. Camesi, T. Gimmi, A. Jenni, M. Kiczka, U. Mäder, M. Mazurek, D. Rufer, H.N. Waber, P. Wersin, C. Zwahlen & D. Traber
IX	TBO Trüllikon-1-1: Rock-mechanical and Geomechanical Laboratory Testing	E. Crisci, L. Laloui & S. Giger
X	TBO Trüllikon-1-1: Petrophysical Log Analysis	S. Marnat & J.K. Becker
	TBO Trüllikon-1-1: Summary Plot	Nagra

1.4 Structure of Dossier VII

The objective of the dossier at hand is to provide a summary of the conducted hydrogeological investigations and acquired hydrogeological data, including assessments of tests and results, but without interpretation.

This report focuses on fluid logging and hydraulic packer testing, and is organised as follows:

- Chapter 2 presents the general strategy for the hydrogeological investigations in the TRU1-1 borehole.
- Chapter 3 is dedicated to fluid logging which was performed in the cored borehole Section II. Due to technical problems, the assessment of the records was purely qualitative in nature.
- Chapter 4 discusses all aspects of the hydraulic packer tests including planning of test strategies, test equipment used, general concerns for the analysis of tests, and test activities in borehole TRU1-1. Selected tests and analyses are presented in detail.
- Chapter 5 summarises and discusses the data and results mainly for the hydraulic packer tests. The results are summarised in tables and plots and some assessments are made.
- Finally, this report includes a set of appendices, which present relevant general project information and further investigation details.

2 Strategy for the hydrogeological investigations

2.1 Hydrogeological objectives of the TBO boreholes

The overall objectives of the hydrogeological investigations are the detailed determination of the hydraulic conductivity and hydraulic head in the aquifers, aquicludes and aquitards on the one hand, and the chemistry and isotopic composition of the deep groundwaters in the aquifers and the porewaters in the aquicludes and aquitards on the other. The results of the hydrogeological investigations in the TBO boreholes form an important dataset for the site selection and the safety case. They are mainly needed for the characterisation of:

- Hydraulic and hydrochemical properties of the containment-providing rock zone, which consists of the host rock Opalinus Clay and the confining geological units above and below.
- Hydrogeological conditions in the aquifers providing the hydraulic and hydrochemical boundary conditions for the containment-providing rock zone and providing input for the identification of potential release paths as well as for the planning of the future access structures.

2.2 Hydrogeological investigation concept for TRU1-1

The hydrogeological investigations for TRU1-1 comprised:

- Fluid logging
- Hydraulic packer testing

Given sufficiently high transmissivity, fluid logging was performed. Water inflows into the borehole were identified with a series of temperature – conductivity logs and/or flowmeter logs. No analysis for transmissivity was possible because of technical issues.

Hydraulic packer tests were used for the detailed hydraulic characterisation of selected borehole sections to determine: transmissivity (T), hydraulic conductivity (K), hydraulic head (h) and to identify the appropriate flow model. Hydraulic packer tests were performed in scheduled testing phases between drilling phases but also during drilling phases when potentially highly transmissive features or faults were encountered. Depending on the transmissivity of the test interval, different test methods were applied in TRU1-1:

- Pumping tests with constant flow rate
- Slug tests
- Pulse tests

These test methods usually are combined, i.e. executed one after the other as a test sequence in test-specific order.

No gas threshold pressure test was conducted in the TRU1-1 borehole and no hydraulic long-term monitoring system was installed.

The detailed groundwater sampling, subsequent hydrochemical and isotope analyses (including results) are documented in Lorenz & Pechstein (2021). Further porewater investigations are the subject of Dossier VIII. The laboratory permeability measurements on drill-core sections are discussed in Dossier IX.

3 Flowmeter logging and fluid logging

3.1 Description of equipment

The fluid logging was performed with the equipment introduced below.

3.1.1 Borehole logging winch

The winch features a mechanical cable spooling device, an electronic and a mechanical depth measurement and a cable tension measurement. For specifications, see Tab. 3-1. It is permanently mounted in the logging van. As soon as the motor is stopped, a break is automatically engaged in the gearbox. Additionally, there are a manual brake and a clutch.

Tab. 3-1: Specifications of borehole logging winch

Manufacturer	HEWA Feinwerktechnik Engineering GmbH, Marie-Curie-Str. 2, 79211 Denzlingen, Germany
Type	TT2000, Electrical, 220 V
Cable type	Rochester 3⁄16" 4-conductor cable Type 4-H-181A
Cable breaking strength	14.7 kN
Max. cable length	2'000 m
Logging speed range	0 – 30 m/min
Depth measurement	IVO BAUMER incremental encoder, 2'500 pulse/rotation; 500 mm circumference wheel mounted on the spooling device, + mechanical depth counter
Cable tension gauge	External display or input for matrix logger
Safety joint	Cable head is set up to form a weak joint. The cable is pulled from the cable head in case of a stuck probe. Cable clamping devices are in stock at the office

3.1.2 Matrix logger

The Matrix logger is a logging surface unit that interfaces the probe with the acquisition PC, using the ALT Matrix Logger software. For specifications, see Tab. 3-2. It records the data, depth and logging speed. It has a digital interface. The unit supports several communication protocols and can therefore be used to run probes built by different manufacturers (among others electromind, Robertson Geologging, ALT). A browser module connects the acquisition software to an ALT WellCAD document and feeds the data directly into WellCAD. The data of several runs is displayed in one document.

The software used to control the unit and the probes is as follows:

- Heat Pulse: Matrix Heat: V3.3 build 2208 © Advanced Logic Technology, 2005 – 2012
- All other probes: Matrix Logger: V 12.1 build 2388 © Advanced Logic Technology, 1995 – 2018
- Processing: WellCAD 5.2 build 1925 © Advanced Logic Technology, 1993 – 2018.

The winch features a mechanical cable spooling.

Tab. 3-2: Specifications of matrix logger

Manufacturer	Advanced Logging Technology, 30H Rue de Niederpallen, Zoning de Solupla, L-8506 Redange, Luxembourg
Type	Matrix borehole logging system
Data transmission	The data is digitised in the probes and sent to the logging system with a resolution of 15 bit (0 – 32'768 cps resolution per channel) and 16 bit (0 – 65'536 cps resolution per channel), respectively, depending on the probe

3.1.3 Flowmeter-temperature-conductivity-gamma probe

The probe is a combination of a LIM logging / electromind temperature-electrical-conductivity-gamma probe with an Intergeo impeller flowmeter head. For this reason, the actual dimensions of the probe as mentioned below differ from the dimensions on the manufacturer's data sheet. It was assembled on the field contractor's request by electromind. The Intergeo flowmeter head combines a larger diameter (88 mm) with jewelled bearings for the impeller instead of ball bearings which provides improved sensitivity compared to the standard electromind impeller head. For specifications, see Tab. 3-3.

This probe measures fluid temperature, electrical fluid conductivity, vertical fluid velocity and natural gamma ray. The electrical conductivity-temperature sensor is mounted on the side of the probe. Fluid can freely flow through it while going down and up. The flowmeter is an impeller type with a cage of 88 mm. It is used if relatively higher fluid flow rates are expected. If lower flow rates are anticipated that might be below the detection limit, the performance of the impeller can be improved by using a diverter disk. It seals the annulus between the impeller cage and the borehole wall and forces most of the fluid through the sensor. This increases the fluid velocity at the sensor. Different disks are available to adjust to the borehole diameter.

The diverter disk assembly is made from a base plate that is attached to the probe, and a flexible plastic disc that can be changed depending on the borehole diameter. The base plate for the FTC60G probe is made of Nylon. Its dimensions are 140 mm outer diameter, 80 mm inner diameter, 42 mm height.

Tab. 3-3: Specifications of the flowmeter-temperature-conductivity-gamma probe

Manufacturer	LIM logging / electromind s.a. 1 Rue de l'Industrie, 4801 Rodange, Grand Duche de Luxembourg + intergeo Haferland AG
Type	FTC60G
Length	1'710 mm
Weight	5.5 kg
Cage diameter	88 mm
Operational temperature range	0 – 70 °C (up to 80 °C for a limited time)
Max. pressure	20 MPa
Borehole diameter range	> 96 mm
Temperature sensor range	0 – 70 °C (up to 80 °C for a limited time)
Temperature sensor accuracy	0.1 °C
Temperature sensor resolution	0.001 °C
Electrical conductivity sensor linear range	0 – 3'000 µS/cm (not on data sheet, information from manufacturer)
Electrical conductivity sensor accuracy	10 µS/cm
Electrical conductivity sensor resolution	1 µS/cm
Flowmeter threshold velocity (static)	1 m/min
Flowmeter impeller sensor resolution (theoretical)	0.003 m/min
Gamma detector	NaI 50 mm × 25 mm Crystal

3.1.4 Temperature-conductivity-gamma probe

The probe measures fluid temperature, electrical fluid conductivity and natural gamma ray. For specifications, see Tab. 3-4. The electrical conductivity is referenced to 25 °C. The temperature-electrical conductivity sensor is mounted at the bottom. In the standard setup, the fluid enters the probe at openings at the bottom, flows through the sensor assembly and leaves the probe through openings at the side of the probe a bit further up. This geometry is optimised for logging going down.

Tab. 3-4: Specifications of the temperature-conductivity-gamma probe

Manufacturer	Robertson Geologging Ltd., York Road, Deganwy, Conwy, LL31 9PX, UK
Type	TCG
Length	1'690 mm
Weight	4.5 kg
Tool diameter	38 mm
Operational temperature range	0 – 70 °C (up to 80 °C for a limited time)
Max. pressure	20 MPa
Borehole diameter range	> 50 mm (> 96 mm with sleeve)
Temperature sensor range	0 – 70 °C (up to 80 °C for a limited time)
Temperature sensor accuracy	±0.5 °C (not on data sheet, information from manufacturer)
Temperature sensor resolution	0.04 °C (not on data sheet, information from manufacturer)
Electrical conductivity sensor range	50 – 50000 µS/cm
Electrical conductivity sensor accuracy	±2.5% at 500 µS/cm (not on data sheet, information from manufacturer)
Electrical conductivity sensor resolution	4 µS/cm (not on data sheet, information from manufacturer)
Electrical conductivity temperature compensation	25 °C
Gamma Detector	NaI 50 mm × 25 mm crystal

3.1.5 High resolution flowmeter-gamma probe

This probe measures vertical fluid velocity and natural gamma ray. For specifications, see Tab. 3-5. The flowmeter is an impeller type with a cage of 45 mm. This probe is used if relatively higher fluid flow rates are expected. If lower flow rates are anticipated which might be below the detection limit, the performance of the impeller can be improved by using a diverter disk.

The diverter disk assembly is made from a base plate that is attached to the probe, and a flexible plastic disc that can be changed depending on the borehole diameter. The base plate for the probe is made of aluminium. The dimensions are: 90 mm outer diameter, 45 mm inner diameter, 11 mm height.

Tab. 3-5: Specifications of the high resolution flowmeter-gamma probe

Manufacturer	Robertson Geologging Ltd., York Road, Deganwy, Conwy, LL31 9PX, UK
Type	HRFM
Length	1'530 mm
Weight	4.0 kg
Cage diameter	45 mm
Operational temperature range	0 – 70 °C (up to 80 °C for a limited time)
Max. pressure	20 MPa
Borehole diameter range	> 50 mm
Flowmeter threshold velocity (static)	1 m/min (not on data sheet, information from manufacturer)
Flowmeter sensor resolution (theoretical)	4 pulses per impeller revolution, the time between pulses is measured. Resolution of time measurement 20 ms (not on data sheet, information from manufacturer)
Gamma detector	NaI 50 mm × 25 mm crystal

3.1.6 Gamma sensors

All probes described above are equipped with similar gamma-ray detectors. The detectors are of the scintillation type, set up for total count measurements. They consist of an NaI-crystal (50 mm × 25 mm), a photomultiplier tube and a counting circuit. The output is counts per second (cps). No background radiation exists and has to be considered in a borehole.

The range of the sensors is 0 – 65'536 cps (16 bit). In a typical geological context of southern Germany and Switzerland the count rates normally do not exceed 300 – 400 cps with the given sensors.

Remarks on accuracy of a gamma measurement (Richards 1981): There is a statistical noise to the data, because it is possible to predict the rate of emission of gamma rays, but not which individual nuclei will disintegrate or not. It is possible to determine the true mean count rate (cps) for a given source of gamma-rays quite accurately by counting and averaging for a long time. The statistical noise produces a fluctuation of the readings around the true mean count rate. The expected standard deviation is the square root of the true mean count rate n.

The fractional standard deviation expresses the standard deviation as percentage of the true count rate:

fractional std. dev. = (std. dev.)/n*100

e.g. n = 10'000 cps → std. dev.: 100 cps, fractional std. dev.: 1%

n = 100 cps → std. dev.: 10 cps, fractional std. dev.: 10%

This means the precision of the measurement increases as the count rate increases.

3.1.7 Temperature-electrical conductivity meter

The WTW (Wissenschaftlich-technische Werkstätten GmbH) instrument pH/Cond 340i is a handheld digital instrument to measure fluid pH, electrical conductivity and temperature. For specifications, see Tab. 3-6. It is used at the workshop to perform the electrical conductivity calibration of the logging tools, and on site to check the calibration of electrical conductivity and temperature.

Tab. 3-6: Specifications of the temperature-electrical conductivity meter

Manufacturer	WTW (Wissenschaftlich-technische Werkstätten GmbH), Dr.-Karl-Slevogt-Straße 1, D-82362 Weilheim
Type	pH/Cond 340 i
Temperature sensor range	0 – 105 °C
Temperature sensor accuracy	±0.1 °C
Electrical conductivity range	0 – 19.99 mS/cm (resolution 0.01), 0 – 199.9 mS/cm (resolution 0.1)
Electrical conductivity accuracy	±0.5 %
Reference temperature	25 °C

3.1.8 Centraliser

When the probes are run in the hole, they are equipped with a set of centraliser blades. The main purpose of the centralisers is to keep the probes off the borehole wall to prevent that the measurements are influenced by any debris that might be scraped off the borehole wall. For specifications, see Tab. 3-7.

The centralisers are made from brass rings with elastic copper – beryllium blades. The centraliser cage can be set up with different blades to cover different borehole diameter ranges. They are fixed to the probe by grub screws.

Tab. 3-7: Specifications of the centraliser

Manufacturer	LIM Logging / electromind s.a.
Type	Bow spring centraliser
Length	420 mm at 165 mm diameter, 530 mm at 215 mm diameter
Weight	Approx. 3 kg
Borehole diameter range	70 – 270 mm

3.1.9 Field analysis IT structure

Logging is performed directly into a WellCAD document to display previous and current measurements. For specifications of the IT structure, see Tab. 3-8.

Tab. 3-8: Specifications of the IT structure for field analysis

Processing software	WellCAD 5.2 build 1925 © Advanced Logic Technology, 1993 – 2018
Logging software	Matrix Logger: V 12.1 build 2388 © Advanced Logic Technology, 1995 – 2018
Logging software (heat pulse flowmeter only)	Matrix Heat: V3.3 build 2208 © Advanced Logic Technology, 2005 – 2012
Uninterrupted power supply	APC Back-UPS Pro 900 BR900-G, 900 VA / 540 Watt
Data back-up	External hard drive
Acquisition computer	Notebook, Windows 10 Pro

3.2 Tool application

Fluid logging was conducted in borehole TRU1-1 on 15 and 16 October 2020 between 479 m and 708 m MD, i.e. in the cored borehole Section II. The test is referred to as TRU1-1-FL1-MAL. The measurements were performed using the temperature-conductivity-gamma probe described in Section 3.1.4. Casing was installed up to a depth of 491.20 m MD with a diameter of 17½". The open borehole section had a diameter of 12¼" between 491.20 m and 501.50 m MD, followed by a section of 8½" diameter (501.50 m – 505.50 m MD) and the cored section of 6⅜" diameter between 505.50 m and 712.00 m MD. Prior to the logging activities, the borehole fluid was exchanged with tap water. During testing, the water level was lowered by pumping. This induced inflow of natural formation fluids into the borehole.

A technical problem (blocking of the probe) occurred during the logging activities (Tab. 3-9) and reduced the number of useable runs. A long period of time passed from when the pump was stopped to when the first useable logs were generated. Because the sleeve of the probe had been taken off, only the down runs could be considered (runs 16, 18 and 20). The corresponding logs gave good results and the acquired data look consistent. A quantitative analysis with regard to the hydraulic transmissivity of the inflow zones was not carried out because of the technical issues.

The basic assumption of the interpretation is that the inflow zones will show peaks with increased values in the electrical conductivity logs. However, there were no sharp limits at the deeper end of the inflow zones as is usual due to the slow back flow from the formation into the borehole. Additionally, the limits of the inflow zones cannot be clearly determined due to the advective and dispersive transport processes of the inflowing formation water of unknown concentration and flow rate.

Two inflow zones were detected qualitatively. The sharp jump in the electrical conductivity at approx. 500 m MD fits the transition into the open borehole section of reduced diameter and is not interpretable.

The lower peak (inflow zone) is more distinct. Mud losses were reported during drilling from 591 m MD (*cf.* Dossier I). The change in temperature gradient between 580 m and 590 m MD can be used as an additional indicator of this inflow zone. However, the extent (thickness) of the inflow zones is highly uncertain. The locations of the inflow zones are defined based on expert opinion reflecting the measured temperature and electrical conductivity logs. It fits perfectly to observations about mud losses during drilling from 591 m MD. Tab. 3-10 lists their positions and Fig. 3-1 shows the runs used for qualitative assessment.

Tab. 3-9: Logging activities of TRU1-1-FL1-MAL

Date	**Time**	**Log-Run No.**	**Remark**
15.10.2019	15:20	1	Water level 0.00 m MD
15.10.2019	16:07	2	Not used, water level 0.00 m MD
15.10.2019	16:18	3	Not used, water level 0.00 m MD
15.10.2019	17:06	4	Not used, water level 0.00 m MD
15.10.2019	18:13	5	Not used, water level 0.00 m MD
15.10.2019	18:15		Start pumping, 250 l/min
15.10.2019	19:11	6	Not used, water level falling
15.10.2019	19:40		Stop pumping, water level 135.88 m MD
15.10.2019	19:53	7	Not used, water level rising
15.10.2019	20:41	8	Not used, water level rising
15.10.2019	20:53	9	Not used, water level rising
15.10.2019	21:21	10	Not used, water level rising
15.10.2019	21:57	11	Not used, water level rising
15:10.2019	22:32	12	Not used, water level rising
15.10.2019	23:06	13	Not used, water level rising
16.10.2019	00:19	14	Not used, water level rising
16.10.2019	00:27		Probe blocked
16.10.2019	02:47		Start pumping, water level 126.33 m MD
16.10.2019	02:56		Stop pumping, water level 135.87 m MD
16.10.2019	03:08		Start pull out of hole of the pump
16.10.2019	05:20		Pull out of hole finished
16.10.2019	07:18	15	Not used, without sleve, water level rising
16.10.2019	07:36	16	Without sleve, water level rising
16.10.2019	08:22	17	Not used, without sleve, water level rising
16.10.2019	08:57	18	Without sleve, water level rising
16.10.2019	09:40	19	Not used, without sleve, water level rising
16.10.2019	10:19	20	Without sleve, water level rising
16.10.2019	10:55	21	Not used, without sleve, water level rising

Tab. 3-10: Inflow zones detected qualitatively by TRU1-1-FL1-MAL

Depth [m MD]	**Remark**
531.31 – 535.21	Indicated by electrical conductivity
590.41 – 594.21	Indicated by electrical conductivity

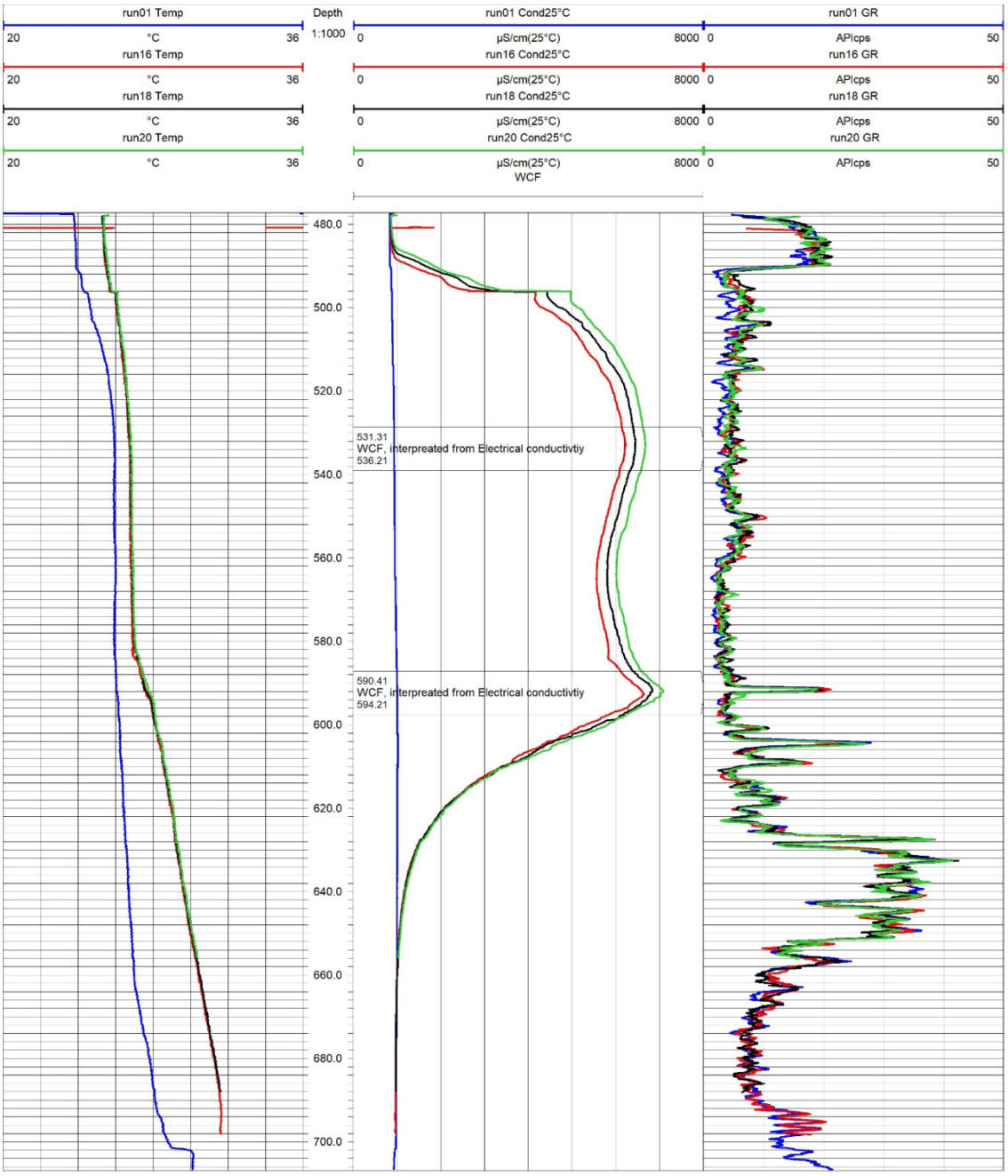

Fig. 3-1: Fluid logging runs used to identify two inflow zones in borehole TRU1-1

4 Hydraulic packer tests

4.1 Test strategy

The geological formations examined in the TBO boreholes exhibit a wide range of transmissivities. The host rock, Opalinus Clay, and its confining units are expected to have very low transmissivities, whilst the regional aquifers like the Malm and the Muschelkalk formations are expected to have relatively high transmissivities.

Nagra has long established hydraulic testing strategies (e.g. Nagra 1997) to extract the maximum information about the hydraulic characteristics of the various geological formations. Two testing strategies are preferred (Tabs. 4-1 and 4-2). A typical test sequence is divided into different test phases: test preparation, diagnostic and main phase. The test sequence may be concluded with a pulse test (PW/PI) to check if the total test interval compressibility changed during the test. Modifications to the strategies are made according to the preliminarily available information, the encountered specific test conditions and obtained results while testing. This may lead to the omission of certain test phases, e.g. the diagnostic phase.

The main difference in the two testing strategies is the selection of appropriate test types and phases as well as the duration of the test phases. In a formation with medium to high transmissivity, pressure disturbances due to drilling or temperature effects dissipate relatively quickly. Accordingly, the test preparation phase is short. The main phase delivers results of sufficient accuracy with respect to the hydraulic properties of the formation in a relatively short period.

In case of formations with low to very low transmissivity, the test types and their duration is different. For the determination of hydraulic head, the borehole pressure history and test duration are an important issue. Depending on the pressure difference between the static formation conditions and the pressure induced in the borehole during the pre-test pressure history, the estimates of hydraulic head can be strongly affected due to non-static pressure conditions in the surrounding borehole area.

A further aspect of the testing strategy is the use of drilling fluid as test fluid (see Tab. 4-1). In contrast to previous exploration boreholes drilled by Nagra (e.g. Benken), no exchange of drilling fluid in the test interval was performed in the TRU1-1 borehole. The main reason was borehole stability. The model implementation as a skin in the test analysis is assumed to address the issues linked with the drilling fluid properties at the borehole wall adequately. During the hydraulic test in the Malm Group, Pure-Bore® was the drilling fluid additive in use, for all the others it was an additive containing potassium silicate (*cf.* Dossier I).

Tab. 4-1: Preferred test sequence for formations with medium to high transmissivity

[1)] For explanation of abbreviations see Tab. A-3.

Test phase	**Phase** [1)]	**Aims**
Test preparation phase	COM	Temperature and pressure equilibration in the test interval
	PSR	Pressure static recovery with closed shut-in tool; create pressure conditions for the initiation of the first test, first estimate of formation pressure; recognition of temperature and pressure trends
Diagnostic phase	PW	First estimates of hydraulic conductivity, which are used to plan the following test sequence
Diagnostic / main phase	SW	Estimation of hydraulic conductivity, which is used to plan the following test sequence, especially the pumping rate and drawdown of the RW phase
	SWS	Estimation of an accurate flow model and hydraulic parameters; hydrostatic pressure for subsequent pumping phase
Main phase	RW	Defined signal with a larger radius of influence; allows a representative groundwater sample of the formation to be taken as well as the detection of boundary conditions
	RWS	Estimation of an accurate flow model and hydraulic parameters as well as boundary conditions
Optional	PW/PI	Estimation of the total test interval compressibility at the end of the test

Tab. 4-2: Preferred test sequence for formations with low to very low transmissivity

Test phase	**Phase**[1]	**Aims**
Test preparation phase	COM	Temperature and pressure equilibration in the test interval
	PSR	Pressure static recovery with closed shut-in tool; create pressure conditions for the initiation of the first test, first estimate of formation pressure; recognition of temperature and pressure trends
Diagnostic phase	PW	First estimates of hydraulic conductivity, which are used to plan the following test sequence
Main phase Version 1	SW	Estimation of hydraulic formation parameters during a flow phase
	SWS	Estimation of an accurate flow model and hydraulic parameters during shut-in conditions
	PW/PI (optional)	Estimation of the total test interval compressibility at the end of the test
Main phase Version 2	PW/PI	Estimation of hydraulic formation parameters (as an alternative to SW/SWS)

[1] For an explanation of the abbreviations see Tab. A-3.

4.2 Test equipment

The most relevant components of the field test contractor's equipment are presented below.

4.2.1 Downhole equipment

The packer system referred to as the heavy-duty double packer system (HDDP) was used for all hydraulic packer tests in open borehole sections. It consists of a top and bottom inflatable packer (non-inflated outer diameter 114 mm for borehole TRU1-1) in order to confine a test interval section of appropriate length for the intended test (Fig. 4-1). Inflow and outflow occurred through a perforated filter segment covered by a filter screen mounted on a 2⅞" tubing above the bottom packer.

Four pressure transducers, mounted in a probe carrier shell above the top packer and referred to as the quadruple sub-surface probe or quadruple probe (QSSP), measured the pressures below (P1), within (interval pressure P2) and above the test interval (annulus pressure P3) as well as in the test tubing above the downhole shut-in tool (P4). In addition, the pressure in the test interval was recorded with an autonomous memory gauge at the bottom of the filter screen (P2*).

Temperatures were measured at the level of the QSSP by the temperature sensors associated with each pressure transducer (referred to as T1, T2, T3, T4, respectively) and additionally by the sensor associated with the memory gauge mentioned above (named T2*).

A hydraulically controlled non-displacement downhole shut-in tool (SIT) placed above the probe carrier shell was used to isolate the test zone from the test tubing (2⅞" EUE API CT5 L80). A progressive cavity (PC) pump or Moyno® type pump or a pump housing with a 4" submersible pump, integrated in the test tubing, can be used for production pumping tests.

Additionally, a piston pulse generator (PPG) can be mounted in the test interval. It introduces a unique and proven technology to reduce the uncertainty associated with determining the test zone compressibility for conducting pulse tests in formations with a low transmissivity.

For testing in a single packer configuration (Fig. 4-2), the system was set up without the bottom packer but with a prolongation of the interval string with the filter at the bottom. Inflow and outflow occurred through a perforated filter segment covered by a filter screen mounted on a 2⅞" tubing at the bottom of the prolongation.

The quadruple flat-pack consists of three hydraulic steel pipes of ¼" outer diameter (OD) and one electrical conductor coated in a thermoplastic protective cover. Two steel pipes were used for packer inflation and one for the control of the SIT and the pressure release valve (PRV), which was only used when the packers could not be sufficiently deflated by opening the packer lines at the surface.

Certain parts of the downhole equipment are described below in more detail.

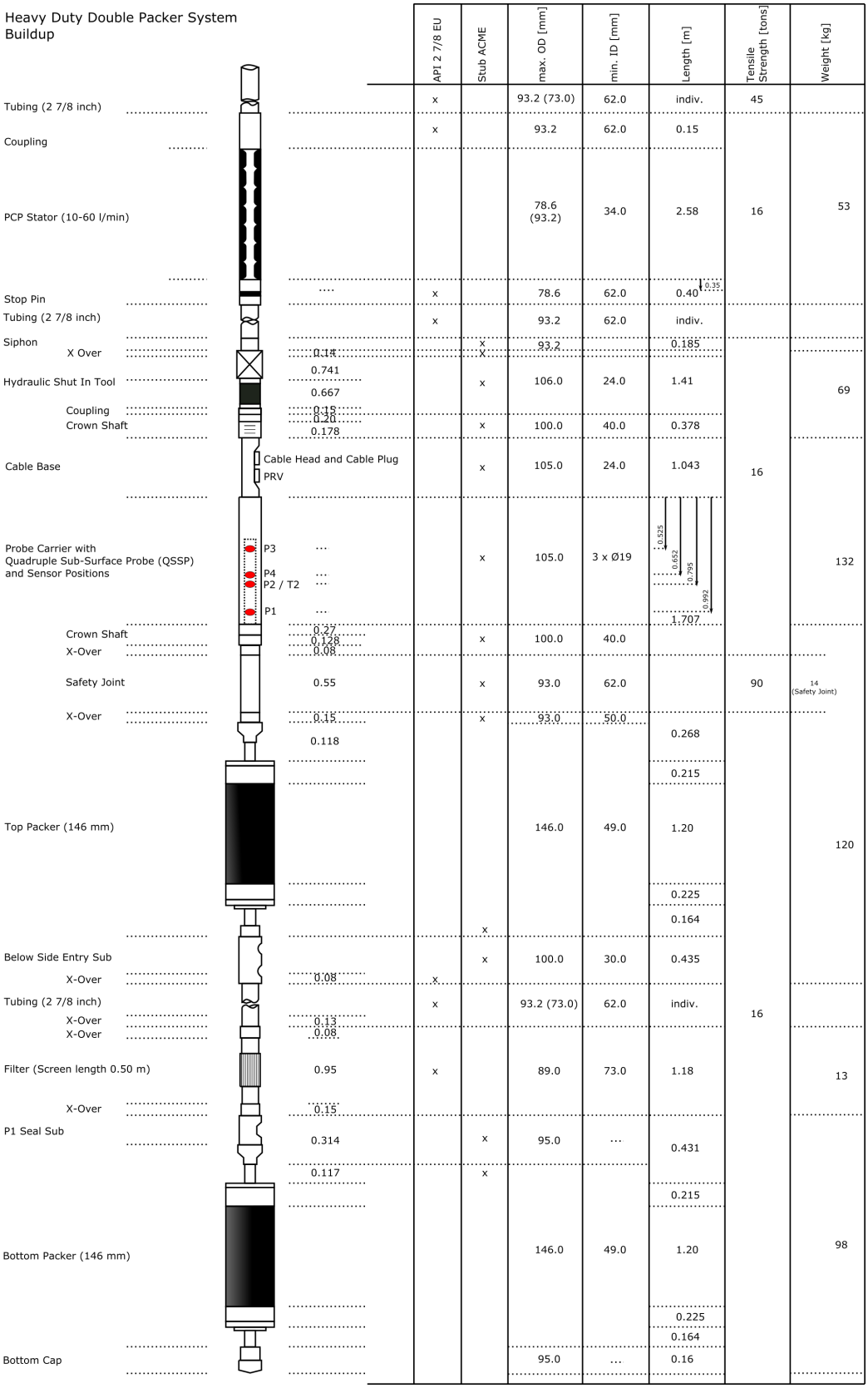

	API 2 7/8 EU	Stub ACME	max. OD [mm]	min. ID [mm]	Length [m]	Tensile Strength [tons]	Weight [kg]
Tubing (2 7/8 inch)	x		93.2 (73.0)	62.0	indiv.	45	
Coupling	x		93.2	62.0	0.15		
PCP Stator (10-60 l/min)			78.6 (93.2)	34.0	2.58	16	53
Stop Pin	x		78.6	62.0	0.40		
Tubing (2 7/8 inch)	x		93.2	62.0	indiv.		
Siphon		x	93.2		0.185		
X Over		x					
Hydraulic Shut In Tool		x	106.0	24.0	1.41		69
Coupling							
Crown Shaft		x	100.0	40.0	0.378		
Cable Base		x	105.0	24.0	1.043	16	
Probe Carrier with Quadruple Sub-Surface Probe (QSSP) and Sensor Positions		x	105.0	3 x Ø19	1.707		132
Crown Shaft		x	100.0	40.0			
X-Over							
Safety Joint		x	93.0	62.0		90	14 (Safety Joint)
X-Over		x	93.0	50.0			
Top Packer (146 mm)			146.0	49.0	1.20		120
Below Side Entry Sub		x	100.0	30.0	0.435		
X-Over	x						
Tubing (2 7/8 inch)	x		93.2 (73.0)	62.0	indiv.	16	
X-Over							
X-Over							
Filter (Screen length 0.50 m)	x		89.0	73.0	1.18		13
X-Over							
P1 Seal Sub		x	95.0	...	0.431		
Bottom Packer (146 mm)			146.0	49.0	1.20		98
Bottom Cap			95.0	...	0.16		

Fig. 4-1: General configuration and specifications of the HDDP in double packer configuration

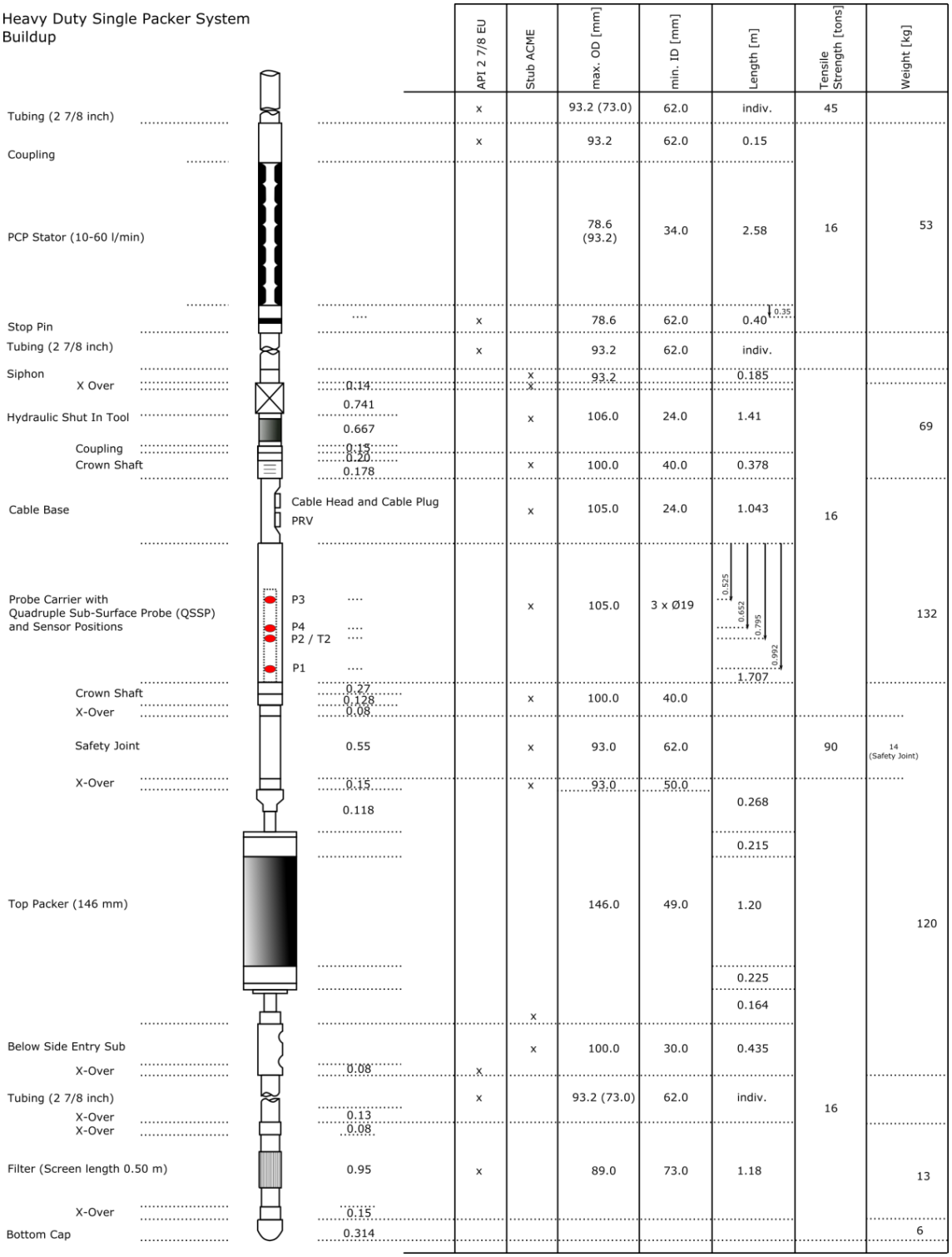

Fig. 4-2: General configuration and specifications of the HDDP in single packer configuration

4.2.1.1 Heavy-duty double packer system

The technical data of the HDDP are provided in Tab. 4-3. A summary of the downhole equipment with the most important specifications is given in Tab. 4-4.

Tab. 4-3: Specifications for the HDDP

Tool Description	**HDDP**
Packer configuration	Double packer or single packer
Maximum installation depth	1'400 m (vertical); 1'500 m (inclined) along borehole axis
Maximum fluid pressure	20'000 kPa
Maximum differential pressure	114 mm packer system for 162 mm borehole: ~ 12'200 kPa 146 mm packer system for 216 mm borehole: ~ 8'000 kPa
Maximum downhole temperature	80 °C
Range of interval length	3 – 100 m
Probe	QSSP
Shut-in tool (SIT)	Zero-displacement valve
Control lines	4 core encapsulated flat-pack • Hydraulic line – bottom packer (PA1) • Hydraulic line – top packer (PA2) • Hydraulic line – shut-in tool (SIT) and packer pressure release valve (PRV) • ⅛" (3.175 mm) OD tubing encased single conductor cable

Tab. 4-4: Specifications for the HDDP components

Component	**Specifications**	**Min. ID** [mm]	**Weight**	**Max. tensile force** [t]
Quadruple flat-pack	3 each ¼" OD × 0.035" WT 316L stainless steel welded and cold drawn annealed tubes 153'339 kPa nominal burst pressure 49'139 kPa maximum test pressure Incorporating 1 each ⅛" OD × 0.022" WT316L stainless steel 16 AWG solid CU conductor /P/N 024440) encapsulated to ¼" OD in TT200 thermoplastic Encapsulated as 33 mm × 11 mm in TT210 thermoplastic, suitable for maximum 98.9 °C brine service		0.637 kg/m	n/a
Tubing	2⅞" EUE API CT5 N80	62	9.68 kg/m	45.3
Pup joints	2⅞" EUE API CT5 L80/N80	62	9.68 kg/m	45.3
Shut-in tool (SIT)	Duplex 1.4462	24	69 kg	16
Pressure release valve (PRV)	Duplex 1.4462	24	132 kg	16
Cable base	Duplex 1.4462			16
Quadruple sub-surface probe (QSSP)	Duplex 1.4462 4 pressure sensors P1, P2, P3 and P4	3 × Ø19		16
Coarse thread safety joint	3 21/32" OD, with 2 7/16" bore with 2⅞" EUE box × pin connections	62	26 kg	90
Packers for large borehole diameter	IPI 5¾" (146 mm), steel wire reinforced, duplex, natural rubber Packer 1 Packer 2	 49 49	 98 kg 106 kg	16
Packers for normal borehole diameter	IPI 4½" (114 mm), steel wire reinforced, duplex, natural rubber Packer 1 Packer 2	 49 49	 78 kg 67 kg	16
Filter	HP well screen: sand free filter screen mounted on 2⅞" tubing L 80 Length: 0.50 m Length: 1.00 m	 73 73	 13 kg 19 kg	16
Total system weight	At 1'400 m depth including PC Pump, quadruple flat-pack cable and centralisers		about 15.2 t	
Maximum applicable tensile force for entire system	Actual system weight at the corresponding depth, plus 16 t (weakest point)			

4.2.1.2 Packers

Two types of packers were available for use, a 114 mm packer for 162 mm diameter boreholes and a 146 mm packer for 216 mm diameter boreholes (Tab. 4-5). The packers were individually inflated with water through the packer inflation line. The inflation line was integrated in the quadruple flat-pack using a booster pump. Depending on the environmental temperatures, an anti-freeze was added to the water. Both packer pressure lines were connected to the packer control board at the winch and equipped with pressure sensors (pressure range 0 – 30'000 kPa) for packer pressure monitoring. The packer pressure sensors were connected to the data acquisition system (DAS) for continuous recording. To keep packer pressures constant, the packers were connected to a pressure vessel via the packer control board for the entire test time. The pressure vessel was placed in a water bath to keep its temperature as constant as possible.

Tab. 4-5: Specifications for the HDDP packers

Manufacturer	Inflatable Packers International, Perth, Australia	
Packer types	IPI 4½" (114 mm)	IPI 5¾" (146 mm)
Material and type	Duplex, natural rubber, sliding end	Duplex, natural rubber, sliding end
Reinforcement type	Steel wire reinforced	Steel wire reinforced
Borehole diameter	162 mm	216 mm
Packer diameters	125 – 230 mm (pressure dependent)	162 – 280 mm (pressure dependent)
Outer diameter, not inflated	114 mm max.	146 mm max.
Inner diameter	49 mm min.	49 mm min.
Overall length: Bottom packer Top packer	 1.93 m 2.08 m	 1.92 m 1.92 m
Rubber sleeve length	1.20 m	1.20 m
Thread connections	2⅞" EUE pin × 2⅞" EUE box	2⅞" EUE pin × 2⅞" EUE box
Max. working temperature for a period > 100 h	+80 °C	+80 °C
Packer inflation lines	Quadruple flat-pack, see Tab. 4-4	Quadruple flat-pack, see Tab. 4-4
Inflation method	Surface controlled	Surface controlled
Inflation fluid	Water and anti-freeze (if necessary)	Water and anti-freeze (if necessary)

4.2.1.3 Downhole sensors in the quadruple sub-surface probe

Four Keller PA-27XW transducers (for transducer types and specifications see Tab. 4-6) were used to monitor fluid pressures in the interval below the bottom packer (P1), within the testing interval (P2), in the annulus between the tubing and borehole wall above the top packer (P3) and in the test string (P4) above the downhole SIT. These four transducers were mounted in the QSSP probe, which was integrated in the probe carrier (see Fig. 4-1). The pressure sensors measured absolute pressure and corrected it to atmospheric pressure; the sensor showed ±0 kPa at atmospheric pressure conditions.

Each pressure transducer had an associated temperature sensor (referred to as T1, T2, T3 and T4) for full thermal compensation of the pressure measurement (Tab. 4-6). The temperature sensor was mounted inside the pressure transducer housing. Because the temperature measurements were taken at the positions of the pressure transducers, they may not represent the effective temperature of the test interval fluid.

Tab. 4-6: Specifications for the pressure transmitters mounted in the QSSP

Pressure transducer type	Keller PA-27XW, custom-made
Manufacturer	Keller, Winterthur, Switzerland
Year of commissioning	2018
Pressure range (full scale)	0 – 20'000 kPa (absolute)
Accuracy	-0.004…0.005% FS[1]
Resolution	< 0.0007% FS
Minimum recording rate	1 Hz
Temperature range (FS)	-10 °C to 80 °C
Accuracy (temperature)	1 °C
Resolution (temperature)	0.01 °C
Output signal	RS485 (digital)

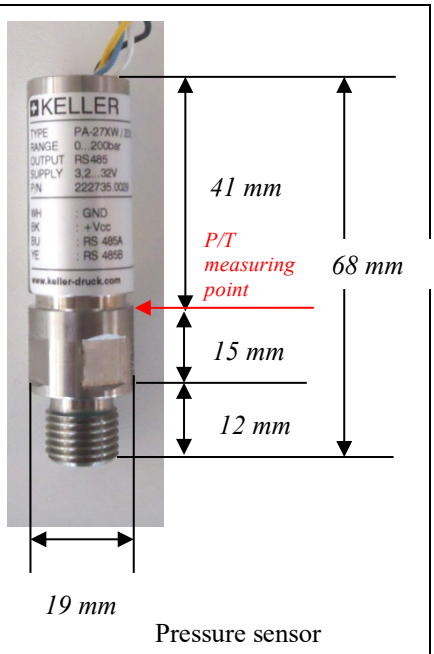

Pressure sensor

[1] FS = full scale

4.2.1.4 Autonomous data logger in test interval

Pressures and temperatures were recorded as redundant measurements in the interval at the lower end of the filter screen (referred to as P2* and T2*, respectively) with an autonomous data logger of the type DataCan Memory Pressure Gauges. The specifications are given in Tab. 4-7. The recorded pressure measurement is an absolute measurement.

Tab. 4-7: Specifications for the data logger

Data logger type	DataCan Memory Pressure Gauge 1.25" Welded Piezo III
Manufacturer	Data Can, Red Deer, Canada
Pressure range (FS)	0 – 20'684 kPa (absolute)
Pressure accuracy	0.03% FS
Resolution	0.0003% FS
Temperature range	0 – 150 °C
Temperature accuracy	0.5 °C
Resolution	0.005 °C
Memory capacity	1'000'000 data sets
Minimum recording rate	10 Hz
Year of commissioning	2018

4.2.1.5 Zero-displacement shut-in tool

The downhole SIT controls the fluid connection between the interior of the test tubing and the test interval. The SIT is a zero-displacement valve that is hydraulically operated via a hydraulic line integrated in the quadruple flat-pack using a booster pump. An axially moveable valve piston opens and closes the valve. The valve piston is moved via the hydraulic (closure) line by applying pressure to close the valve. Releasing the pressure with a pre-stressed spring resets the valve piston and opens the valve (pressure-free opening).

With a pressure compensation element, the pressure at interval depth (annulus pressure) is used to support the spring and to keep the opening/closing pressure constant for the entire borehole depth. The spring force is high enough to ensure a proper functioning of the valve also at low groundwater levels. The specifications are given in Tab. 4-8.

Tab. 4-8: Specifications for the zero-displacement shut-in tool

Zero displacement shut-in tool (SIT)	Manufactured by Solexperts
Maximum water flow rate	Below 40 l/min without friction loss, max. 350 l/min
Pressure loss caused by SIT at a flow rate of 1 l/min and 10 l/min	±0 kPa
Closing pressure	9'000 – 10'500 kPa
Maximum applicable tensile force	16 t

4.2.1.6 Test tubing

API Spec. 5 CT-05 2⅞" tubing was used as test rods. The detailed specifications of the test tubing are summarised in Tab. 4-9.

Tab. 4-9: Specifications for the test tubing

Test tubing type	Seamless steel tubing and pup joints: 2⅞" 6.5 ppf L80 B*P EUE R2 API 5CT
Manufacturer	Normec, Celle, Germany
Steel grade	L80
Inner diameter	62.00 mm
Outer diameter	73.02 mm
Coupling outer diameter	93.20 mm
Thread	API 2⅞" EUE
Weight per meter	9.68 kg
Volume per meter	3.02 l
Individual tubing length	Range 2, ~ 9.5 m
Number of individual tubings	162
Total length of test tubing	Ca. 1'500 m
Lengths of pup joints	Length, quantity 0.5 m, 2 1.0 m, 2 2.0 m, 2 3.0 m, 4 4.5 m, 4
Maximum applicable tensile force	45.3 t

4.2.1.7 Slim tubing

The rate of pressure increase during the flow phase of a slug test depends on the formation transmissivity and the diameter of the test tubing, which defines the wellbore storage of the test system during the slug. To improve the resolution of the pressure change, a slim tubing was used to reduce the diameter of the test tubing for slug tests in formations with low transmissivity.

The slim tubing consists of a stiff tube, which is installed into the test tubing. A packer at the bottom of the slim tubing with an outer diameter of 56 mm sealed the annulus between the 2 ⅞" tubing and the slim tubing. The water level in the slim tubing was measured with the P4 sensor from the QSSP and additionally with a backup pressure sensor installed at the top of the slim tubing packer, referred to as P4-slim. P4-slim has a smaller pressure range and thus a higher precision compared to P4. The technical specifications of the slim tubing are summarised in Tab. 4-10.

After lowering the water level in the 2⅞" test tubing for a slug withdrawal test to the specified depth, the slim tubing was installed in the tubing below the water level. Afterwards, the slim tubing packer was inflated, and the test was started by opening the SIT valve. The water only increased in the pipe. The use of a stiff tube ensured a constant inner diameter independent of the pressure (fluid level).

Tab. 4-10: Specifications for the slim tubing

Slim tubing	Manufactured by Solexperts	
Types	Polyethylene tube	Stainless steel tube
Inner diameter	12 mm	6 mm
Outer diameter	16 mm	8 mm
Length	300 m	300 m
Packer specifications	Diameter 56 mm, sealing length 1'000 mm, working pressure 1 – 13.5 MPa	
Packer pressure line	Polyamide OD: 6 mm; ID: 3 mm	
Packer pressure sensor	Keller PA-23SY, 0 – 5'000 kPa, accuracy 0.25% FS	
Pressure sensor (P-slim)	Keller PA-27XW, 0 – 3'000 kPa, accuracy < 0.07% FS, linearity 0.2% FS	
Installation procedure	Wireline system of the drill rig	

4.2.1.8 Submersible pumps

Frequency driven 3" and 4" Grundfos submersible pumps can be used for pumping tests and during open-hole pumping, e.g. for fluid logging. The specifications are included in Tab. 4-11. The flow rate can be arbitrarily adjusted because of the frequency control of the pump.

Tab. 4-11: Specifications for the submersible pumps

Submersible pump types	4" down-hole pump	3" down-hole pump
Manufacturer	Grundfos, Fällanden, Schweiz	
Type	SP14-27E	SQE1-110
Regulation	Frequency-controlled	Frequency-controlled
Dimensions	101 × 3040 mm	74 × 852 mm
Pumping rate at 150 m	100 l/min	10 l/min
Range of pumping rates	Max. 300 l/min	Max. 28 l/min
Maximum installation depth	160 m	160 m
Maximum temperature	40 °C	35 °C
Weight	57 kg (pump) 31 kg (motor)	6 kg
Pump housing	Yes	No
Specifications of pump housing	Length: 4.22 m OD max: 180 mm Weight: 130.3 kg	
Purpose	Pumping tests	Pumping tests, fluid logging

4.2.1.9 Progressive cavity pump

For constant rate or constant head withdrawal tests (pumping tests) a progressive cavity (PC) pump, a so-called Moyno® type pump, was used. The PC pump consists of a helical rotor and a twin helix in a rubber stator. The stator is integrated into the test tubing string and allows for pumping, if necessary, but does not preclude any other test methods. For pumping, a suitable rotor had to be installed by means of the so-called sucker rods until the rotor had fully penetrated the stator. The specifications are listed in Tab. 4-12.

Tab. 4-12: Specifications for the PC pump

PC pump type	Progressive cavity pump
Manufacturer	Netzsch
Dimensions	Drive head: L × W × H: 1'375 × 767 × 1'263 mm
Pumping rates	1.7 – 60 l/min Pumping rates of < 1.7 l/min can be reached by closing the valve installed in-line at the wellhead.
Maximum installation depth	300 m
Temperature	10 °C to 70 °C
Sucker rods, type	¾" × 7.62 m
Sucker rods, quantity	45
Total length	Approx. 300 m
Available stators	1 for pump rates 10.4 – 60 l/min, Temp. 10 °C to 70 °C 1 for pump rates 1.7 – 5.5 l/min, Temp. 10 °C to 70 °C
Available rotors	3 for pump rates 10.4 – 60 l/min, Temp. 10 °C to 30 °C, 30 °C to 50 °C, 50 °C to 70 °C 3 for pump rates 1.7 – 5.5 l/min, Temp. 10 °C to 30 °C, 30 °C to 50 °C, 50 °C to 70 °C

4.2.1.10 Piston pulse generator

The piston pulse generator (PPG) is an optional downhole tool. It brings a unique and proven technology for conducting pulse tests to the more traditional low-permeability hydraulic testing realm. In an effort to reduce the uncertainty associated with determining the test zone compressibility, a hydraulic piston (i.e. the PPG) of known volume is incorporated into the hydraulic test tool, in this case the HDDP. This PPG resides within the test zone but not conventionally in between the packers. The PPG is contained within a housing that is located above the top packer and below the downhole SIT.

When deployed in a borehole, the packers are inflated, the piston is put into the appropriate position (fully extended or fully retracted), the SIT is closed, thereby isolating the test zone from the rest of the borehole, and the test zone is allowed to equilibrate for a period of time.

When it has been decided to initiate a pulse with the PPG, fluid from the pressurised fluid reservoir is routed to the appropriate hydraulic line (piston extend or piston retract) through the hydraulic control panel, thereby changing the position of the piston and changing the test zone volume by a known amount during a few minutes. The resulting test zone pressure change is measured and can be used for the calculation of the interval storage / test zone compressibility. The pressure transducers used to monitor the PPG state are linked to the DAS. The specifications are listed in Tab. 4-13.

It should be noted that only one piston can be deployed at a time and the piston must be either fully extended or fully retracted. Therefore, only displacement volumes of 50 ml, 250 ml or 500 ml can be achieved once the HDDP is deployed.

Tab. 4-13: Specifications for the PPG

PPG type	INTERA-PPG-1
Manufacturer	HydroResolutions
Dimensions	OD: 0.1143 m Length: max. 2.54 m
Weight	Max. 79.38 kg
Material	Steel
Maximum applicable tensile force	Approx. 30 t

4.2.2 Surface equipment

The surface equipment consisted of the following equipment:

- Winch for quadruple flat-pack cable
- Flow control system
- Pressure vessel for packer pressure stabilisation
- Injection and pumping head
- PC pump drive head and control unit
- Data acquisition system

The surface equipment was installed in a mobile measuring container.

4.2.2.1 Flow board

For the control and measuring of pump (and injection) rates, a flow board with two flowmeters of type Yokogawa AXF were available. The flowmeters covered a flow rate range between 0.01 and 100 l/min (Tab. 4-14). The schematic layout of the flow control unit is displayed in Fig. 4-3.

Tab. 4-14: Specifications for the flowmeters

	Measuring range and accuracy			
	Lower limit		**Upper limit**	
	[l/min]	[% FS]	[l/min]	[% FS]
AXF 010	0.1	1	11.78	0.35
AXF 025	1.0	1	100	0.35

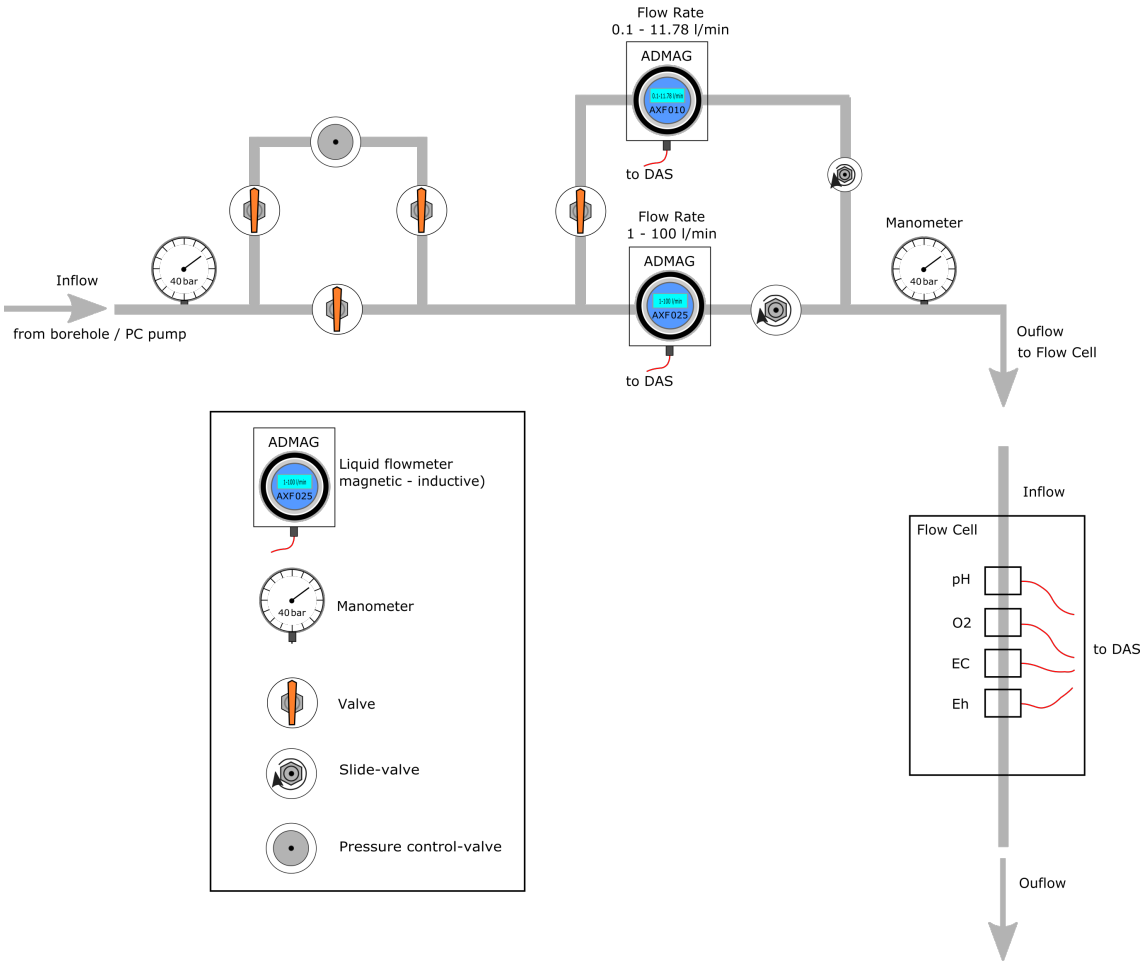

Fig. 4-3: Schematic layout of the flow control unit

4.2.2.2 Packer pressure control unit

Two transducers (type Keller PA-23SY, 30'000 kPa) mounted on the surface inflation control panel were used to monitor the packer inflation pressures (Fig. 4-4).

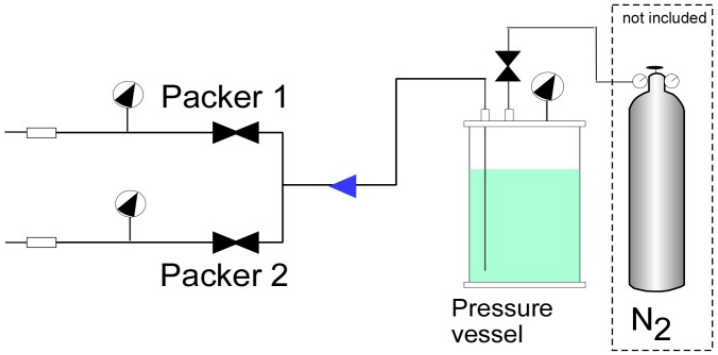

Fig. 4-4: Schematic layout of the packer control unit

4.2.2.3 Additional recorded measurements at surface

A single pressure transducer (type Keller PAA-33X, 80 – 120 kPa absolute) was mounted in the monitoring trailer and used to monitor barometric pressure (Tab. 4-15).

During pumping tests, the physico-chemical parameters (e.g. pH, EC, Eh, temperature and oxygen concentration) and the temperature of the extracted fluid were recorded. The specifications of the physico-chemical sensors are given in Tab. 4-16. The specifications of the temperature sensor are also given in Tab. 4-16. The sensors were calibrated on-site before each use.

Tab. 4-15: Specifications for the atmospheric pressure sensor

Temperature sensor type	Keller PAA-33X
Manufacturer	Keller, Winterthur, Switzerland
Pressure range	80 – 120 kPa
Accuracy	0.02% FS
Resolution	0.002% FS

Tab. 4-16: Specifications for the physico-chemical sensors

Sensor type	**EC**	**pH**	**Eh**	**O_2**	**Temp**
Manufacturer	Xylem analytics, Weilheim, Germany				IST AG
Model	WTW TetraCon 325	WTW SensoLyt DW	WTW SensoLyt PtA/Pt	WTW FDO 700 IQ	Pt 1000
Range	1 µS/cm – 2 S/cm	0 – 14	±2'000 mV	0 – 20 mg/l	-50 – 650 °C
Accuracy	n/a	n/a	n/a	n/a	±0.15 °C at 0 °C ±0.35 °C at 100 °C
Resolution	n/a	n/a	n/a	0.01 mg/l (0.01 ppm)	1.5×10^{-3} °C
Temperature range	0 °C to 100 °C	0 °C to 60 °C	0 °C to 60 °C	-5 °C to 50 °C	-50 °C to 650 °C

4.2.2.4 Data acquisition system

The data acquisition system (DAS) consisted of industrial PCs, screens and keyboard. Data acquisition was performed through the Solexperts GeoMonitor II (GMII) software. The downhole pressures (P1, P2, P3, P4) and temperature measurements (T1, T2, T3, T4) were recorded in real time through the quadruple flat-pack cable assembly. Surface measurements like flowmeter rates, packer pressures, atmospheric pressure and temperature, slim tubing packer pressure and the physico-chemical parameters were recorded either permanently or, if required, with an interface with the same scan rate as the downhole pressures from the QSSP.

The scan rates could be adjusted as required between 0.5 s (using a reduced number of sensors) and > 30 s.

The measurements were written to a data file on the PC hard drive in real-time with a continuous data collection and database model. From the PC hard drive, the data were transferred to another network PC every 20 s for 'online' analysis and data back-up. An uninterruptible power supply was utilised to protect the system from short power interruptions.

4.3 Test analyses

4.3.1 Workflow

For TRU1-1, the general on-site analysis approach involved mainly numerical techniques considering the whole borehole pressure history. Analytical solutions were used mainly to present the results and to conduct more detailed consistency checks between measurements and simulations. This ensured a comprehensive evaluation of the recorded data. The numerical solutions were assessed further with a perturbation analysis. Prior to commencement of the hydraulic tests, particularly the representation of the borehole history period and the starting input parameters were defined.

The on-site analysis workflow supported the test design to achieve the quality objectives defined by Nagra:

- Identification of the flow model, e.g. by flow dimension diagnostic (Beauheim et al. 2004)
- Numerical simulation of individual test sequences in Cartesian coordinates

  The suitability of the applied flow model was checked with diagnostic representations of the recorded and simulated pressure data, and limited perturbation analysis was used to assess the suitability of the numerical solution.
- Numerical simulation of the entire test sequence in Cartesian coordinates using the optimised parameter set obtained from the analysis of the individual phases

  This final step was used to check the consistency of the model to the entire data set.
- Consistency check of the test analysis as well as estimated parameters by the technical supervisor

The results were used to continuously optimise the test design to achieve the quality objectives within the dedicated time of testing. A general flowchart of the analysis work is provided in Fig. 4-5.

The test data were analysed numerically using the nSIGHTS software (Geofirma Engineering Ltd. & INTERA 2011). For slug and pulse tests, the consistency check typically involved one or more of the semi-log and log-log plots developed by Ramey et al. (1975). Recovery tests were presented according to Horner (1951). A summary of the applied test analysis methods is presented in Tab. 4-17.

Tab. 4-17: Summary of analytical analysis methods

Test phase	**Analysis method**	**Reference**
Pulse test	Semi-log and log-log representations of the transient pressure change and derivative versus time	Ramey et al. (1975)
	Diagnostics: analysis on transient pressure data	Beauheim et al. (2004)
Slug test (flow phase SW)	Semi-log and log-log representations of the transient pressure change and derivative versus time	Ramey et al. (1975)
	Diagnostics: analysis on transient pressure data	Beauheim et al. (2004)
Slug test (pressure recovery after slug flow phase, SWS)	Semi-log and log-log representations of the transient pressure change and derivative versus time	Ramey et al. (1975)
	Diagnostics: analysis on transient pressure data	Beauheim et al. (2004)
Constant rate test	Log-log representations of the transient pressure change and derivative versus time	Bourdet et al. (1989)
	Diagnostics: analysis on transient pressure data	Horne (1995), Beauheim et al. (2004)
Pressure recovery after constant rate tests	Log-log representations of the transient pressure change and derivative versus 'superposition time'	Bourdet et al. (1989)
	Semi-log representations of the transient pressure change	Horner (1951)
	Diagnostics: analysis on transient pressure data	Horne (1995), Beauheim et al. (2004)

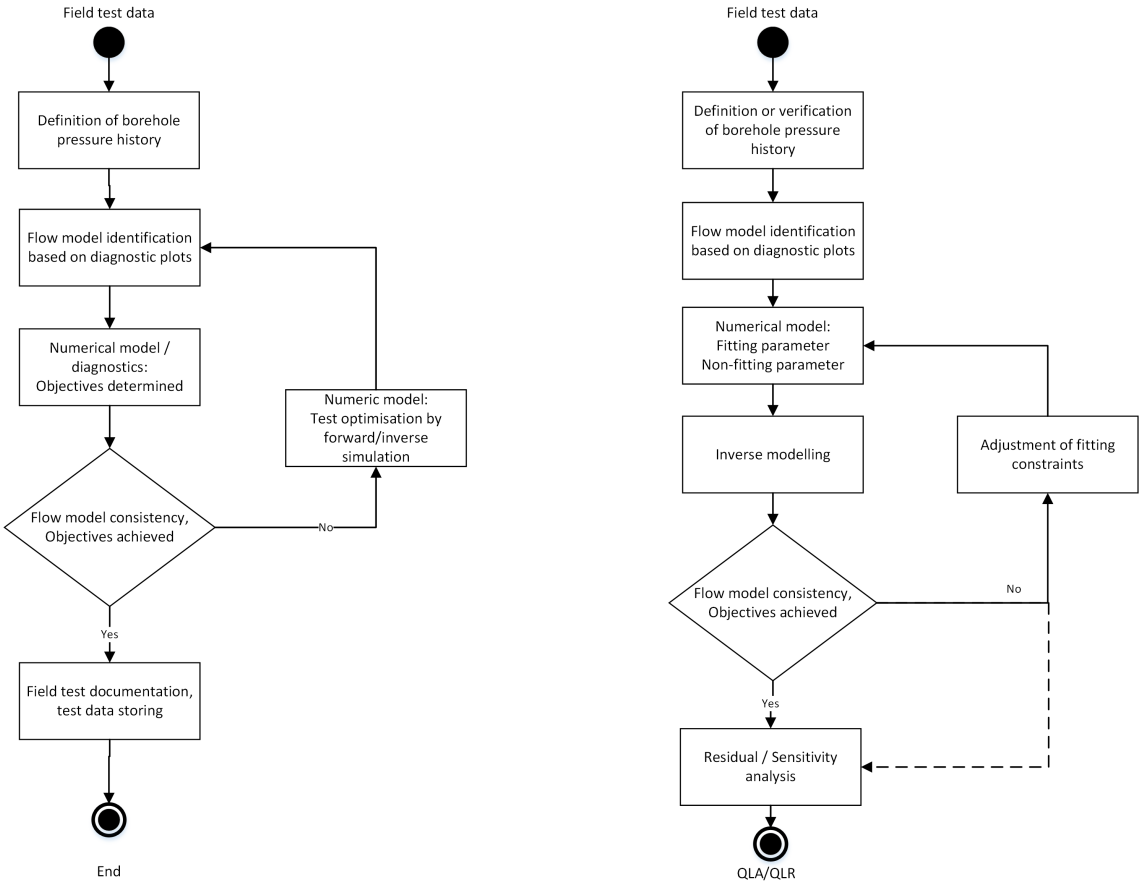

Fig. 4-5: Flowcharts for the on-site hydraulic packer test analysis (left) and Quick Look Analysis (QLA) (right)

The detailed analysis (DA) was performed off-site after the test was completed and is based on the QLA. The QLA was reviewed as part of the Quality Control (QC) programme. During this task, open questions and potential ambiguities of the analysis were defined. Based on the outcome of the QC review, further specifications and, if necessary, further analyses were implemented. Fig. 4-6 provides the general flowchart of the DA, which includes perturbation and non-fitting parameter analysis, to obtain the most reasonable parameter results and ranges of uncertainty.

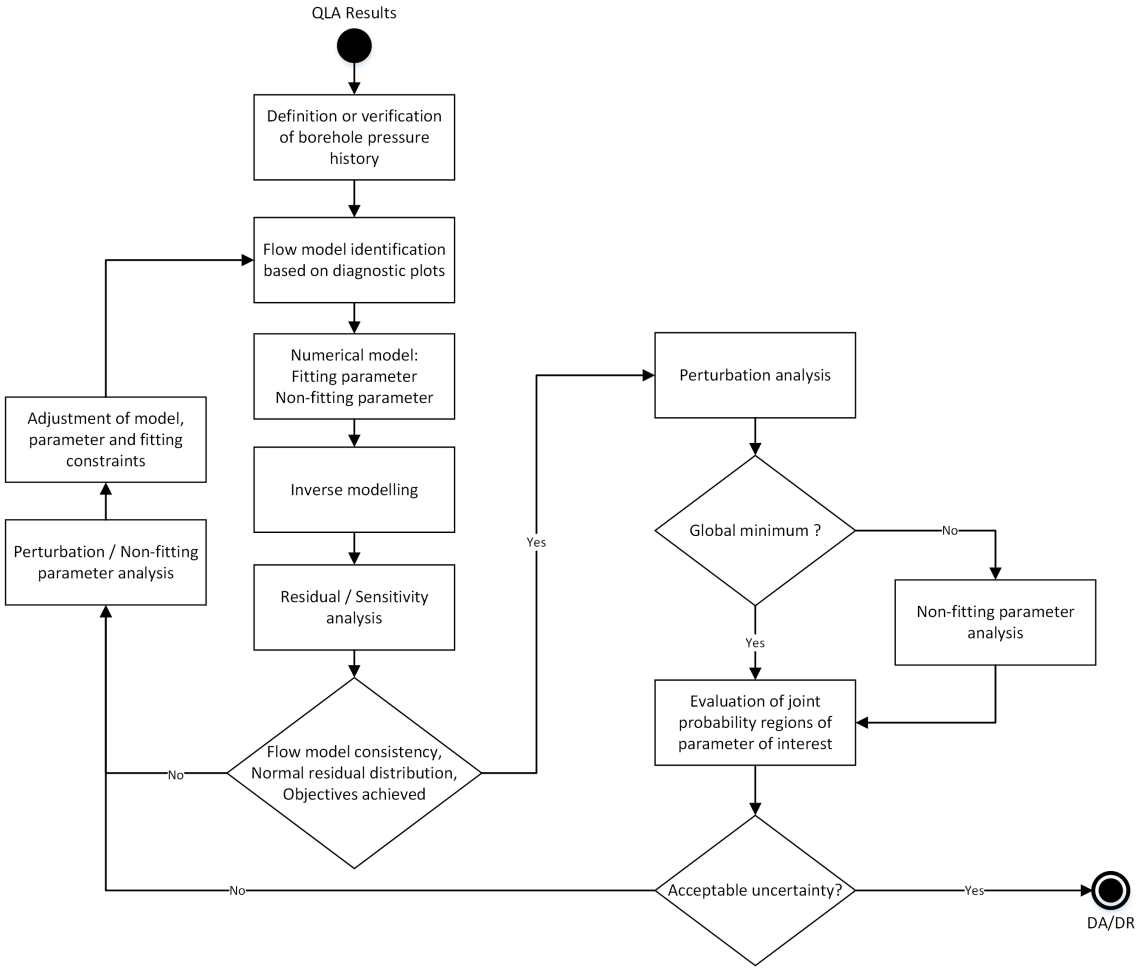

Fig. 4-6: Flowchart for the off-site DA of a hydraulic packer test

4.3.2 Special effects

The time series measured during hydraulic packer tests are the pressure and temperature inside the test interval. Their development over time was analysed to estimate the hydraulic properties of the formation surrounding the test interval. Various factors affected the recorded time series. All hydraulic tests are affected by factors beyond the test execution and the model used for their analysis (analytical solutions based on assumptions to derive them, numerical models based on the physical processes included in their base equation system). They are referred to as disturbances because they are not considered in the analysis. However, it is possible to describe the development of temperature and pressure signals by the diffusion equation. Disturbances are of short duration in formations with medium to high transmissivity. In formations with low transmissivity, disturbances of the pressure or temperature field can have a significant influence on the pressure signal measured during the test in the test interval (e.g. Grauls 1999, Nagra 2001).

Any disturbances of the pressure field during the time before the hydraulic test is started, are summarised under the name 'borehole pressure history'. Disturbances in the pressure and temperature fields can be caused by drilling and other activities before testing. In addition, disturbances can occur even during testing, e.g. mechanical effects due to changes in the stress field surrounding the interval, or osmosis due to the chemical interaction of the formation and drilling

fluid. However, results from the experiment 'Deep Borehole Hydraulic Testing Experiment' in the Mont Terri Rock Laboratory show that osmotic effects have no significant impact on the determination of transmissivity and hydraulic head (Marschall et al. 2003).

As the TBO boreholes are multi-purpose boreholes with many other objectives besides hydraulic packer testing, there is always a trade-off between disciplines in regard to optimal test conditions. The hydraulic packer tests were performed without exchange of drilling fluid with testing fluid with the aim to reduce potential pressure and temperature disturbances. In addition to this preventive measure, the numerical analysis tool can estimate the effect of these influences, so that plausibility ranges for the parameter estimations can be defined. In the following, possible individual special effects that had already been identified, e.g. for borehole Benken (Nagra 2001), are discussed in more detail.

4.3.2.1 Borehole history

All numerical analyses took into account the borehole pressure history. The borehole pressure history was constructed based on activities that took place prior to hydraulic testing. Drilling through the midpoint of the test interval was used as the starting point of the pressure history. The borehole pressure history data were incorporated into the numerical analyses. The following information was used:

- Date and time of drilling through the interval midpoint, from drilling logs
- Drilling fluid density
- Pressure records of preceding hydraulic testing

Most affected by the borehole pressure history is the determination of the static formation pressure (hydraulic potential), which in turn depends on the transmissivity of the formation. In formations with low transmissivity, like Opalinus Clay, the determination of the static formation pressure can be impossible in a reasonable time due to the long duration of the pressure history. This was proven by the measurements of the Benken long-term monitoring system, which demonstrated that the static formation pressures of Opalinus Clay determined by hydraulic tests were much higher than those subsequently determined by long-term measurements (e.g. Jäggi & Vogt 2020).

The specific periods of the borehole pressure history taken into account for the analysis of the hydraulic packer tests in borehole TRU1-1 are provided in Tab. 4-18.

Tab. 4-18: Specific periods of the pre-test borehole pressure history

Pre-test refers to the period prior to the separation of the test interval from the rest of the borehole through the inflation of the last packer.

Test name	**Drilling through midpoint: date and time**	**Start hydraulic testing: date and time**	**Borehole history duration** [h]
TRU1-1-MAL1	24.09.2019, 08:30	26.09.2019, 00:40	40.17
TRU1-1-BDO2[1]	24.11.2019, 22:46	27.11.2019, 15:53	65.12
TRU1-1-BDO1	23.11.2019, 19:48	02.12.2019, 12:54	209.10
TRU1-1-OPA2	09.12.2019, 21:51	20.12.2019, 03:11	245.33
TRU1-1-LIA1	16.12.2019, 16:35	29.12.2019, 17:00	312.42
TRU1-1-LIA2	15.12.2019, 12:10	01.01.2020, 15:12	411.03
TRU1-1-OPA3	11.12.2019, 13:44	07.01.2020, 14:16	648.53
TRU1-1-KEU1	31.01.2020, 12:06	03.02.2020, 14:58	74.87
TRU1-1-MUK1	14.02.2020, 23:04	22.02.2020, 14:39	183.58

[1] Test re-named from OPA1 to BDO2 during final reporting.

4.3.2.2 Interval temperature changes during testing

All activities inside the open borehole also affect the temperature field in and around the borehole. In formations with low transmissivity this temperature disturbance affects the pressure field surrounding the borehole due to coupled thermo-hydraulic processes. The analysis of hydraulic tests using the numerical software packages nSIGHTS, Multisim and WellSi can incorporate temperature changes during the hydraulic test that lead to a change in fluid volume and thus pressure within a confined test interval volume. The fluid volume change in the test interval was calculated using the volumetric thermal expansion coefficient of the fluid (water), which itself is temperature-dependent. The pressure change is linearly dependent on the interval fluid volume change using a proportionality factor, the compressibility of the interval.

The temperature exchange between the surrounding rock and the borehole fluid is neglected in the above-mentioned numerical analysis tools with the exception of nSIGHTS which can handle this process from version 3 onward. The rock surrounding the test interval is heated up during hydraulic testing, while it is cooled down by the fluid circulation during drilling. These changes in the temperature field around the borehole affect the pressure field around the borehole. In formations with low transmissivity, the thermal effects can perturb the pore pressure in the surrounding formation, resulting in an additional observable effect to the temperature changes inside the test interval volume, which in turn may also affect the estimation of the formation parameters, especially the static formation pressure. The coupled thermo-hydraulic processes in Opalinus Clay have been investigated by Nagra in previous studies (e.g. in experiments in the Mont Terri Rock Laboratory and deep boreholes, Gaus et al. 2014a and 2014b, Nagra 2019; predictive modelling of the post-closure period, Senger et al. 2014).

4.3.2.3 Mechanical effects

The mechanical deformations caused by drilling- and testing-related stress redistribution in the formation can also influence the pressure response during a hydraulic test. Normally, the conceptual model for the description of the storage coefficient used in the underlying hydraulic models assumes a compressible pore volume and an incompressible grain structure. In this model, changes in pore pressure are considered as movement of the fluid into and out of the pore volume. The coupling between fluid volume change and mechanical deformations results in a time-dependent deformation for an elastic media (Detournay & Cheng 1988). The Opalinus Clay formation has shown a time-dependent deformation during the excavation of tunnel in Mont Terri (see Lisjak et al. (2015) for a sum-up of the observations and for a numerical interpretation of the data). Opalinus Clay time-dependent behaviour is most likely due to the undrained and drained excavation response, rather than mechanical creep phenomena. In formations with low transmissivity, time-dependent deformations can have an influence on the pressure signal observed in the test interval.

However, there are no data on mechanical deformations available for the tests in borehole TRU1-1 that would allow the characterisation of mechanical effects on the tests in formations with low transmissivity. Deformations of the borehole wall can be included in the analysis by all of the numerical software packages used by means of an appropriate parameterisation during the analysis in the same way as for temperature changes inside the interval. The resulting pressure change is caused by volume changes, which can be either linear or quadratic. The proportionality factor between the volume change and the pressure change is the interval compressibility.

4.4 Test activities

A total of nine test intervals were investigated in borehole TRU1-1 using the HDDP in single and double packer configuration. The most important test specifications are summarised in Tab. 4-19. The initial plan called for eight test intervals. During drilling, an additional hydraulic test was performed to investigate fractured zones in the Opalinus Clay discovered between 870.6 m and 870.7 m as well as between 878.0 m and 882.5 m. The hydraulic packer tests were performed in the following geological formations (*cf.* Dossier III):

- Malm Group («Felsenkalke» + «Massenkalk») with a focus on a porous and a fractured zone (TRU1-1-MAL1)
- Dogger Group, with a focus on the marls, limestones and iron oolites of the «Humphriesioolith Formation» as well as the sandy marls, sandy limestones and sandstones of the Wedelsandstein Formation (TRU1-1-BDO1), on the transition from the Wedelsandstein Formation and the «Murchisonae-Oolith Formation» to Opalinus Clay (TRU1-1-BDO2 [6]), and on typical Opalinus Clay (TRU1-1-OPA2) as well as slightly fractured Opalinus Clay (TRU1-1-OPA3)
- Lias Group, with a focus on the Staffelegg Formation including Rietheim, Breitenmatt/ Rickenbach, Grünschholz, Frick and Beggingen Members (TRU1-1-LIA1) and the transition of Opalinus Clay to the Staffelegg Formation including Gross Wolf and Rietheim Members (TRU1-1-LIA2)

[6] NB: During test execution and analysis, this test interval was referred to as TRU1-1-OPA1. It was re-named to TRU1-1-BDO2 while this final field report was being prepared, i.e. after the finalisation of the relevant DR. The reason is that the test interval covers 9.0 m of Wedelsandstein Formation, 0.9 m of «Murchisonae-Oolith Formation» and merely 5.8 m of Opalinus Clay. Accordingly, the acronym BDO better reflects the thicker formation section located in the test interval. For the sake of traceability in previous test documentation, the names of TRU1-1-OPA2 and TRU1-1-OPA3 remain unchanged.

- Keuper Group (Klettgau Formation and Bänkerjoch Formation) including a heterogeneous sequence of mainly sandstone, argillaceous marl, claystone and anhydrite (TRU1-1-KEU1)
- Muschelkalk Group (Schinznach Formation) with a focus on sub-vertical fractures (TRU1-1-MUK1)

All tests were performed in the cored borehole section with a borehole diameter of 6⅜", with 114 mm (deflated diameter) packers, and without any prior fluid exchange, i.e. with the drilling fluid being used as the interval test fluid. The density and viscosity of the drilling fluid were reported by the mud engineer in daily mud reports. The tubing was typically filled with traced tap water (Na-naphthionate, at a concentration of approximately 10 ppm); for the hydraulic test within the shales 1.5-naphthalene disulfonate (1 ppm) was used as a tracer. The SIT was closed during the whole time of lowering to and installing the HDDP at the test depth. Therefore, in test intervals with low transmissivity, the interval fluid density was not affected by traced water in the test tubing as mostly withdrawal tests were performed and no or only very little fluid flow occurred. If a pressure increase of more than 100 kPa was observed in the test interval during inflation of the top packer, the SIT was opened and the COM phase started. Due to the higher density of the mud in the test interval, for formations with low transmissivity it can be assumed that no flow occurred from the test tubing into the test interval during the COM phase. It was possible to create flow from the formation into the borehole by means of slug and pumping tests only during the following tests: TRU1-1-MAL1, TRU1-1-BDO1, TRU1-1-LIA1, TRU1-1-LIA2, TRU1-1-KEU1 and TRU1-1-MUK1.

A swabbing tool was used to create the pressure difference between the test tubing and the test interval.

For each of the pumping tests the PC pump was used, and the position of the stator of the PC pump in the test string was optimised. If two tests were performed sequentially without pulling the HDDP out of the borehole between tests, a stator was already installed for the first test (usually the deeper test).

For the tests TRU1-1-MAL1 and TRU1-1-KEU1 drilling was stopped for hydraulic testing. For the other tests, a longer section was drilled and then the hydraulic tests were performed. The curves of measured pressures (measured by the downhole sensors in the QSSP and the autonomous data logger in the interval) and pumping rates (measured by the flow board at the surface) for all tests conducted in borehole TRU1-1 are provided in Figs. 4-7 to 4-15. The figures are taken directly from the DRs of the field test contractor.

The temperature increase was included in the analysis for formations without a pumping period (low transmissivity). The temperature increase in the test interval from the start of the initial pressure recovery after closing the shut-in valve (PSR) until the end of the test ranged from 0.6 °C to 3.6 °C for all tests.

Tab. 4-19: Hydraulic packer testing in borehole TRU1-1: Test interval and test specifications

Test name[1]	**Interval depth** [m bgl]	**Interval midpoint [m bgl]**	**Packer configuration**	**Test phases**[1]	**Testing period** (duration)	**Lithology and structural geology features** (formation) [depth and length values rounded]	**Objectives**[2]
TRU1-1-MAL1	589.00 – 600.38	594.69	Single	INF1, PSR1, PW, SW, INF2, INF3, RW, RWS, PI	26.09. – 30.09.2019 (109 h)	«Felsenkalke»+ «Massenkalk» of the Malm Group: porous zone from approx. 592.2 to 593.1 m bgl; fractured zone from approx. 593.5 to 595.4 m bgl (visually highest permeability from approx. 593.5 to 594.3 m bgl); single packer seated in massive limestone above the porous zone	T, h_s, FM, WS
TRU1-1-BDO1	782.25 – 805.30	793.8	Double	INF, COM, PSR, PW, SW, SWS, DEF	02.12. – 05.12.2019 (82 h)	From top down: 5.25 m of «Humphriesioolith Formation», 17.8 m of Wedelsandstein Formation; packers seated in competent sections of «Humphriesioolith Formation» and Wedelsandstein Formation	T, h_s, FM
TRU1-1-BDO2[3]	806.50 – 822.20	814.35	Single	INF, COM, PSR, PW1, PW2, DEF	27.11. – 29.11.2019 (45 h)	From top down: 9.0 m of Wedelsandstein Formation, 0.9 m of «Murchisonae-Oolith Formation», and 5.8 m of Opalinus Clay; the strata covered by the test interval are 63% BDO and 37% OPA; packer was seated in a competent siltstone section of the Wedelsandstein Formation	T, h_s, FM
TRU1-1-OPA2	829.00 – 854.00	841.50	Double	INF, COM, PSR, PW, PI, DEF	20.12. – 23.12.2019 (87 h)	Entirely within Opalinus Clay; packers seated in competent sections of Opalinus Clay	T, h_s, FM
TRU1-1-OPA3	868.50 – 887.45	877.98	Double	INF, COM, PSR, PW, PI, DEF	07.01. – 10.01.2020 (97 h)	Entirely within Opalinus Clay including fractures of unknown hydraulic significance between 870.6 and 870.7 m bgl and between 878.0 and 882.5 m bgl; packers seated in competent sections of Opalinus Clay	T, h_s, FM
TRU1-1-LIA2	923.72 – 944.50	934.11	Double	INF, COM, PSR, PW, SW, DEF	01.01. – 04.01.2020 (76 h)	From top down: 4.2 m of Opalinus Clay and 16.6 m of Staffelegg Formation (incl. 6.8 m of Gross Wolf Member and 9.8 m Rietheim Member); this part of the Staffelegg Formation consists mainly of calcareous to argillaceous marls and bituminous shales	T, h_s, FM
TRU1-1-LIA1	944.50 – 965.28	954.89	Double	INF, COM, PSR, PW, SW, DEF	29.12.2019 – 01.01.2020 (68 h)	Entirely within the Staffelegg Formation (incl. 0.2 m of Rietheim Member, 4.5 m of the Breitenmatt/Rickenbach Member, 0.8 m of Grünschholz Member, 12.2 m of Frick Member and 3.2 m of Beggingen Member); this part of the Staffelegg Formation consists mainly of sandy to silty claystone with some limestone intercalations.	T, h_s, FM

Tab. 4-19: continued

Test name[1]	**Interval depth** [m bgl]	**Interval midpoint** [m bgl]	**Packer configuration**	**Test phases**[1]	**Testing period** (duration)	**Lithology and structural geology features** (formation) [depth and length values rounded]	**Objectives**[2]
TRU1-1-KEU1	990.70 – 1'035.00	1'012.85	Single	INF1, COM1, PSR1, SW1, SW2, DEF1, INF2, COM2, RW1, RWS1, INF3, RW2, RWS2, DEF2	03.02. – 07.02.2020 (85 h)	44.3 m of Keuper including (from top to bottom) 36.5 m of Klettgau Formation and 7.8,m of Bänkerjoch Formation; the Klettgau section includes 13.3 m of Seebi Member (formerly «Stubensandstein», primarily a breccia, rauhwacke, dolostone and sandstone), 9.4 m Gruhalde Member (primarily an argillaceous marl with dolostone layers), 2.1 m of Gansingen Member (primarily an anhydrite) and 11.7 m of Ergolz Member (primarily a sandstone and argillaceous marl); the 7.8 m of Bänkerjoch Formation (formerly «Gipskeuper») consisting of an intercalation of claystone, dolostone and anhydrite	T, h_s, FM, WS
TRU1-1-MUK1	1'085.30 – 1'110.30	1'097.80	Double	INF, COM, PSR, SW, SWS, RW1, RWS1, RW2, RWS2, RW3, RWS3, DEF	22.02. – 25.02.2020 (70 h)	25.0 m of Schinznach Formation including (from top to bottom) 5.2 m of Asp Member (primarily a dolostone and bituminous shale) and 19.6 m of Stamberg Member (formerly «Trigonodus dolomite»), mainly a fractured dolostone	T, h_s, FM, WS

[1] For an explanation of the test names and test phases see Tabs. A-2 and A-3, respectively.
[2] FM = flow model, T = transmissivity, K = hydraulic conductivity, h_s = static formation head, WS = water sample
[3] Test re-named from OPA1 to BDO2 during final reporting.

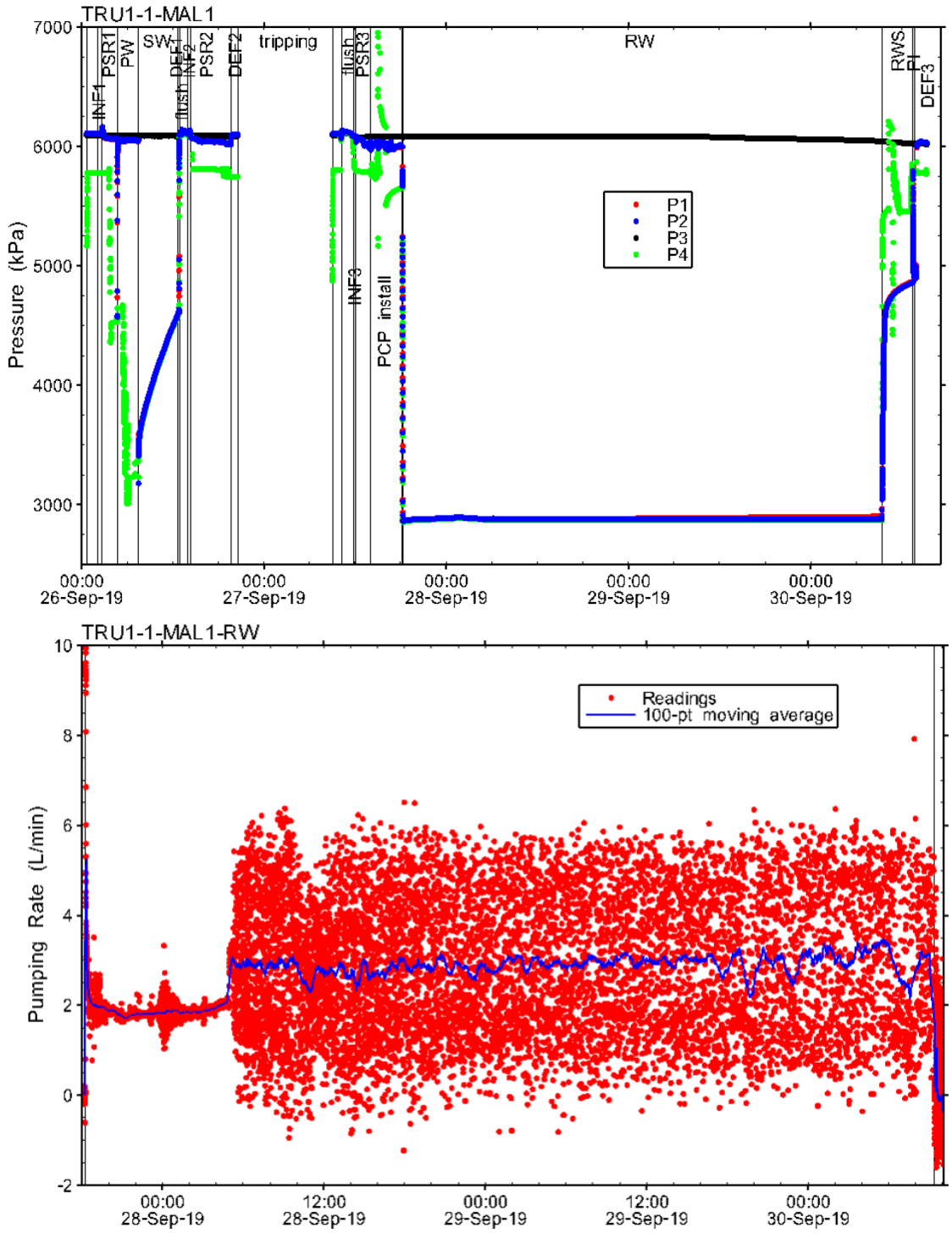

Fig. 4-7: Hydraulic packer test TRU1-1-MAL1: Overview plot of pressure vs. time (top) and pumping rate vs. time (bottom)

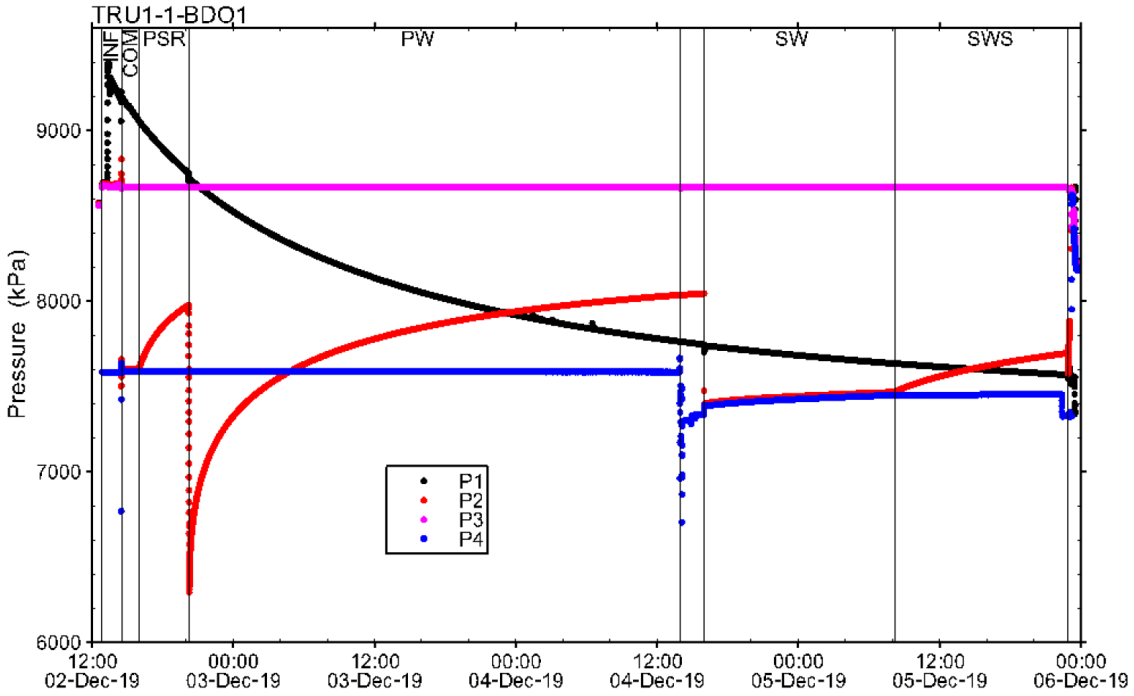

Fig. 4-8: Hydraulic packer test TRU1-1-BDO1: Overview plot of pressure vs. time

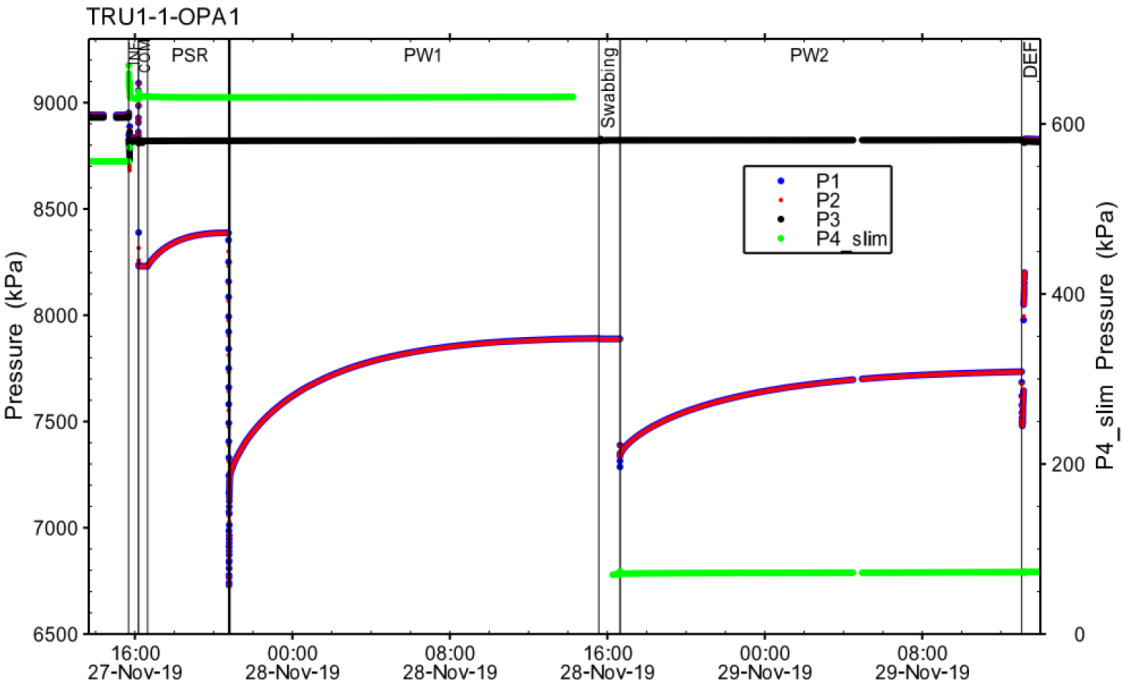

Fig. 4-9: Hydraulic packer test TRU1-1-BDO2: Overview plot of pressure vs. time

Test re-named from OPA1 to BDO2 during final reporting.

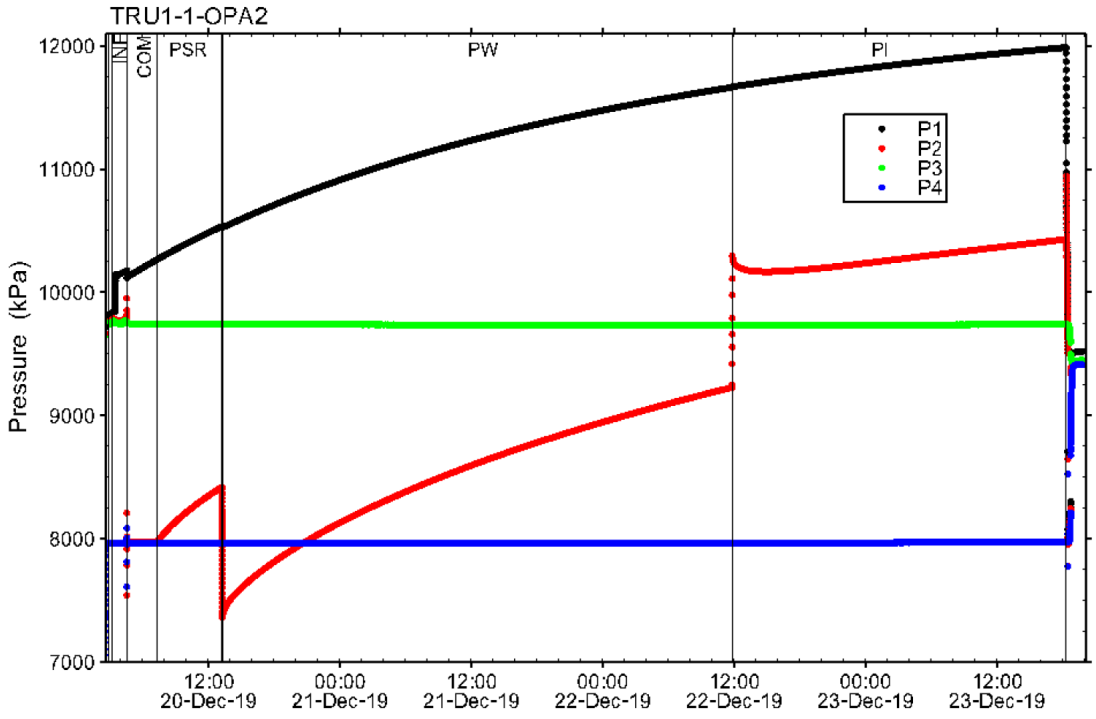

Fig. 4-10: Hydraulic packer test TRU1-1-OPA2: Overview plot of pressure vs. time

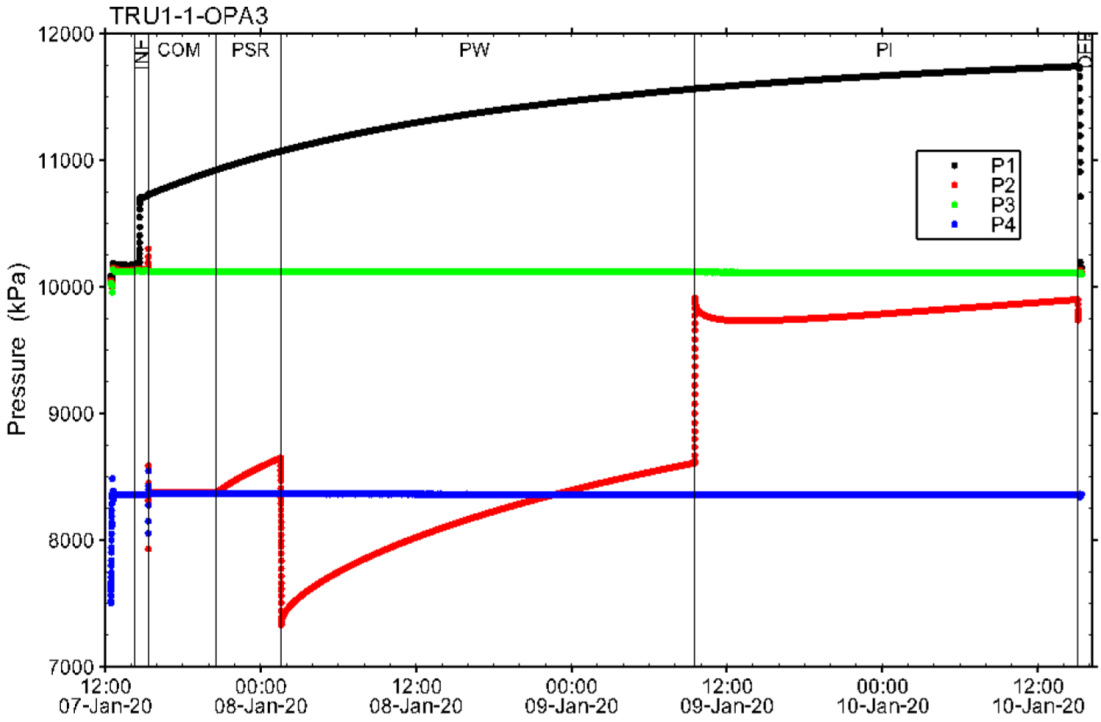

Fig. 4-11: Hydraulic packer test TRU1-1-OPA3: Overview plot of pressure vs. time

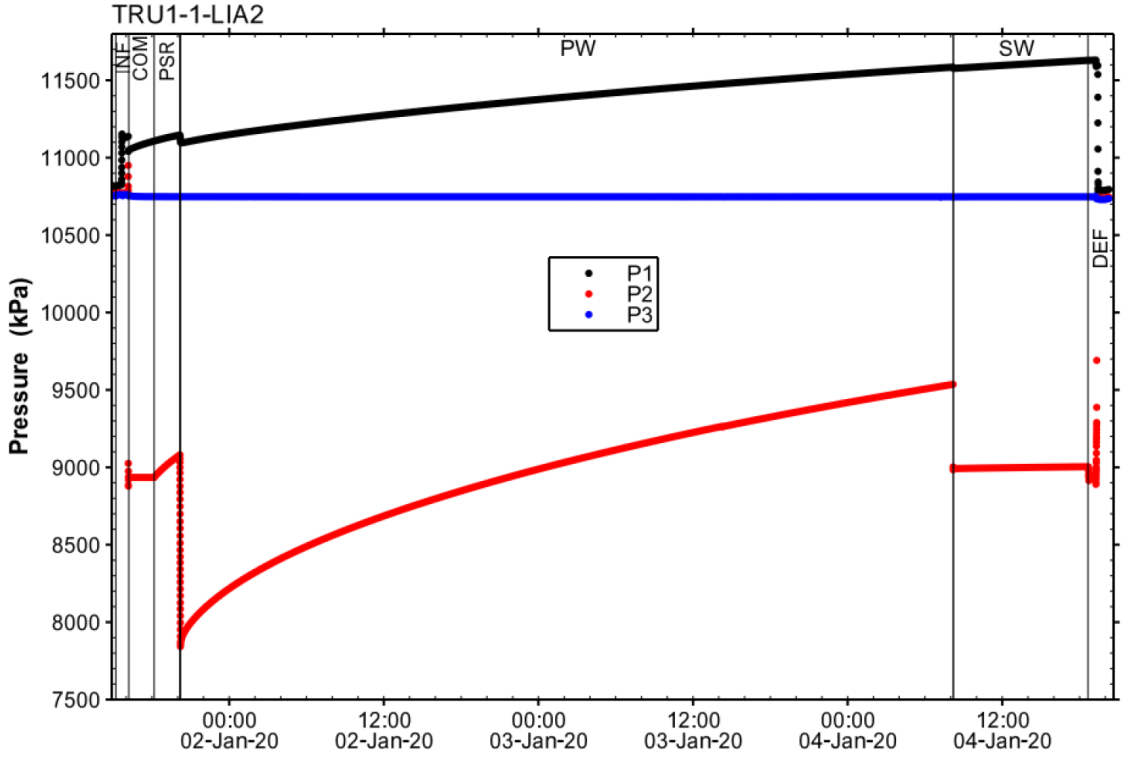

Fig. 4-12: Hydraulic packer test TRU1-1-LIA2: Overview plot of pressure vs. time

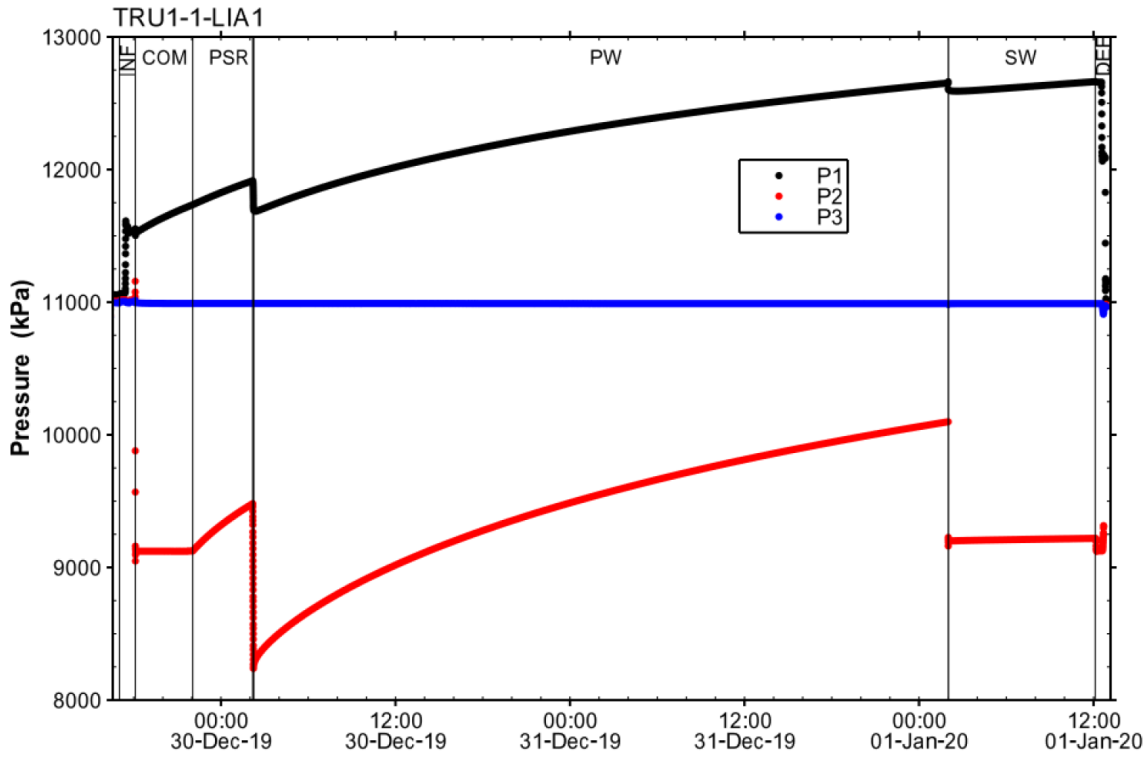

Fig. 4-13: Hydraulic packer test TRU1-1-LIA1: Overview plot of pressure vs. time

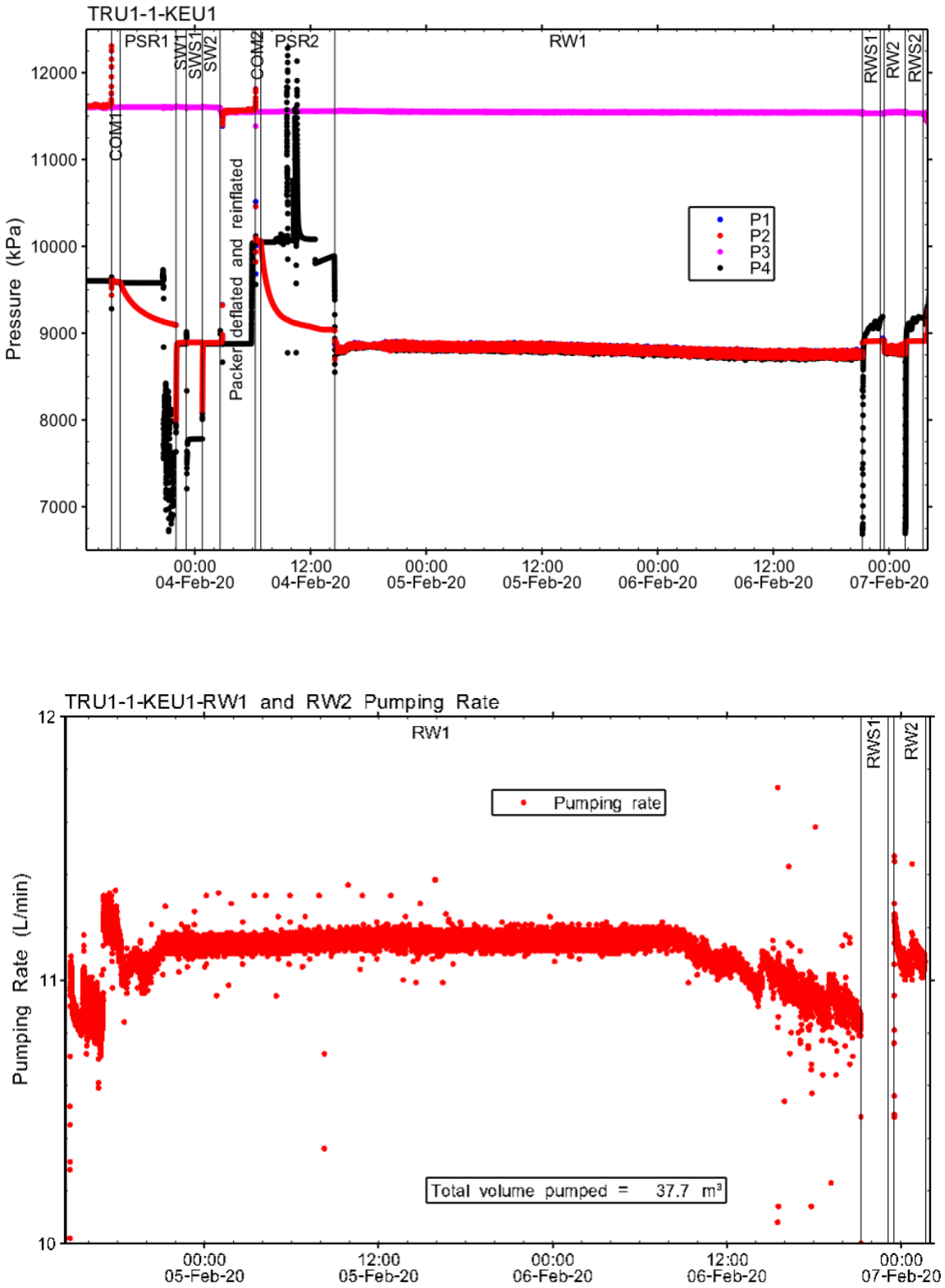

Fig. 4-14: Hydraulic packer test TRU1-1-KEU1: Overview plot of pressure vs. time (top) and pumping rate vs. time (bottom)

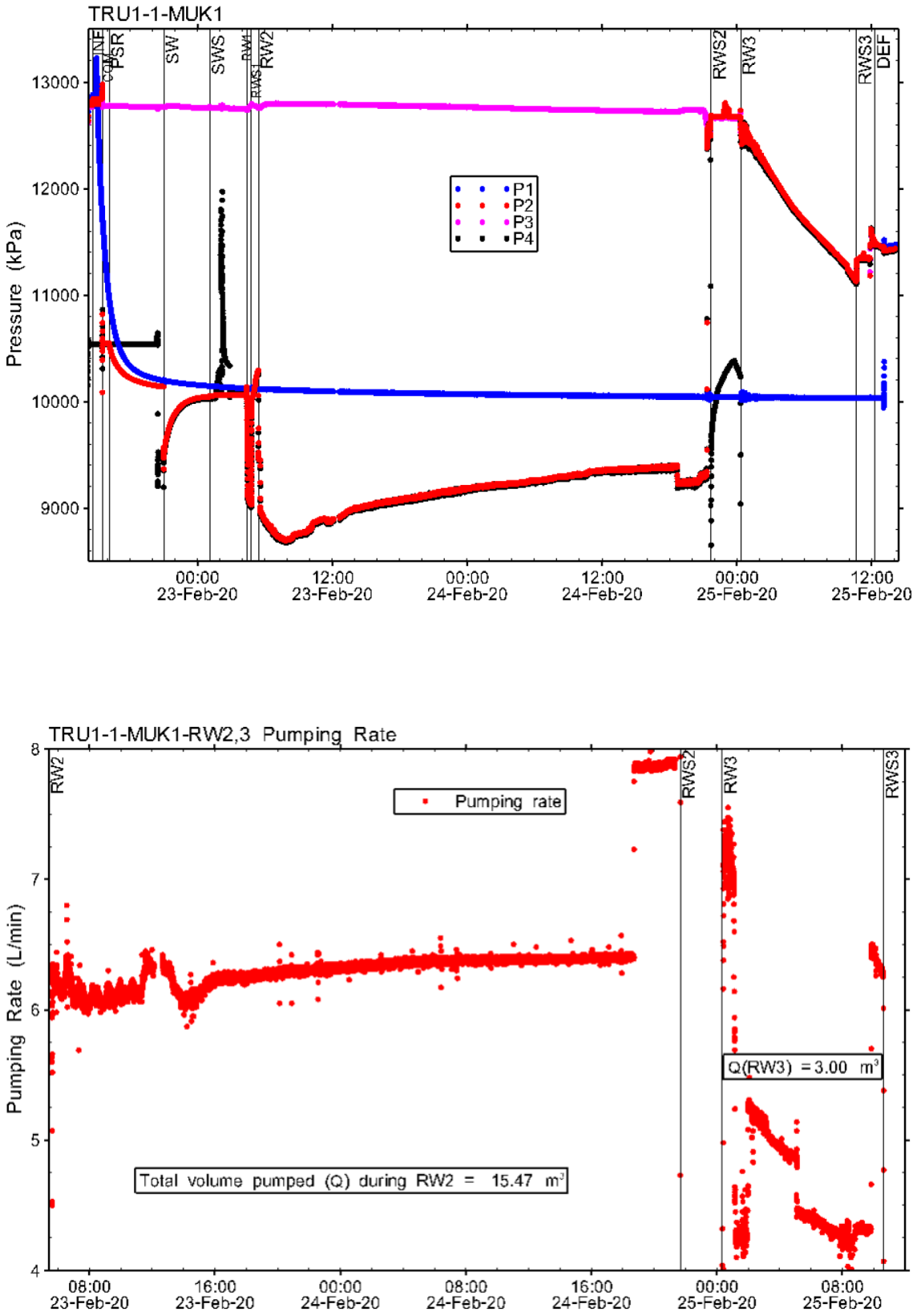

Fig. 4-15: Hydraulic packer test TRU1-1-MUK1: Overview plot of pressure vs. time (top) and pumping rate vs. time (bottom)

4.5 Details of selected tests

Two of the hydraulic packer tests are presented below in more detail: TRU1-1-OPA2 and TRU1-1-MUK1. TRU1-1-OPA2 was focused on the estimation of formation parameters of the Opalinus Clay under undisturbed conditions. TRU1-1-MUK1 was performed to characterise one of the bounding aquifers.

The selected examples reflect the wide range of hydraulic conditions in the borehole. They show the applied analysis strategy and the influence of different effects on, e.g. packer pressure changes due to surface temperature changes, interval temperature changes during testing and borehole pressure history. The results of the two test analyses are provided in the summary chapter (Chapter 5) together with the results of all other tests performed.

4.5.1 Hydraulic packer test TRU1-1-OPA2

The hydraulic packer test TRU1-1-OPA2 represents an example of testing in formations with low transmissivity.

4.5.1.1 Interval characterisation

The hydraulic test TRU1-1-OPA2 was performed in a double packer configuration. The entire interval is located in the Opalinus Clay. The test interval was selected because it is located in the undisturbed layer of the Opalinus Clay. The primary test objectives were to obtain reliable estimates of T (and K) for the formation, and the freshwater hydraulic head. Details of the interval and test duration are provided in Tab. 4-20.

Tab. 4-20: Hydraulic test TRU1-1-OPA2: Information on the test interval

Test	**Depth**		**Length**	**Packer confi-guration**	**Hydraulic testing**		
	from [m bgl]	to [m bgl]	[m]		Start date	End date	Duration [h]
TRU1-1-OPA2	829.00	854.00	25.00	DP [1]	20.12.2019	23.12.2019	87.2

[1] DP: Double packer

4.5.1.2 Test execution

Fig. 4-16 provides the system installation record as provided by the field test contractor. The equipment components are those described above.

The HDDP was lowered to the test interval position with regular checks every 10 tubing joints so that the tubing could be filled with traced freshwater (1.5-naphthalene disulfonate) and a communications check between the gauges and the DAS could be performed. The test was started by inflating the bottom packer (test phase INF part 1) followed by the top packer (INF part 2) using a 2:1 mixture of anti-freeze:water. The 250-mL piston in the PPG housing was extended after the lower packer had been inflated so that a pulse-withdrawal test could be performed later. The SIT was opened when the top packer began to isolate the interval volume. The COM phase lasted 2.8 h before the SIT was again closed to initiate the PSR phase. The PSR phase lasted 5.9 h. After the PSR phase, a pulse withdrawal (PW) was initiated by retracting the 250-mL piston that had previously been extended. The PW phase lasted for 46.54 h. Next, the piston was extended to initiate a pulse injection (PI) phase of a duration of 30.5 h. The P2 pressure decreased during the first 3 hrs of the test phase and then rolled over and increased for the rest of the duration of the 30.5 h PI phase. At the conclusion of the PI phase, the packers were deflated and the HDDP was removed from the borehole with SIT closed.

The surface equipment included the packer pressure control unit, which automatically stabilised the packer pressures over the whole test duration.

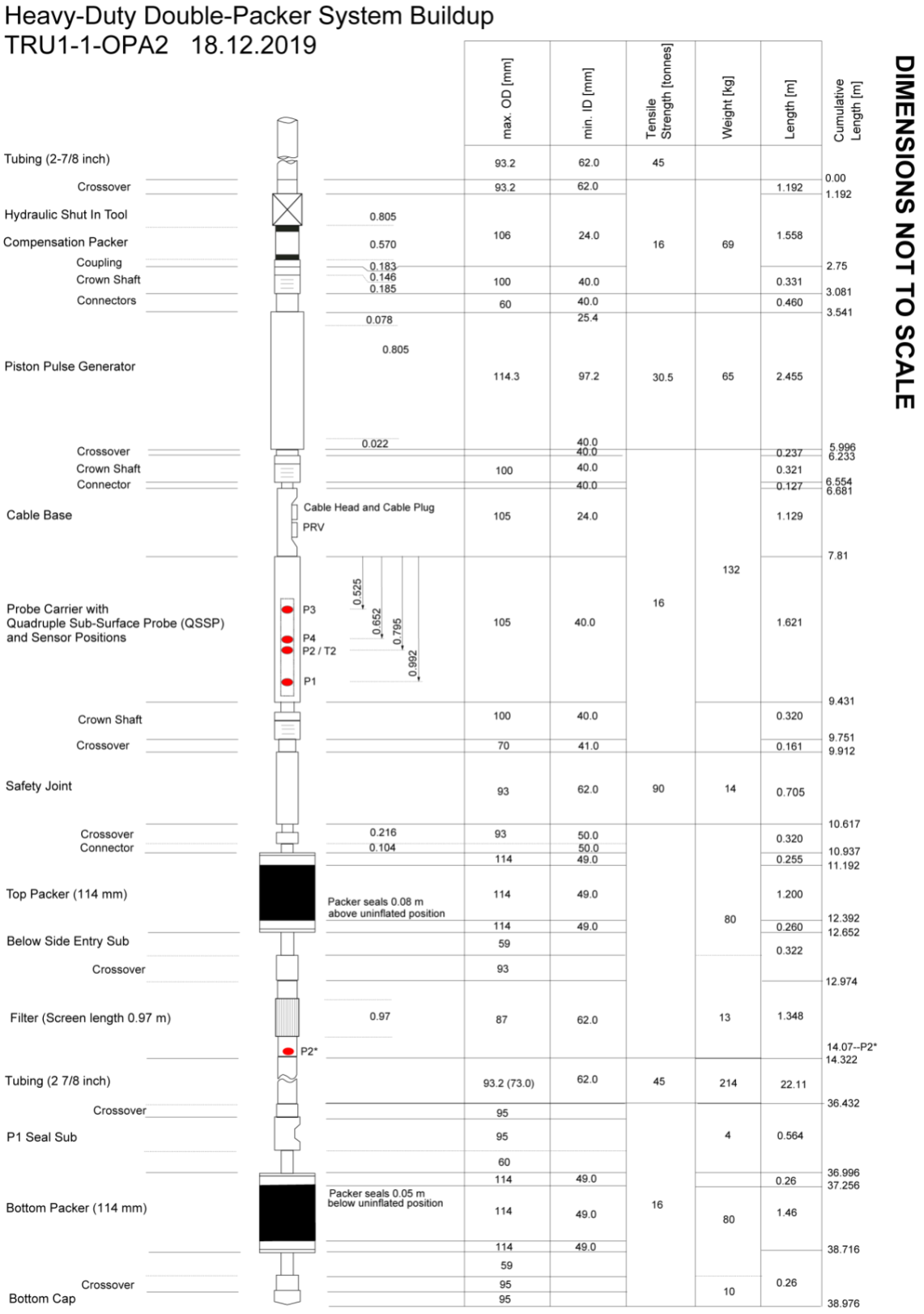

Fig. 4-16: Hydraulic test TRU1-1-OPA2: Downhole equipment installation record with system layout as used in the field tests

4.5.1.3 Analysis

Borehole pressure history

The borehole history used for the analysis of the TRU1-1-OPA2 tests is shown in Fig. B-1 and summarised in Tab. 4-21. The history after the midpoint of the test interval had been cored was developed by first extrapolating the mud circulation pressures measured by GEO-data (see Dossier I), using a pressure gauge mounted 1.6 m above the rig floor, to the depth of the P2 transducer using the reported mud density of 1'200 kg/m^3. For periods with no active mud circulation, the drillers generally kept the borehole full up to the level of the flow line 3.5 m above ground. The resulting pressure was calculated using the reported mud density. Once the HDDP was at test depth and data acquisition began, the P2 gauge measured pressure directly.

Tab. 4-21: Hydraulic test TRU1-1-OPA2: Borehole pressure history

Description	**Start date and time**	**Duration** [h]	**Pressure**[1] [kPa]	
			Start	**End**
Drilling[2]	09.12.2019, 21:51	229.7	12'582	9'757
Preparation[3]	19.12.2019, 11:30	15.7	9'757	9'757
Start TRU1-1-OPA2	20.12.2019, 03:11	-	9'784	-

[1] Interval pressure at P2 sensor level (825.30 m bgl)
[2] Drilling through interval midpoint (841.5 m bgl)
[3] Includes POOH wireline coring system string, preparation and installation of hydraulic testing equipment

Flow model evaluation

All test phases were analysed using a radial homogeneous flow model that included a skin zone around the borehole. The PW was analysed using a discrete numerical description of the inner / skin zone adapting only the inner zone hydraulic conductivity (nSIGHTS: 2-zone radial-composite model) in which the hydraulic conductivity of the inner/skin zone transitions logarithmically to the formation hydraulic conductivity with distance from the borehole wall, while the PI was analysed using a radial homogeneous model with a discrete numerical description of the inner / skin zone whereby all hydraulic parameters of this zone can be defined separately (nSIGHTS: homogeneous model with skin).

Analysis of the pulse withdrawal (PW)

The analysis of the PW was based on an initial fitting followed by a perturbation analysis of 2'000 optimisations. A 2-zone radial-composite model was used matching the measured pressure of P2 in a Cartesian format while optimising the hydraulic conductivity of the formation and the skin zone (K, K_s), the static formation pressure (P_s), the specific storage (S_s), used for both zones, and the thickness of the inner / skin zone (t_s). Fig. B-2 shows all 2'000 optimisation results plotted with the simulated pressure data in a Cartesian horsetail plot.

707 perturbation optimisations were selected as representative by normalised fit values lower than or equal to 6, matching a correct range for the hydraulic conductivity of the inner / skin zone and formation as well as showing a coherent structure of the normalised fit values. Figs. B-3 and B-4 show Ramey A and B horsetail plots, respectively, of the PW data and these 707 optimisation results. The ranges and best-fit values for the fitting parameters obtained from the perturbations that satisfied the filters are given in Tab. 4-22. The corresponding mappings of the parameter space according to the formation parameter are presented in Fig. B-5 to B-7.

Tab. 4-22: Hydraulic test TRU1-1-OPA2: Perturbation results applied for the analysis of PW

PW results	**K** [m/s]			**S_S** [1/m]			**P_f** [kPa]		
Perturbation result	2.2×10^{-14}			3.0×10^{-6}			12'949		
Uncertainty ranges	1×10^{-14}	-	5×10^{-14}	5×10^{-7}	-	8×10^{-6}	11'800	-	13'920

All formation parameters are clearly correlated. A negative correlation exists between the static formation pressure and the hydraulic conductivity of the formation as well as between the specific storage and the hydraulic conductivity of the formation. A positive correlation exists between the static formation pressure and the specific storage of the formation. All three correlations are presented in Figs. B-8 to B-10.

The residuals (difference between the recorded data and simulated values) from the PW are plotted against time in Fig. B-11. For the majority of the test, they are less than 1 kPa, reflecting a good quality of the fit. The quantile-normal plot of the residuals (Fig. B-12) shows a reasonably normal distribution for the smallest residuals and deviations from normal for the beginning of the test. The observed normal distribution of residuals supports the choice of the flow model used to simulate the PW phase.

Analysis of the pulse injection (PI)

Like the analysis of PW, the PI analysis was based on an initial fitting followed by a perturbation analysis of 500 optimisations. The data were fitted, using a homogeneous model with an inner / skin zone in which the hydraulic conductivity (K_s) was allowed to be different for the fall-off and pressure-rise periods of the PI, by matching in a Cartesian format, optimising on hydraulic conductivity of the formation (K), the period of decreasing pressure (K_{s1}) and separate the period of rising pressure (K_{s2}), the static formation pressure (P_s), the specific storage of the inner/skin zone (S_{ss}), and the thickness of the inner/skin zone (t_s). The specific storage of the formation (S_s) was fixed to the theoretical value of 2×10^{-6} 1/m. Fig. B-13 shows all 500 simulations plotted with the data in a Cartesian horsetail plot.

A threshold value (fit discriminant) of 1.75 was defined, which allowed to differentiate between optimisation results that were ‘acceptable’ and those which should be rejected. This resulted in 118 of the simulations being accepted as reasonable fits of the data, which represent the isolated global minimum. Figs. B-14 and B-15 show Ramey A and B horsetail plots, respectively, of the PI data and these 118 optimisation results. The ranges and best-fit values for the fitting parameters obtained from the perturbations are given in Tab. 4-23. The corresponding mappings of the parameter space according to the formation parameter are presented in Figs. B-16 and B-17.

Tab. 4-23: Hydraulic test TRU1-1-OPA2: Perturbation results applied for the analysis of PI

PI results	**K** [m/s]			**Ss** [1] [1/m]			**Pf** [kPa]		
Perturbation result	5.2×10^{-14}			2.0×10^{-6}			11'929		
Uncertainty ranges	3×10^{-14}	-	6×10^{-14}	-	-	-	11'870	-	12'240

[1] Fixed to the theoretical value.

As expected, a negative correlation exists between the static formation pressure and the hydraulic conductivity of the formation (Fig. B-18).

The residuals (difference between the recorded data and simulated values) from the PW are plotted against time in Fig. B-19. The residuals are greatest during the fall-off period. For the majority of the test, they are less than 0.5 kPa, reflecting a good fit. The quantile-normal plot of the residuals (Fig. B-20) shows a reasonably normal distribution for the smallest residuals and deviations from normal for the higher magnitude residuals at the beginning of the test. These plots suggest that the selected model provides a better representation of the late-time formation response when the pressure was rising than it does of the early-time period when pressure was decreasing. Most probably, this relates to some difference in skin properties between injecting fluid (drilling mud filtrate) into the formation during the early portion of the PI and withdrawing fluid from the formation during the latter part of the PI.

Overall confirmation simulation (PW-PI)

Finally, a perturbation of 1'000 parameter optimisations over the testing period was performed for the hydraulic conductivity of the formation (K) and the inner/skin zone during the PW (K_{s1}), during the fall-off period of the PI (K_{s2}), during the pressure-rise period of the PI (K_{s3}), the static formation pressure (P_s), the specific storage of the inner/skin zone (S_{ss}), and inner/skin zone thickness (t_s). The specific storage of the formation (S_s) was fixed at the theoretical value of 2×10^{-6} 1/m. The simulations of all 1'000 optimisation results were plotted with the data in a Cartesian horsetail plot of the PW (Fig. B-21) and PI phase (Fig. B-22).

A threshold value of 2.5 was defined, which allowed to differentiate between optimisation results that were ‘acceptable’ and those that should be rejected, and to isolate the global minimum that resulted in 599 of the simulations being accepted as reasonable fits of the recorded data. Figs. B-23 and B-24 show Ramey A and B horsetail plots, respectively, of the PW and PI data and these 599 optimisation results. The ranges and best-fit values for the fitting parameters obtained from the perturbations are given in Tab. 4-24. The corresponding mappings of the parameter space according to the formation parameter are presented in Figs. B-25 and B-26.

Tab. 4-24: Hydraulic test TRU1-1-OPA2: Perturbation results applied for the analysis of the sequence PW-PI

PW-PI results	**K** [m/s]			**Ss** [1] [1/m]			**Pf** [kPa]		
Perturbation result	2.8×10^{-14}			2.0×10^{-6}			12'679		
Uncertainty ranges	1×10^{-14}	-	3×10^{-14}	-	-	-	12'470	-	13'550

[1] Fixed to the theoretical value.

As expected, a negative correlation exists between the static formation pressure and the hydraulic conductivity of the formation (Fig. B-27).

A Jacobian plot showing parameter sensitivity in the best-fit simulation as a function of time during the PW and PI is presented in Fig. B-28. Sensitivity to the formation parameters steadily increased through the phases.

The residuals from the PW and PI are plotted against time in Fig. B-29. The residuals are greatest at the beginning of the tests when skin effects were most important, but the compromises made by optimising on both phases simultaneously prevented the model from matching the curvature of the pulse recovery responses in the same quality as for the individual phases. The quantile-normal plots of the residuals for the PW and PI (Fig. B-30) show the same behaviour. The failure of the model to produce a simulation with normally distributed residuals for both test phases indicates that some parameter(s) are different between the PW and the PI. Most probably, this relates to some difference in the skin between injecting fluid (drilling mud filtrate) into the formation during the early portion of the PI and withdrawing fluid from the formation during the PW and later part of the PI. However, the formation parameters range in the same limits.

4.5.2 Hydraulic packer test TRU1-1-MUK1

The hydraulic packer test TRU1-1-MUK1 is an example for testing in formations with medium to high transmissivity.

4.5.2.1 Interval characterisation

The test TRU1-1MUK1 was performed in a double packer configuration. The 25.0 m test interval contained 0.9 m of the Bänkerjoch Formation and 24.1 m of the Schinznach Formation. The Bänkerjoch Formation consists of gypsum and other sulphatic facies. The Schinznach interval included (from top to bottom) 4.5 m of the Asp Member (primarily dolomite and marl) and 19.6 m of the Stamberg Member (vuggy bivalve and gastropod-rich dolomite). The primary test objectives were to obtain representative water samples from the Schinznach Formation and estimates of the transmissivity (and K) for the Schinznach Formation, and the freshwater hydraulic head of the test interval. A secondary objective was to define an appropriate flow model for the hydraulic conditions surrounding the test interval. Details are provided in Tab. 4-25.

Tab. 4-25: Hydraulic test TRU1-1-MUK1: Information on the test interval

Test	**Depth**		**Length**	**Packer configuration**	**Hydraulic testing**		
	from [m bgl]	to [m bgl]	[m]		Start date	End date	Duration [h]
TRU1-1-MUK1	1'025.30	1'110.30	25.00	DP[1]	22.02.2020	25.02.2020	69.6

[1] DP: Double packer

4.5.2.2 Test execution

Fig. 4-17 provides the system installation record as provided by the field test contractor. The equipment components are those described above.

The HDDP was lowered to the test interval position with regular checks every 10 tubing joints so that the tubing could be filled with traced freshwater (naphthionate) and a communications check between the gauges and the DAS could be performed. The test was started by inflating the bottom packer (test phase INF part 1) followed by the top packer (INF part 2) using a 2:1 mixture of anti-freeze:water. The SIT was opened to begin the COM phase just as the top packer started to squeeze the fluid in the test interval. The COM phase lasted 34 minutes during which the P2 pressure did not change. The SIT was then closed to initiate the PSR phase. The PSR phase lasted 4.85 h. Late in the PSR phase, the test tubing was swabbed to lower the pressure in the tubing (P4) below the pressure in the test interval (P2), so that a slug withdrawal (SW) test could be initiated by opening the SIT. The SW was terminated after 4.1 h by closing the SIT. The installation of the rotor and sucker rods for the PCP did not affect the test-interval pressure. The SWS phase was stopped after 3.3 h. When pumping first began (RW1), no water was observed at the surface after 23 minutes even though the downhole transducer clearly showed drawdown. The pump was turned off for a system check (RWS1), during which the flow lines from the wellhead to the flowmeter were filled with water to speed detection of flow when pumping resumed (RW2). Flow was observed almost immediately after pumping resumed. Pumping continued at an approximate rate of 6.2 to 6.4 l/min for 37.3 h, during which the test-interval pressure, after an immediate decline, showed a slow but steady increase. At 21:20 on 24.02.2020, isolation of the test interval was lost because a leak developed in the top packer. The pump was turned off (RWS2) 20 minutes after isolation was lost, but was turned back on (RW3) after 2 h and 40 minutes to pump out the 3 m^3 of formation water that had already entered the test tubing and was still suitable for sampling.

The surface equipment included a hydrochemistry cabinet and the packer pressure control unit, which automatically stabilised the packer pressures over the whole test duration. Once the tubing and approximately five test-interval volumes had been evacuated, a portion of the pump discharge was channelled through the hydrochemistry cabinet. Electrical conductivity (EC) and pH dropped for the duration of pumping, nearing stabilised values by the end of RW2. Eh displayed rather erratic behaviour, while dissolved oxygen quickly dropped to zero. The density of the discharge was measured at 1'004 kg/m^3 near the end of the RW2 phase.

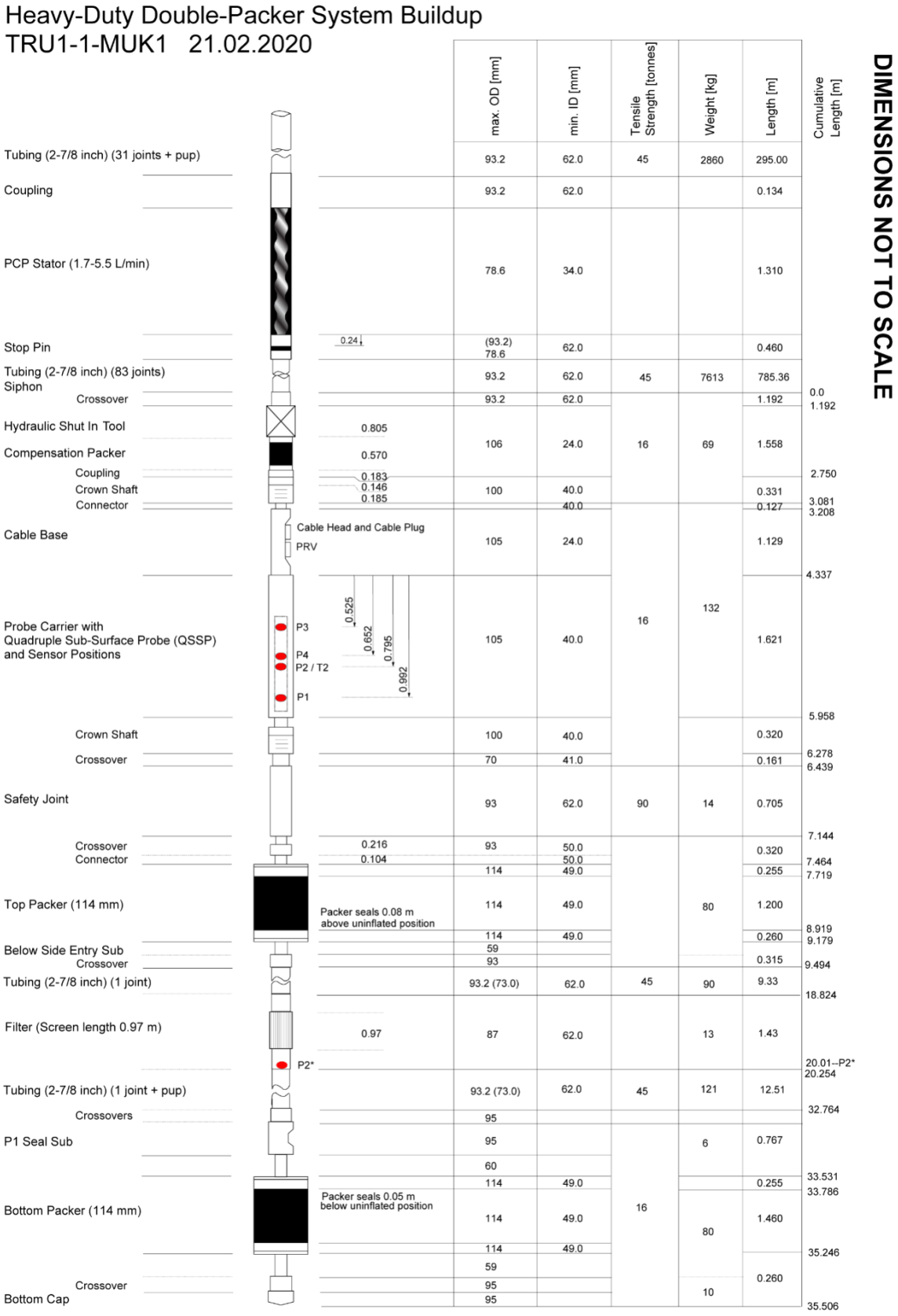

Fig. 4-17: Hydraulic test TRU1-1-MUK1: Downhole equipment installation record with system layout as used in the field tests

4.5.2.3 Analysis

Borehole pressure history

The borehole history used for the analysis of the TRU1-1-MUK1 tests is shown in Fig. B-31 and summarised in Tab. 4-26. The history, after the midpoint of the test interval had been cored, was developed by first extrapolating the mud circulation pressures measured by GEO-data (see Dossier I; including the coring and the check-tip before testing), using a pressure gauge mounted 1.6 m above the rig floor, to the depth of the P2 transducer using the reported mud density of 1'200 kg/m^3. For periods with no active mud circulation, the drillers generally kept the borehole full up to the level of the flow line 3.5 m above ground. The resulting pressure was calculated using the reported mud density. Once the HDDP was at test depth and data acquisition began, the P2 gauge measured pressure directly.

Tab. 4-26: Hydraulic test TRU1-1-MUK1: Borehole pressure history

Description	**Start date and time**	**Duration** [h]	**Pressure**[1] [kPa]	
			Start	**End**
Drilling[2]	14.02.2020, 23:04	165.2	18'832	12'771
Preparation[3]	21.02.2020, 20:18	18.4	12'773	12'773
Start TRU1-1-OPA2	22.02.2020, 14:39	-	12'784	-

[1] Interval pressure at P2 sensor level (1'081.6 m bgl)
[2] Drilling through interval midpoint (1'097.8 m bgl)
[3] Includes POOH wireline coring system string, preparation and installation of hydraulic testing equipment

Flow model evaluation

The Ramey (Ramey et al. 1975) A and B plots and log-log plots for pressure change and the derivative of pressure change developed by Bourdet et al. (1989) for constant-rate pumping tests, and variable-rate tests with the appropriate time superposition function, were used for the identification of the flow model.

The early-time derivative data of the Ramey B plot of SW (Fig. B-32) do not suggest the presence of a negative skin. However, both the normalised pressure and derivative data show anomalous inflections during the test. The log-log diagnostic plot for the SWS phase (Fig. B-33) was generated with the assumption of a constant flow rate during the preceding SW phase, which was calculated from the SW pressure data. If the SWS had followed an ideal constant-rate flow period, the slight upward trends in both the pressure change and derivative data at late time of the SWS would suggest a system in which K is decreasing slightly with radial distance from the borehole.

All analyses were performed using a simple radial homogeneous flow model. Additional elements were added to the model as found necessary to achieve an acceptable fit. For the independent SW analysis, a radial homogeneous model without an inner/skin zone was adequate to match the collected data. For the independent SWS analysis and for the joint SW-SWS analysis, a radial homogeneous model with a discrete inner/skin zone was used.

Analysis of the slug withdrawal (SW)

The analysis of the SW was based on an initial fitting using a radial homogeneous flow model followed by a perturbation analysis of 2'000 optimisations. The early time data showed inertia-related oscillations followed by anomalous concave-upward rather than concave-downward curvature, therefore, these data were treated as a prescribed pressure phase. Figs. B-34 and B-35 present the horsetail plot of all optimisation results as Ramey A respectively the Ramey B of the slug phase. The ranges and best-fit values for the fitting parameters obtained from the perturbations are given in Tab. 4-27. They satisfied a normalised fit value of 1.6 (1'992 results). Fig. B-36 shows a Cartesian horsetail plot of all selected optimisation results. The corresponding mappings of the parameter space according to the formation parameter are presented in Figs. B-37 to B-39.

Tab. 4-27: Hydraulic test TRU1-1-MUK1: Perturbation results applied for the analysis of SW

SW results	**K** [m/s]			**S_S** [1/m]			**P_f** [kPa]		
Perturbation result	4.6×10^{-8}			1.8×10^{-8}			10'064		
Uncertainty ranges	4×10^{-8}	-	5×10^{-8}	1×10^{-8}	-	8×10^{-8}	10'063	-	10'066

All formation parameters are clearly correlated. A negative correlation exists between the static formation pressure and the hydraulic conductivity of the formation as well as between the specific storage and the hydraulic conductivity of the formation. A positive correlation exists between the static formation pressure and the specific storage of the formation. All three correlations are presented in Figs. B-40 to B-42.

A Jacobian plot showing normalised parameter sensitivity in the best-fit Cartesian simulation as a function of time during the SW is presented in Fig. B-43. The hydraulic conductivity and specific storage of the formation reached their maximum sensitivity during the first hour of the test. The sensitivity to the static formation pressure levelled out at the end of the test.

The residuals (difference between the recorded data and simulated values) from the SW are plotted against time in Fig. B-44. The residuals range from -3 to +4 kPa reflecting good agreement between the data and simulation. Early oscillations in the residuals reflect an anomalous inflection in the data. However, the quantile-normal plot of the residuals (Fig. B-45) shows a reasonably normal, although somewhat oscillatory, distribution for most of the residuals except for the tails of the distribution and supports the choice of a radial homogeneous flow model.

Analysis of the slug withdrawal recovery (SWS)

A simulation of the slug recovery phase (SWS) using the best-fit parameter values from the slug phase (SW analysis) does not accurately capture the slope of the pressure recovery. It predicts more rapid recovery (Fig. B-46).

The analysis of the SWS was based on an initial fitting using a radial homogeneous flow model with a discrete skin zone considering a smoothed temperature measured by the memory gauge inside the interval. The hydraulic conductivity of the formation and the inner/skin zone, the static formation pressure, the extension of the inner/skin zone and the specific storage (one for the whole model) were optimised followed by a perturbation analysis of 500 optimisations. A threshold value of 1.005 (fit discriminant) was defined for the normalised fit value that resulted in 350 of optimisation results being accepted as providing reasonable fits to the measurement of the SWS phase. Fig. B-47 shows a Cartesian horsetail plot of the reliable optimisation results.

Fig. B-48 shows a log – log horsetail plot and Fig. B-49 a Horner horsetail plot of reliable optimisation results and the measurement during the slug recovery phase (SWS). The ranges and best-fit values for the fitting parameters obtained from the perturbations are given in Tab. 4-28, the hydraulic conductivity of the inner / skin zone ranges from 1×10^{-11} to 1×10^{-8} (best value: 4.4×10^{-9}) with a corresponding extension of the inner / skin zone between 0.015 m and 17.5 m (best value: 2.07 m). The corresponding mappings of the parameter space according to the formation parameter are presented in Figs. B-50 to B-52.

Tab. 4-28: Hydraulic test TRU1-1-MUK1: Perturbation results applied for the analysis of SWS

SWS results	**K** [m/s]			**S_S** [1/m]			**P_f** [kPa]		
Perturbation result	4.4×10^{-8}			2.6×10^{-8}			10'063		
Uncertainty ranges	3×10^{-8}	-	5×10^{-8}	1×10^{-8}	-	2×10^{-5}	10'063	-	10'063

Combined SW-SWS analysis

The simulation of the TRU1-1-MUK1 SW-SWS test sequence using the best-fit parameter values from the SWS analysis, shows a significant underestimation of the pressure recovery during the slug phase (SW). However, the formation parameters estimated from the independent SW and SWS analyses are very similar (*cf.* Tabs. 4-27 and 4-28). It is probably the positive skin added for the SWS that causes the SW recovery to be underestimated.

In addition to the analyses of the individual SW and SWS test phases, a combined or joint SW-SWS analysis was performed fitting to both phases with a single set of parameters. A radial homogeneous flow model with a discrete inner/skin zone was used for the simulations, using the Cartesian data, SW Ramey A normalised pressure and derivative, and SWS log-log pressure-change data as constraints and optimising on the hydraulic conductivity of the formation and the inner / skin zone, static formation pressure, unique specific storage of the formation and inner / skin zone, and the extension of the inner / skin zone. Temperature compensation was applied during the SWS phase. 500 perturbation optimisations were performed. 362 of these were selected as reasonable by a threshold value of 1.00049 (fit discriminant) defined to eliminate the outliers of the estimated hydraulic conductivity of the formation. Fig. B-53 shows these 362 simulations plotted with the measured data in a Cartesian horsetail plot of the SW-SWS testing sequence. The ranges and best-fit values for the fitting parameters obtained from the perturbations are given in Tab. 4-29, the hydraulic conductivity of the inner / skin zone ranges from 2×10^{-11} to 1×10^{-8} (best value: 2.9×10^{-10}) with a corresponding extension of the inner/skin zone between 0.010 m and 13.9 m (best value: 0.16 m). The corresponding mappings of the parameter space according to the formation parameter are presented in Figs. B-54 to B-56.

Tab. 4-29: Hydraulic test TRU1-1-MUK1: Perturbation results applied for the analysis of SW-SWS

SW-SWS results	**K** [m/s]			**S_S** [1/m]			**P_f** [kPa]		
Perturbation result	4.6×10^{-8}			9.0×10^{-6}			10'064		
Uncertainty ranges	4.6×10^{-8}	-	4.6×10^{-8}	1×10^{-7}	-	2×10^{-5}	10'064	-	10'064

The correlations are presented in Figs. B-57 to B-59 for the formation parameters. A negative correlation exists between the specific storage and the hydraulic conductivity of the formation as well as between the static formation pressure and the hydraulic conductivity of the formation. A positive correlation exists between the static formation pressure and the specific storage of the formation.

A Jacobian plot showing normalised parameter sensitivity in the best-fit Cartesian simulation as a function of time is presented in Fig. B-60. The hydraulic conductivity of the formation (K) and inner/skin zone (K_s), the unique specific storage value (S_s) and extension of the inner/skin zone (t_s) had reached their maximum sensitivity during the slug phase (SW), and had low sensitivity during the slug recovery phase (SWS), reflecting the relatively low weight given to the SWS during the parameter optimisation. Sensitivity to static formation pressure (P_s) was still increasing slightly through the SWS.

The Cartesian residuals (difference between the data and simulated values) from SW and SWS are plotted against time in Fig. B-61. The SW residuals range from -3 to +4 kPa, reflecting good agreement between the recorded data and simulation. Early oscillations in the residuals reflect an anomalous inflection in the data. Fig. B-61 is virtually identical to Fig. B-44, indicating that the joint SW-SWS optimisation focused on the SW data and produced results almost identical to those from the individual SW analysis. The SWS residuals transition from positive to negative as the simulation, which did not match the slope of the data, crosses the data. However, the quantile-normal plot of the SW and SWS Cartesian residuals presented in Fig. B-62 shows that the residuals oscillate around a normal distribution and support the choice of the flow model.

Uncertainty analysis considering RW2

In order to evaluate the uncertainty in the results, the longest production phase (RW2) was analysed by a single optimisation. A radial homogeneous flow model was used with a time dependent inner/skin zone and a prescribed rate measured during RW2. Thirteen transition times for skin changes were identified. The hydraulic conductivity of the inner/skin zone increased from 3.3×10^{-11} m/s to 3.1×10^{-10} m/s over the duration of the RW2. These changes apply to only the very small optimised skin thickness of 0.045 cm. In terms of skin factor, skin decreased from 11.6 to 1.22 during this production phase, reflecting removal of the drilling mud from the formation. Tab. 4-30 summarises the formation parameters that are similar to the values from the analysis of the SW and SWS test phases. Fig. B-63 shows the simulated pressure during RW2 in relation to the changing hydraulic conductivity of the inner/skin zone (K_s).

Tab. 4-30: Hydraulic test TRU1-1-MUK1: Results of the single optimisation of RW2

RW2 results	**K** [m/s]	**S_S** [1/m]	**P_f** [kPa]
Perturbation result	7.0×10^{-8}	5.2×10^{-6}	10'096

5 Summary and discussion

5.1 Flowmeter logging and fluid logging

A quantitative analysis of the fluid logging measurements (TRU1-1-FL1-MAL) with regard to the hydraulic transmissivity of the inflow zones was not carried out because of the technical issues. Two inflow zones were detected qualitatively at depths of 531.31 – 535.21 m MD and 590.41 – 594.21 m MD.

5.2 Hydraulic packer test data and results

5.2.1 Description of tests

Nine hydraulic packer test sequences were performed within nine test intervals in the borehole TRU1-1 between September 2019 and February 2020. All tests were performed in the cored borehole section using an HDDP packer system in single packer or double packer configuration (*cf.* Tab. 4-19).

- One hydraulic packer test investigated the partially fractured and porous limestones of the Malm Group («Felsenkalke» + «Massenkalk»): TRU1-1-MAL1.
- One hydraulic packer test was targeted at the Dogger Group («Humphriesioolith Formation» to Wedelsandstein Formation): TRU1-1-BDO1.
- One hydraulic packer test focused on the transition from Wedelsandstein Formation and «Murchisonae-Oolith Formation» to Opalinus Clay: TRU1-1-BDO2.
- Two hydraulic packer tests were seated in the Opalinus Clay; one in typical Opalinus Clay (TRU1-1-OPA2) and one in Opalinus Clay with fractures of unknown hydraulic significance from 870.6 to 870.7 m bgl and from 878.0 to 882.5 m bgl (TRU1-1-OPA3).
- Two hydraulic packer tests focused on the Lias Group: TRU1-1-LIA1 was located entirely within the Staffelegg Formation, whereas TRU1-1-LIA2 also included 4.2 m of Opalinus Clay.
- One hydraulic packer test was performed in the heterogeneous sequence of mainly sandstone, argillaceous marl, claystone and anhydrite of the Keuper Group (Klettgau Formation and Bänkerjoch Formation): TRU1-1-KEU1.
- The final hydraulic packer test investigated the fractured section of the Muschelkalk Group (Schinznach Formation): TRU1-1-MUK1.

5.2.2 Overview tables and plots

The results of the transmissivity and hydraulic conductivity estimations for all tested intervals are summarised in Tab. 5-1. The estimated freshwater hydraulic heads and static formation pressures are documented in Tab. 5-2. Both tables present the best estimates along with confidence ranges as determined by the field test contractor in the corresponding DR.

The permeabilities for all tested intervals are summarised in Tab. 5-3. They were calculated based on the hydraulic conductivities provided in Section 4.5 and Tab. 5-1 and assumed a density of 1'000 kg/m^3 and dynamic viscosity of 1×10^{-3} Pa s.

As the implementation of a skin differs from the analytical description, the implementation by nSIGHT needs to be noted. A skin is implemented by a radial composite model in nSIGHTS, where the hydraulic conductivity of the skin zone does not have a single fixed value but varies logarithmically with distance from the reported value of the hydraulic conductivity at the borehole wall to the reported hydraulic conductivity value of the formation at the radius of discontinuity. Similarly, the hydraulic conductivity is transitioned logarithmically inside one zone of a two or three zone composite flow model with the distance to the next radius of discontinuity. Only the value of the last zone is a fixed value, which has been reported in Tab. 5-1. In the same way, a time varying skin transitioned logarithmically within the period of validity from the hydraulic conductivity at the beginning to the reported hydraulic conductivity value of the next definition and is fixed for the last period.

The hydraulic parameters T, K, P_f and h (in terms of m bgl and m asl) are illustrated with respect to the borehole depth and the geological profile in Figs. 5-1 to 5-5. The best estimates are indicated by vertical lines in the corresponding interval position. The confidence ranges are shown as dashed rectangles, delimited vertically by the corresponding interval extent and laterally by the minimum and maximum values.

Tab. 5-1: Summary of hydraulic packer testing in borehole TRU1-1: Transmissivity and hydraulic conductivity

Test interval details and hydraulic model							**Transmissivity and hydraulic conductivity**					
Test name	**Interval depth**				**Interval length**	**Hydraulic model**	**Best estimates**		**Lowest estimates**[1]		**Highest estimates**[1]	
	From [m bgl]	**To** [m bgl]	**From** [m asl]	**To** [m asl]	[m]		**T** [m^2/s]	**K** [m/s]	T_{min} [m^2/s]	K_{min} [m/s]	T_{max} [m^2/s]	K_{max} [m/s]
TRU1-1-MAL1	589.00	600.38	-114.00	-125.38	11.38	Radial composite with changing wellbore storage	5×10^{-07}	4×10^{-08}	2×10^{-08}	2×10^{-09}	2×10^{-06}	2×10^{-07}
TRU1-1-BDO1	782.30	805.30	-307.30	-330.30	23.00	Homogeneous with skin	5×10^{-12}	2×10^{-13}	2×10^{-12}	8×10^{-14}	2×10^{-11}	8×10^{-13}
TRU1-1-BDO2[2]	806.50	822.20	-331.50	-347.20	15.70	Homogeneous with skin	3×10^{-11}	2×10^{-12}	2×10^{-12}	1×10^{-13}	7×10^{-11}	4×10^{-12}
TRU1-1-OPA2	829.00	854.00	-354.00	-379.00	25.00	Homogeneous with skin	8×10^{-13}	3×10^{-14}	3×10^{-13}	1×10^{-14}	1×10^{-12}	5×10^{-14}
TRU1-1-OPA3	868.50	887.45	-393.50	-412.45	18.95	2 zones radial composite	8×10^{-13}	4×10^{-14}	4×10^{-13}	2×10^{-14}	2×10^{-12}	8×10^{-14}
TRU1-1-LIA2	923.72	944.50	-448.72	-469.50	20.78	2 zones radial composite	5×10^{-13}	2×10^{-14}	1×10^{-13}	7×10^{-15}	2×10^{-12}	7×10^{-14}
TRU1-1-LIA1	944.50	965.28	-469.50	-490.28	20.78	3 zones radial composite	3×10^{-12}	1×10^{-13}	1×10^{-12}	5×10^{-14}	7×10^{-12}	3×10^{-13}
TRU1-1-KEU1	990.70	1'035.00	-515.70	-560.00	44.30	Homogeneous with time varying skin	6×10^{-05}	2×10^{-06}	3×10^{-05}	9×10^{-07}	8×10^{-05}	2×10^{-06}
TRU1-1-MUK1	1'085.30	1'110.30	-610.30	-635.30	25.00	Homogeneous with skin	1×10^{-06}	5×10^{-08}	8×10^{-07}	3×10^{-08}	2×10^{-06}	6×10^{-08}

[1] The lowest and highest estimates for a given parameter are based on uncertainty intervals presented by the field test contractor in the corresponding DR.
[2] Test re-named from OPA1 to BDO2 during final reporting.

Tab. 5-2: Summary of hydraulic packer testing in borehole TRU1-1: Hydraulic head estimates

Test interval details and hydraulic model							**Hydraulic head** [m bgl]			**Hydraulic head** [m asl]			**Formation pressure**		
Test name	**Interval depth**				**Interval length**	**Hydraulic model**	**Best h**	**Lowest[1] h_{min}**	**Highest[1] h_{max}**	**Best h**	**Lowest[1] h_{min}**	**Highest[1] h_{max}**	**Best P_S**	**Lowest[1] $P_{S\,min}$**	**Highest[1] $P_{S\,max}$**
	From [m bgl]	**To** [m bgl]	**From** [m asl]	**To** [m asl]	[m]		[m bgl]	[m bgl]	[m bgl]	[m asl]	[m asl]	[m asl]	[kPa]	[kPa]	[kPa]
TRU1-1-MAL1	589.00	600.38	-114.00	-125.38	11.38	Radial-composite with changing wellbore storage	60	63	33	415	412	442	5'247	5'213	5'512
TRU1-1-BDO1	782.30	805.30	-307.30	-330.30	23.00	Homogeneous with skin	-22	-3	-51	497	478	526	7'999 [2]	7'817 [2]	8'289 [2]
TRU1-1-BDO2 [3]	806.50	822.20	-331.50	-347.20	15.70	Homogeneous with skin	29	69	28	446	406	447	7'706	7'310	7'714
TRU1-1-OPA2	829.00	854.00	-354.00	-379.00	25.00	Homogeneous with skin	-454	-381	-597	929	856	1'072	12'710 [2]	11'993 [2]	14'109 [2]
TRU1-1-OPA3	868.50	887.45	-393.50	-412.45	18.95	2 zones radial composite	-309	-187	-422	784	662	897	11'647 [2]	10'446 [2]	12'753 [2]
TRU1-1-LIA2	923.72	944.50	-448.72	-469.50	20.78	2 zones radial composite	-395	-241	-525	870	716	1'000	13'041 [2]	11'528 [2]	14'309 [2]
TRU1-1-LIA1	944.50	965.28	-469.50	-490.28	20.78	3 zones radial composite	-193	-57	-308	668	532	783	11'260 [2]	9'924 [2]	12'384 [2]
TRU1-1-KEU1	990.70	1'035.00	-515.70	-560.00	44.30	Homogeneous with time varying skin	77	78	76	398	397	399	9'143 [2]	9'137 [2]	9'157 [2]
TRU1-1-MUK1	1'085.30	1'110.30	-610.30	-635.30	25.00	Homogeneous with skin	52	53	52	423	422	423	10'255	10'251	10'261

[1] The lowest and highest estimates for a given parameter are based on uncertainty intervals presented by the field test contractor in the corresponding DR.
[2] Not provided by field test contractor. Calculated for interval midpoint, based on the hydraulic head estimates.
[3] Test re-named from OPA1 to BDO2 during final reporting.

Tab. 5-3: Summary of hydraulic packer testing in borehole TRU1-1: Permeability

Test interval details						**Permeability estimate**[1]		
Test name	**Interval depth**				**Interval length**	**Best k**	**Lowest**[2] **k_{min}**	**Highest**[2] **k_{max}**
	From [m bgl]	**To** [m bgl]	**From** [m asl]	**To** [m asl]	[m]	[m^2]	[m^2]	[m^2]
TRU1-1-MAL1	589.00	600.38	-114.00	-125.38	11.38	4.1×10^{-15}	1.8×10^{-16}	2.1×10^{-14}
TRU1-1-BDO1	782.30	805.30	-307.30	-330.30	23.00	2.0×10^{-20}	8.2×10^{-21}	8.2×10^{-20}
TRU1-1-BDO2 [3]	806.50	822.20	-331.50	-347.20	15.70	2.0×10^{-19}	1.0×10^{-20}	4.1×10^{-19}
TRU1-1-OPA2	829.00	854.00	-354.00	-379.00	25.00	3.1×10^{-21}	1.0×10^{-21}	5.1×10^{-21}
TRU1-1-OPA3	868.50	887.45	-393.50	-412.45	18.95	4.1×10^{-21}	2.0×10^{-21}	8.2×10^{-21}
TRU1-1-LIA2	923.72	944.50	-448.72	-469.50	20.78	2.4×10^{-21}	6.8×10^{-22}	7.5×10^{-21}
TRU1-1-LIA1	944.50	965.28	-469.50	-490.28	20.78	1.4×10^{-20}	5.1×10^{-21}	3.5×10^{-20}
TRU1-1-KEU1	990.70	1'035.00	-515.70	-560.00	44.30	1.6×10^{-13}	8.7×10^{-14}	2.2×10^{-13}
TRU1-1-MUK1	1'085.30	1'110.30	-610.30	-635.30	25.00	4.7×10^{-15}	3.1×10^{-15}	6.1×10^{-15}

[1] The calculation is based on the hydraulic conductivity provided by the field test contractor in the corresponding DR and standard conditions (density: 1'000 kg/m^3, dynamic viscosity: 1×10^{-3} Pa s).

[2] The lowest and highest estimates for a given parameter are based on uncertainty intervals presented by the field test contractor in the corresponding DR.

[3] Test re-named from OPA1 to BDO2 during final reporting.

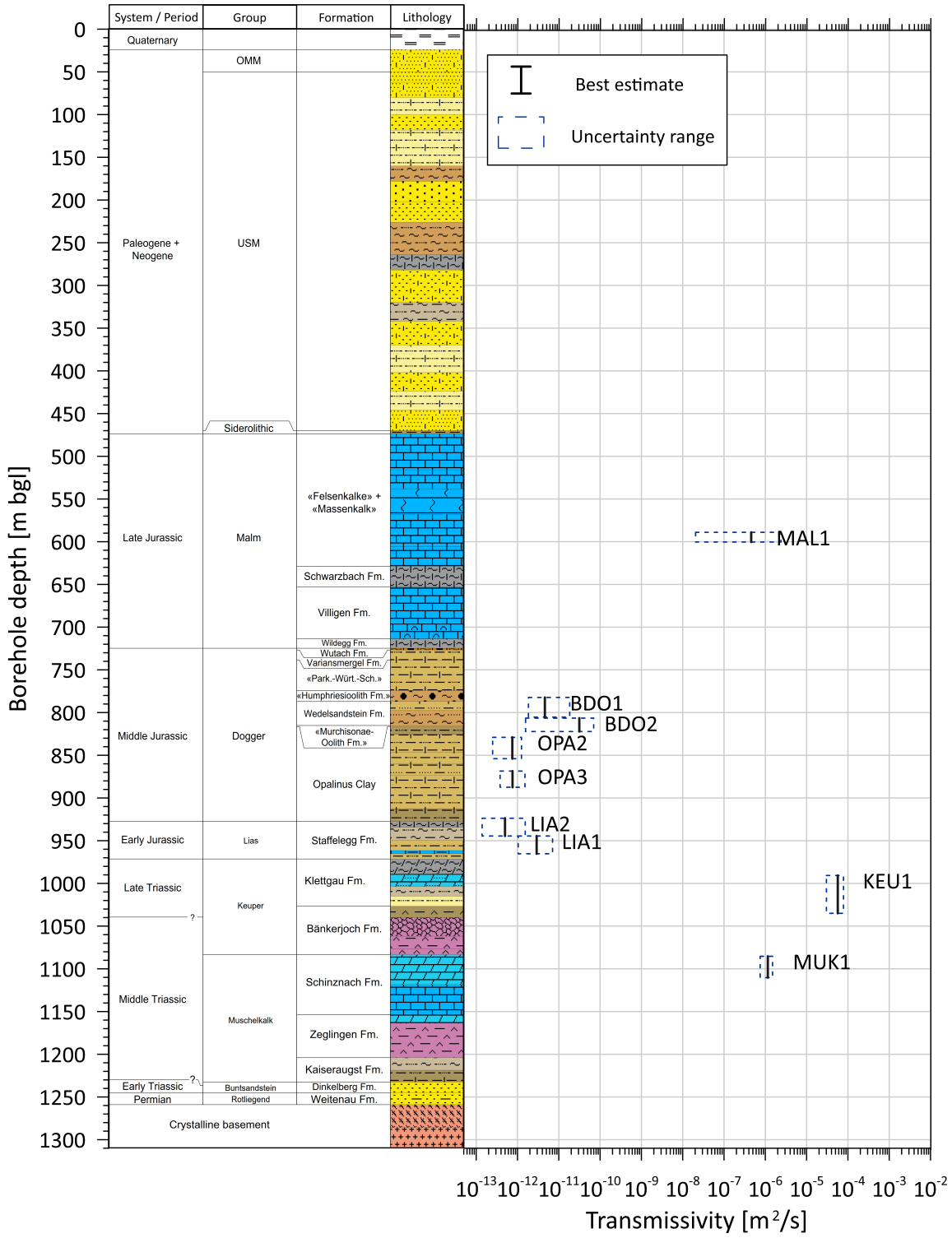

Fig. 5-1: Summary of hydraulic testing in borehole TRU1-1: Formation transmissivity profile

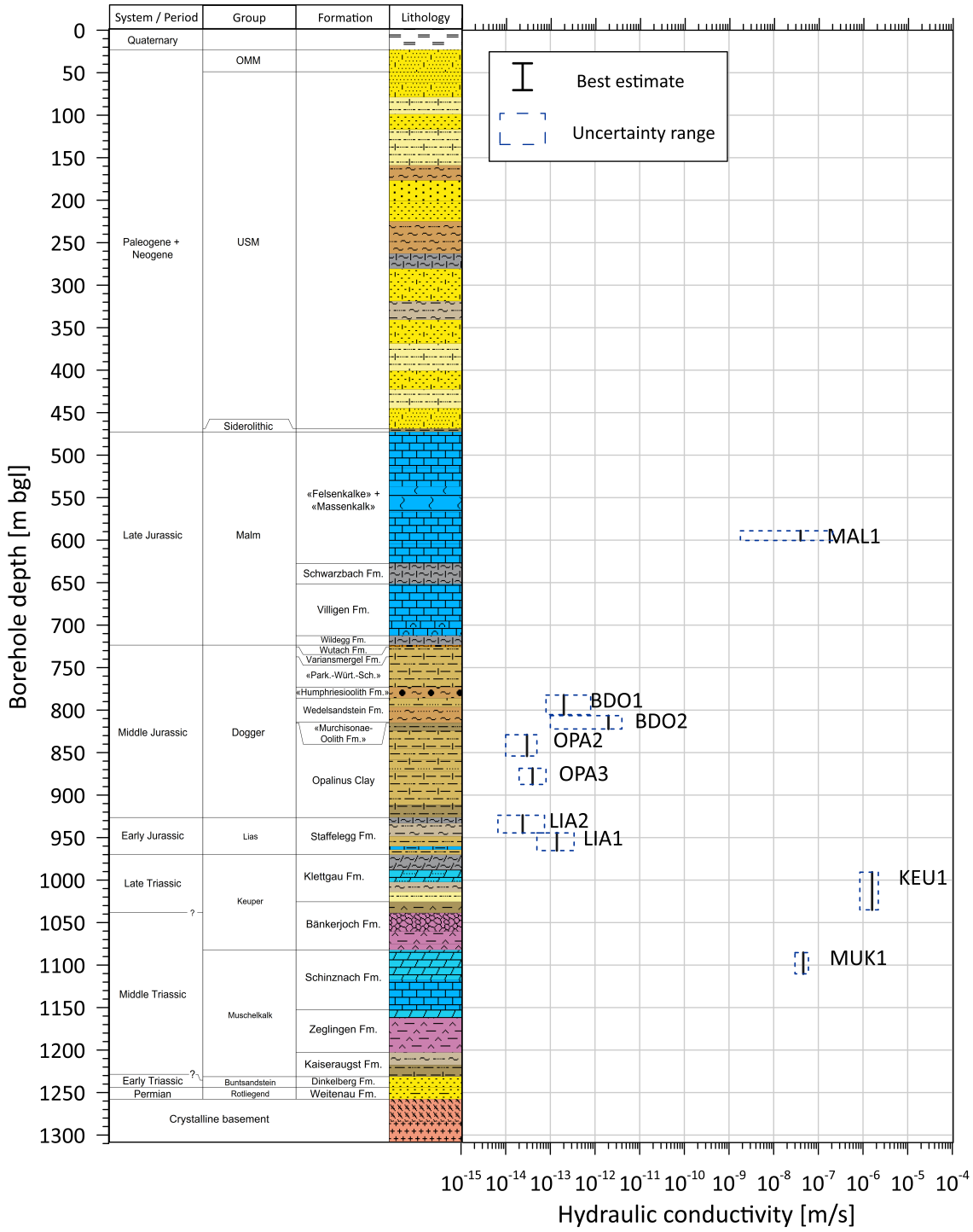

Fig. 5-2: Summary of hydraulic testing in borehole TRU1-1: Formation hydraulic conductivity profile

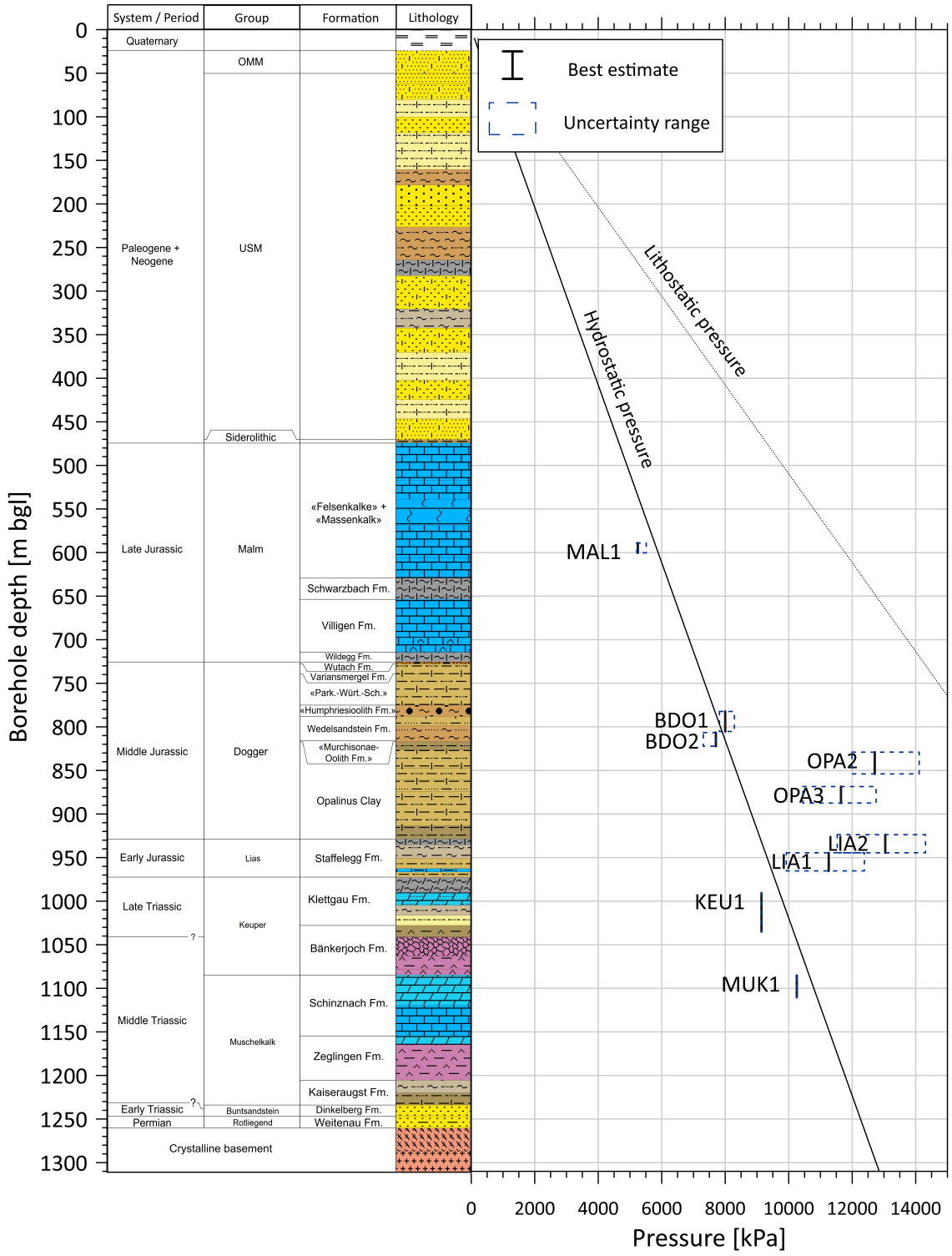

Fig. 5-3: Summary of hydraulic testing in borehole TRU1-1: Static formation pressure profile

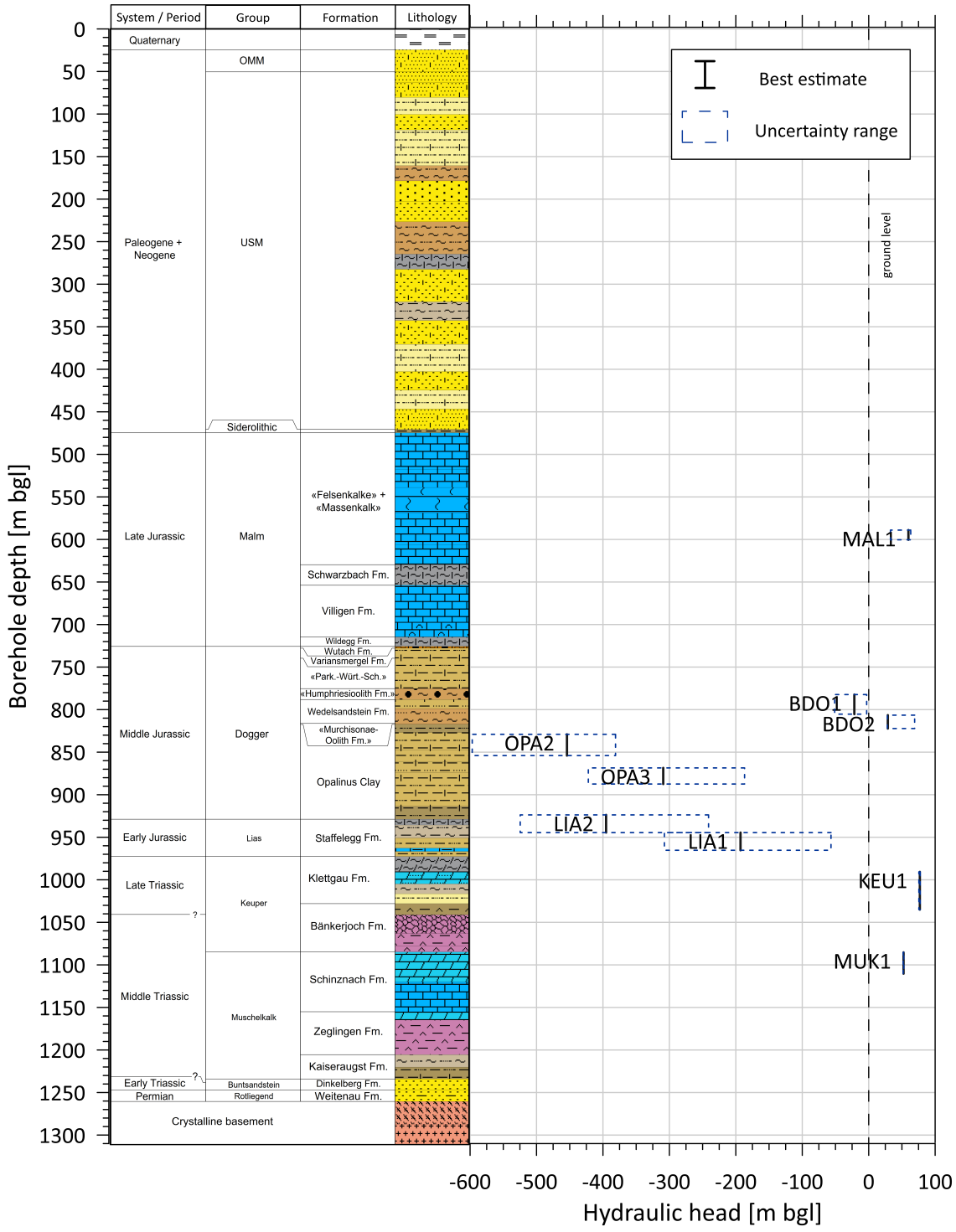

Fig. 5-4: Summary of hydraulic testing in borehole TRU1-1: Formation hydraulic head profile (m bgl)

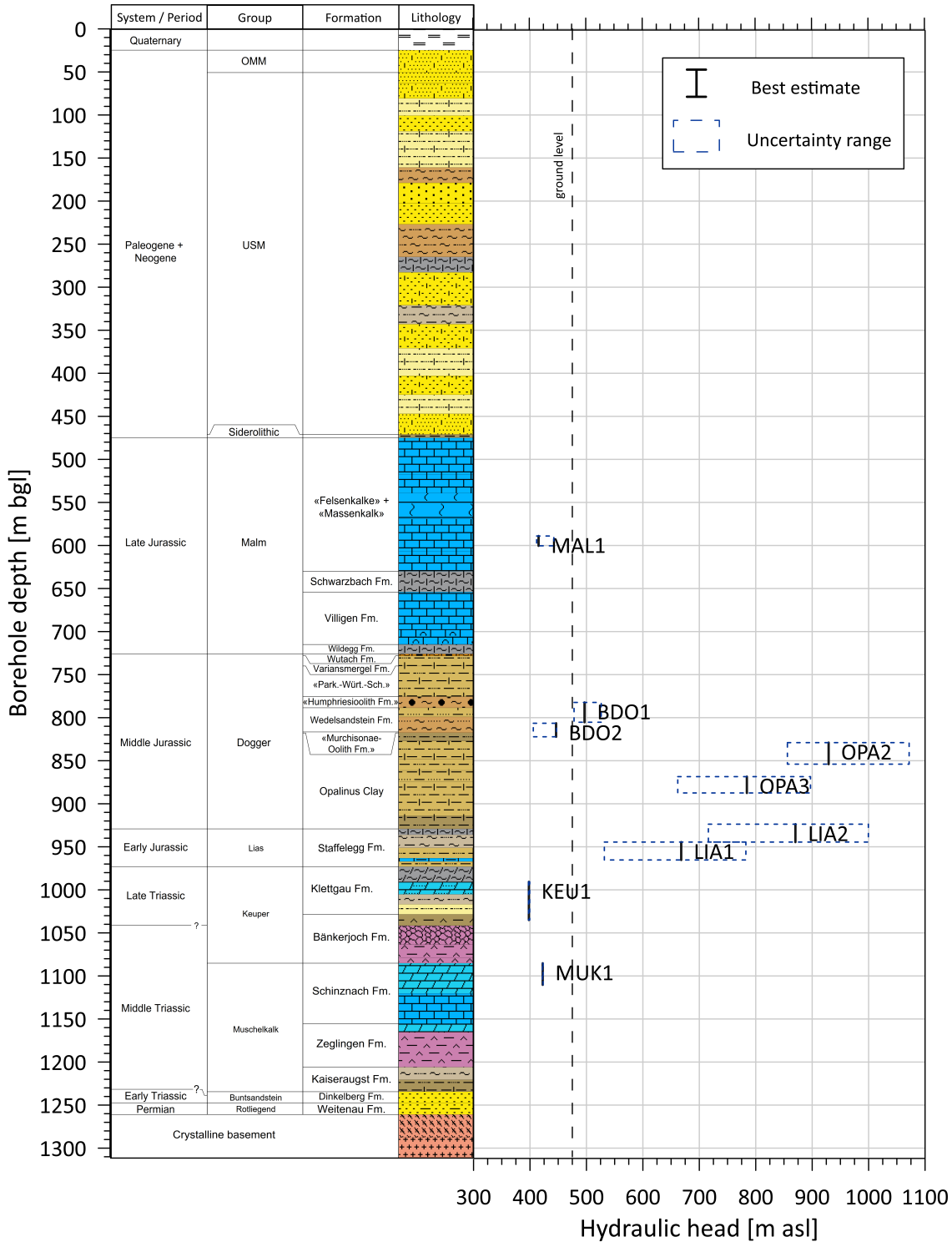

Fig. 5-5: Summary of hydraulic testing in borehole TRU1-1: Formation hydraulic head profile (m asl)

5.2.3 Discussion of data and results

The recorded measurements are of high accuracy and quality. Very few short interruptions in the data acquisition were reported and did not influence the analyses due to their times of occurrence and duration. They were, consequently, neglected.

The best estimates and the uncertainty of all results were quantitatively assessed and are defendable. The results of the analysis for the hydraulic conductivities and transmissivities were found to be reliable. They lie within a reasonable range within the expected spectrum of values for the evaluated formations (e.g. Nagra 2008, Nagra 2014a and 2014b).

Similarly, the extrapolated hydraulic heads are within an expected range (Luo et al. 2014), except for the hydraulic tests performed in the Opalinus Clay and the Lias Group. The hydraulic heads estimated for TRU1-1-OPA2, TRU1-1-OPA3, TRU1-1-LIA2 and TRU1-1-LIA1 appear to be affected by a large overestimation. They are not reliable and have to be considered as 'apparent'. A similar large overestimation of the hydraulic head is documented for the test in the Opalinus Clay in the Benken borehole. The reason for this overestimation may be the long duration of the pressure history. These hydraulic tests were executed with a delay of over 200 hours after drilling through the interval midpoint.

Temperature effects and mechanical processes were accounted for in the numerical implementation of the test intervals. However, these physical processes may not have been represented adequately in the numerical model of the formation. Only for hydraulic test TRU1-1-OPA3 was it attempted to account for the temperature induced pressure changes in the formation fluid using nSIGHTS, though it was not possible to reduce the apparent overestimation of the hydraulic head with this approach. Mechanical processes were not considered for TRU1-1-OPA3 because the required data were not available. General investigations into the physical explanation for the overestimation of the hydraulic head are continuing. The current analysis of all other tests considers only the temperature effects in the test interval and the pressure induced effects resulting from the high-density drilling mud during the entire time since drilling through the interval midpoint.

5.3 Summary

Borehole Trüllikon-1-1 (TRU1-1) was the first TBO borehole drilled in the siting region Zürich Nordost (ZNO).

A total of nine test intervals were investigated in this borehole by means of hydraulic packer tests. The hydrogeological investigations focused on the properties of Opalinus Clay (TRU1-1-OPA2, TRU1-1-OPA3) as well as the confining units above (TRU1-1-BDO1, TRU1-1-BDO2) and below (TRU1-1-LIA2, TRU1-1-LIA1). In addition, the regional aquifers of the Malm Group (TRU1-1-MAL1) and the Muschelkalk Group (TRU1-1-MUK1) as well as the potential aquifer of the Keuper Group (TRU1-1-KEU1) were investigated.

The general objectives were achieved to a large extent and the results were assessed as reliable, except for the hydraulic head estimation in association with TRU1-1-OPA2, TRU1-1-OPA3, TRU1-1-LIA2 and TRU1-1-LIA1, which could not be narrowed down and was therefore assessed as 'apparent'.

The pressures and rates measured during all tests are illustrated in Figs. 4-7 to 4-15. Two hydraulic test analyses were selected to present the general analysis procedure as well as single effects taken into account for the analyses of hydraulic tests in formations with low or medium to high transmissivity. Sections 4.5.1 and 4.5.2 provide overviews of parts of the performed analyses for the hydraulic tests TRU1-1-OPA2 and TRU1-1-MUK1, respectively.

One hydraulic test was conducted in the «Felsenkalke» + «Massenkalk» of the Malm Group including a porous and fractured zone with a higher hydraulic transmissivity (TRU1-1-MAL1) allowing for a groundwater sample to be taken. Additionally, a pumping test and groundwater sampling was performed in the Klettgau Formation and Bänkerjoch Formation of the Keuper Group (TRU1-1-KEU1) as well as in the Schinznach Formation of the Muschelkalk Group (TRU1-1-MUK1).

In the Dogger Group the «Humphriesioolith Formation» and the Wedelsandstein Formation were investigated by test TRU1-1-BDO1. The transition from Wedelsandstein Formation and «Murchisonae-Oolith Formation» to Opalinus Clay was covered by test TRU1-1-BDO2.

The properties of typical Opalinus Clay were measured with test TRU1-1-OPA2 whereas test TRU1-1-OPA3 focused on fractured Opalinus Clay; both showing low hydraulic transmissivities.

Two tests were conducted in the Lias Group confirming low transmissivities at the transition of Opalinus Clay to Staffelegg Formation (TRU1-1-LIA2) and within the Staffelegg Formation (TRU1-1-LIA1).

All hydraulic tests were supported by an on-site field analysis to optimise the test procedure.

Fluid-logging was conducted in borehole section II resp. the Malm Group (TRU1-1-FL1-MAL) that could only be analysed qualitatively as a technical problem occurred during the logging activities and reduced the number of useable runs.

6 References

Barker, J.A. (1988): A generalized radial flow model for hydraulic tests in fractured rock. Water Resources Research 24/10, 1796-1804.

Beauheim, R.L., Roberts, R.M. & Avis, J.D. (2004): Well testing in fractured media: Flow dimensions and diagnostic plots. Journal of Hydraulic Research 42 (Extra Issue), 69-76.

Bourdet, D., Ayoub, J.A. & Pirard, Y.M. (1989): Use of pressure derivative in well-test interpretation. Society of Petroleum Engineers, SPE Formation Evaluation, 293-302.

Detournay, E. & Cheng, A.H.-D. (1988): Poroelastic response of a borehole in a non-hydrostatic stress field. International Journal of Rock Mechanics and Mining Sciences & Geomechanics Abstracts 25/3, 171-182.

Gaus, I., Garitte, B., Senger, R., Gens, A., Vasconcelos, R., Garcia-Sineriz, J.-L., Trick, T., Wieczorek, K., Czaikowski, O., Schuster, K., Mayor, J.C., Velasco, M., Kuhlmann, U. & Villar, M.V. (2014a): The HE-E Experiment: Layout, interpretation and THM modelling. Nagra Arbeitsbericht NAB 14-53.

Gaus, I., Wieczorek, K., Schuster, K., Garitte, B., Senger, R., Vasconcelos, R. & Mayor, J.C. (2014b): EBS behaviour immediately after repository closure in a clay host rock: HE-E experiment (Mont Terri URL). *In:* Norris et al. (eds): Clays in Natural and Engineered Barriers for Radioactive Waste Confinement. Geological Society, London, Special Publications, 400.

Geofirma Engineering Ltd. & INTERA Inc. (2011): nSIGHTS Version 2.50 User Manual. INTERA Inc., Austin, TX, USA.

Grauls, D. (1999): Overpressures: Causal mechanisms, conventional and hydromechanical approaches. Oil & Gas Science and Technology – Rev. IFP 54, 667-678.

Horne, R.N. (1995): Modern Well Test Analysis, A Computer-Aided Approach. 2nd ed. Petroway, Palo Alto, CA, USA.

Horner, D.R. (1951): Pressure Buildup in Wells. Proceedings Third World Petroleum Congress, 2:503-523, The Hague, Netherlands. Reprinted 1967. Pressure Analysis Methods, AIME Reprint Series 9, 45-50, Richardson, TX, USA, Society of Petroleum Engineers.

Isler, A., Pasquier, F. & Huber, M. (1984): Geologische Karte der zentralen Nordschweiz 1:100'000. Herausgegeben von der Nagra und der Schweiz. Geol. Komm.

Jäggi, K. & Vogt, T. (2020): OPA: Sondierbohrung Benken, Langzeitbeobachtung 2019, Dokumentation der Messdaten. Nagra Arbeitsbericht NAB 20-05.

Lisjak, A., Garitte, B., Grasselli, G., Müller, H.R. & Vietor, T. (2015): The excavation of a circular tunnel in a bedded argillaceous rock (Opalinus Clay): Short-term rock mass response and FDEM numerical analysis. Tunnelling and Underground Space Technology 45, 227-248.

Lorenz, G.D. & Pechstein, A. (2021): Borehole TRU1-1 (Trüllikon): Fluid sampling and analytical hydrochemical data report. Nagra Arbeitsbericht NAB 21-24.

Luo, J., Monningkoff, B. & Becker, J.K. (2014): Hydrogeological model Nördlich Lägern. Nagra Arbeitsbericht NAB 13-25.

Marschall, P., Croisé, J., Schlickenrieder, L., Boisson, J.Y., Vogel, P. & Yamamoto, S. (2003): Synthesis of hydrogeological investigations at the Mont Terri site (Phases 1 – 5). Mont Terri Technical Report TR 01-02. Mont Terri Project, Switzerland.

Nagra (1997): Hydrological investigations at Wellenberg: Hydraulic packer testing in boreholes SB4a/v and SB4a/s. Methods and field results. Nagra Technischer Bericht NTB 95-02.

Nagra (2001): Sondierbohrung Benken – Untersuchungsbericht. Nagra Technischer Bericht NTB 00-01.

Nagra (2008): Vorschlag geologischer Standortgebiet für das SMA- und das HAA-Lager –Geologische Grundlagen. Nagra Technischer Bericht. NTB 08-04.

Nagra (2014a): SGT Etappe 2: Vorschlag weiter zu untersuchender geologischer Standortgebiete mit zugehörigen Standortarealen für die Oberflächenanlage. Geologische Grundlagen. Dossier II: Sedimentologische und tektonische Verhältnisse. Nagra Technischer Bericht NTB 14-02.

Nagra (2014b): SGT Etappe 2: Vorschlag weiter zu untersuchender geologischer Standortgebiete mit zugehörigen Standortarealen für die Oberflächenanlage. Geologische Grundlagen. Dossier VI: Barriereneigenschaften der Wirt- und Rahmengesteine. Nagra Technischer Bericht. NTB 14-02.

Nagra (2019): Implementation of the Full-scale Emplacement Experiment at Mont Terri: Design, construction and preliminary results. Nagra Technischer Bericht NTB 15-02.

Pietsch, J. & Jordan, P. (2014): Digitales Höhenmodell Basis Quartär der Nordschweiz – Version 2013 (SGT E2) und ausgewählte Auswertungen. Nagra Arbeitsbericht NAB 14-02.

Ramey, H.J. Jr., Agarwal, R.G. & Martin, I. (1975): Analysis of 'Slug Test' or DST Flow Period Data. Journal of Canadian Petroleum Technology 14/3, 37-47.

Richards, D.J. (1981): Technical Manual on Radiometrics – Geophysical Field Manual for Technicians No.2. South African Geophysical Association.

Senger, R., Papafotiou, A. & Marschall, P. (2014): Thermo-hydraulic simulations of the near-field of a SF/HLW repository during early- and late-time post-closure period. Nagra Arbeitsbericht NAB 14-11.

App. A Abbreviations, nomenclature and definitions

Tab. A-1: Lithostratigraphy abbreviations for test names in TRU1-1

Lithostratigraphy	**Abbreviation**
Malm Group	MAL
Brauner Dogger (Dogger parts above OPA in regions NL and ZNO)	BDO
Opalinus Clay	OPA
Lias Group	LIA
Keuper Group	KEU
Muschelkalk Group	MUK

Tab. A-2: Test name definitions for hydraulic packer testing

Abbreviation	**Example**
Drill site abbreviation – lithostratigraphy abbreviation[1] + number of test	TRU1-1-MUK1: First test interval in Muschelkalk aquifer in borehole TRU1-1

[1] Based on the preliminary information

Tab. A-3: Test event abbreviations for hydraulic packer testing

Test phase	**Abbr.**
Compliance phase	COM
Packer deflation phase	DEF
Packer inflation phase	INF
Multi-rate pumping test with stepwise constant flow rates	MR
Pressure recovery after multi-rate pumping test (shut-in)	MRS
Pulse injection test	PI
Initial pressure recovery 'static pressure recovery' (SIT closed)	PSR
Pulse withdrawal test	PW
Pumping test with constant flow rate ('rate withdrawal test')	RW
Pressure recovery after pumping test with constant flow rate (shut-in)	RWS
Slug withdrawal test (flow phase)	SW
Slug withdrawal test – pressure recovery with closed SIT (shut-in)	SWS

Tab. A-4: Parameter definitions

Abbreviation / symbol	**Description**	**Unit**
h_s	Static hydraulic head (freshwater head) $h_s = z_{ref} - z_{int} + \left[\frac{P_f + \rho_{int}\, g\, (z_{int} - z_2) - P_{atm} - P_{offset}}{\rho_w\, g}\right]$	m asl
k	Intrinsic permeability	m^2
K	Hydraulic conductivity	m/s
K_s	Hydraulic conductivity of skin zone	m/s
n	Fractural flow dimension, e.g. Barker (1988)	-
P	Pressure (at QSSP-P2 level, if not otherwise specified)	Pa, kPa
P1	Pressure below bottom packer/ P1-interval (downhole probe)	Pa, kPa
P2	Pressure in test interval (downhole probe)	Pa, kPa
P2*	Pressure in test interval (memory gauge)	Pa, kPa
P3	Pressure in annulus (above top packer, downhole probe)	Pa, kPa
P4	Pressure in test tubing above SIT (downhole probe)	Pa, kPa
P_{atm}	Atmospheric pressure	Pa, kPa
P_f	Static formation pressure (fitting parameter, at QSSP-P2 level)	Pa, kPa
P_{int}	Pressure at midpoint of test interval	Pa, kPa
P_{offset}	Offset of a pressure probe at atmospheric pressure	Pa, kPa
P_s	Static formation pressure (at midpoint of test interval if not specified otherwise)	Pa, kPa
q	Flow rate	m^3/s
Q, Q_{tot}	Cumulative flow volume	m^3
ρ_{int}	Density of interval fluid	kg/m^3
ρ_w	Density of formation water (fluid)	kg/m^3
S	Storage	-
s	Skin factor	-
S_s	Specific storage	1/m
S_{ss}	Specific storage of skin zone	1/m
T	Transmissivity	m^2/s
t, dt	Time, elapsed time	s
T_{int}, T_2	Temperature in test interval, temperature triple probe (Sensor 2)	°C
z_2	Depth of pressure sensor of test interval P2	m bgl
z_{int}	Depth interval midpoint	m bgl
z_{ref}	Reference point elevation	m asl

App. B Analysis plots of the hydraulic packer tests TRU1-1-OPA2 and TRU1-1-MUK1

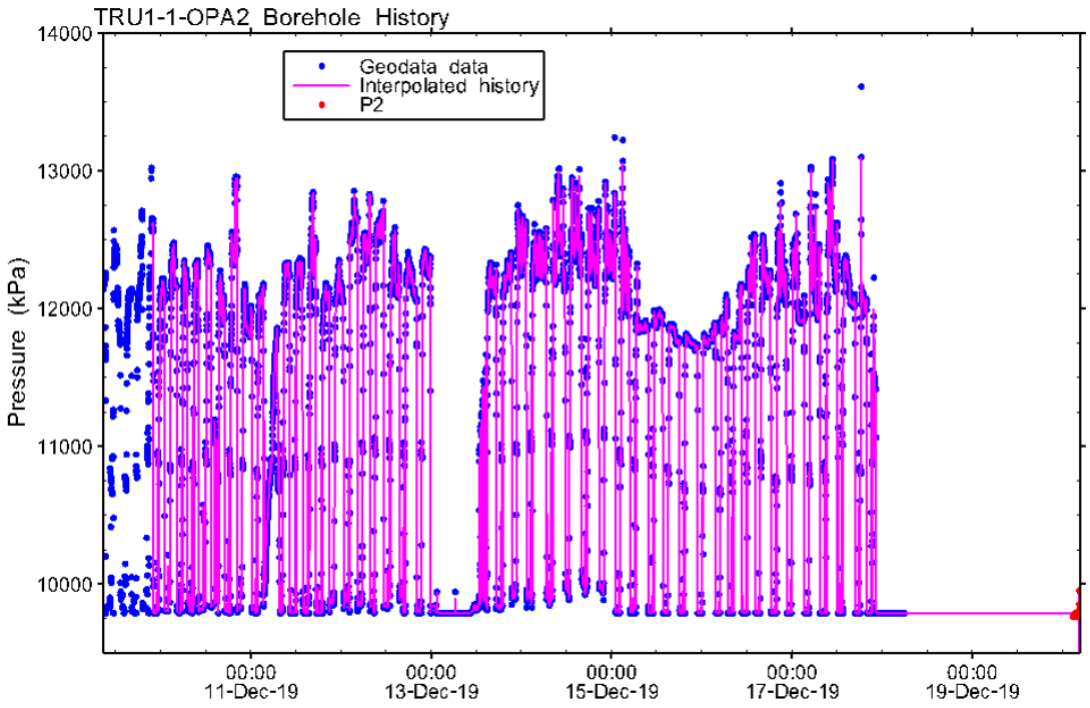

Fig. B-1: Hydraulic test TRU1-1-OPA2: Entire record of the borehole pressure history used in the analysis

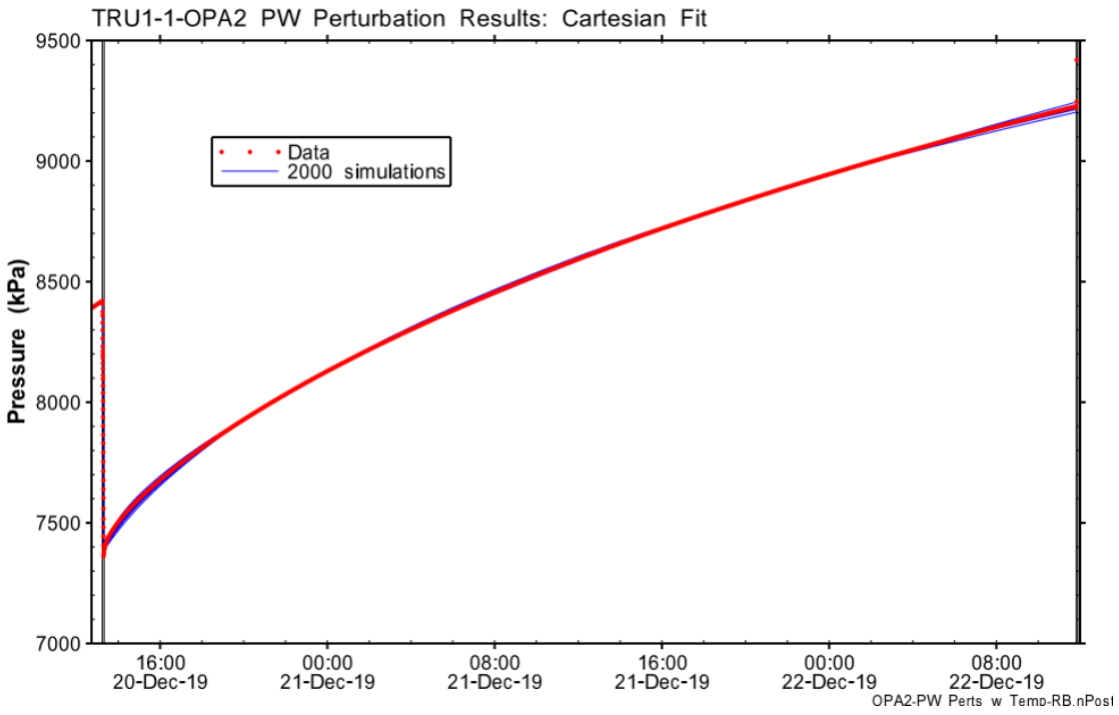

Fig. B-2: Hydraulic test TRU1-1-OPA2: Cartesian horsetail plot showing 2'000 simulations of PW attributed to optimisation results of the perturbation

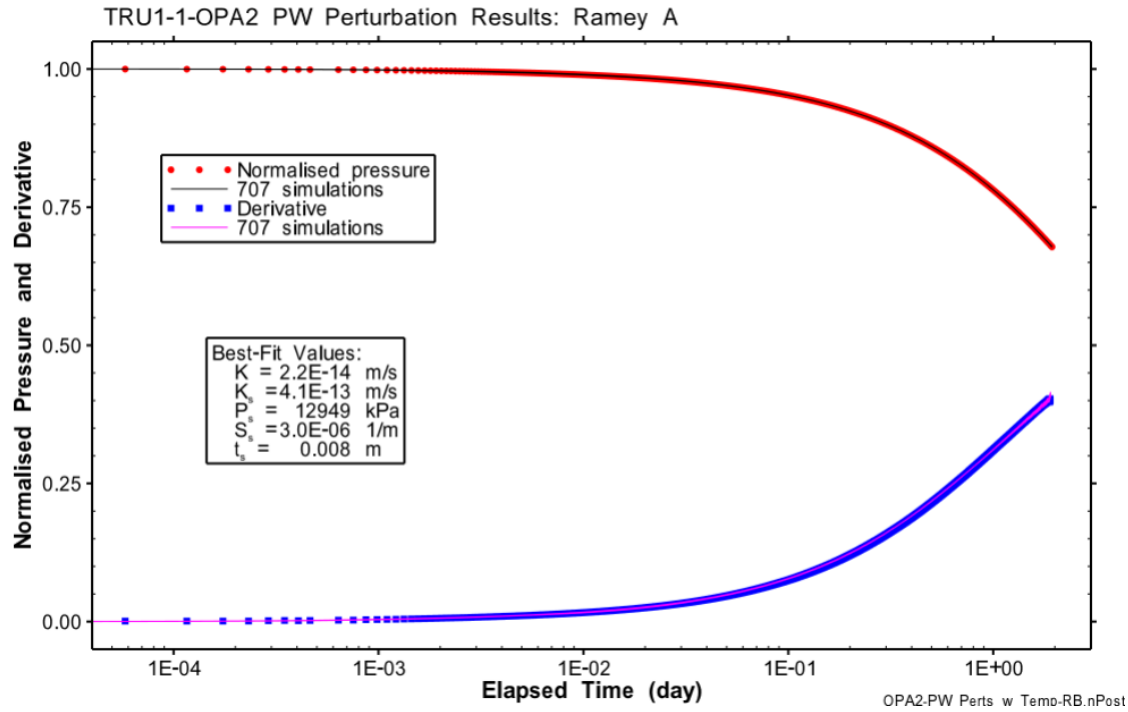

Fig. B-3: Hydraulic test TRU1-1-OPA2: Ramey A horsetail plot showing the 707 simulations of PW attributed to the selected optimisation results of the perturbation

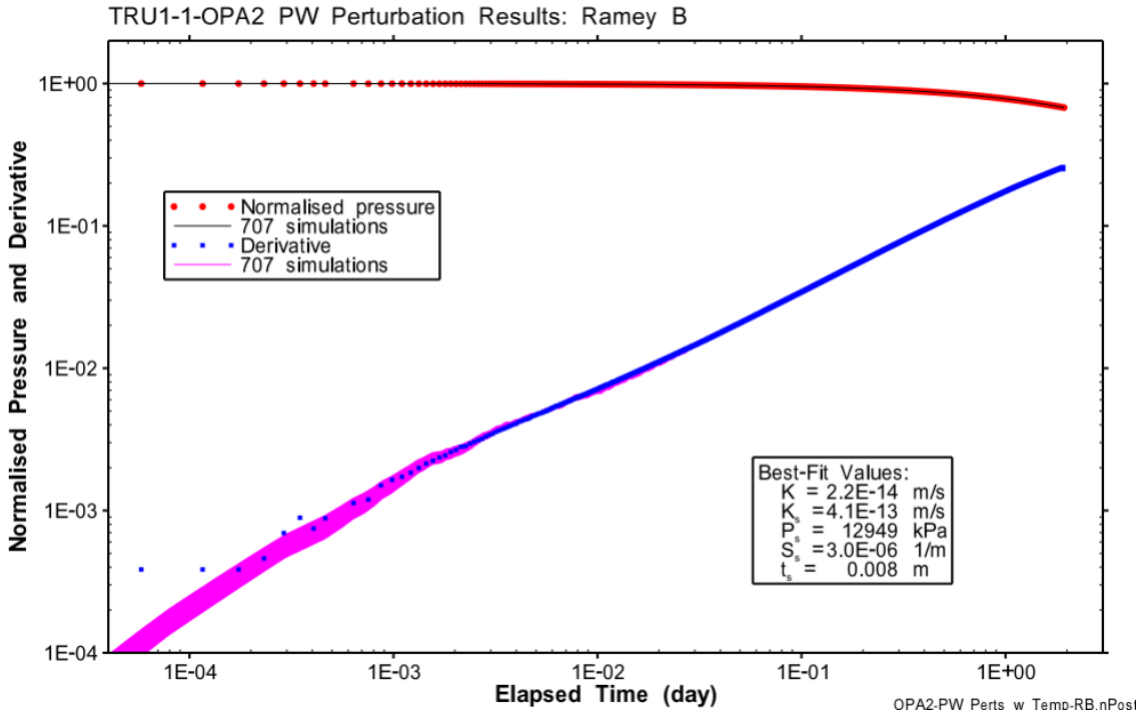

Fig. B-4: Hydraulic test TRU1-1-OPA2: Ramey B horsetail plot showing the 707 simulations of PW attributed to the selected optimisation results of the perturbation

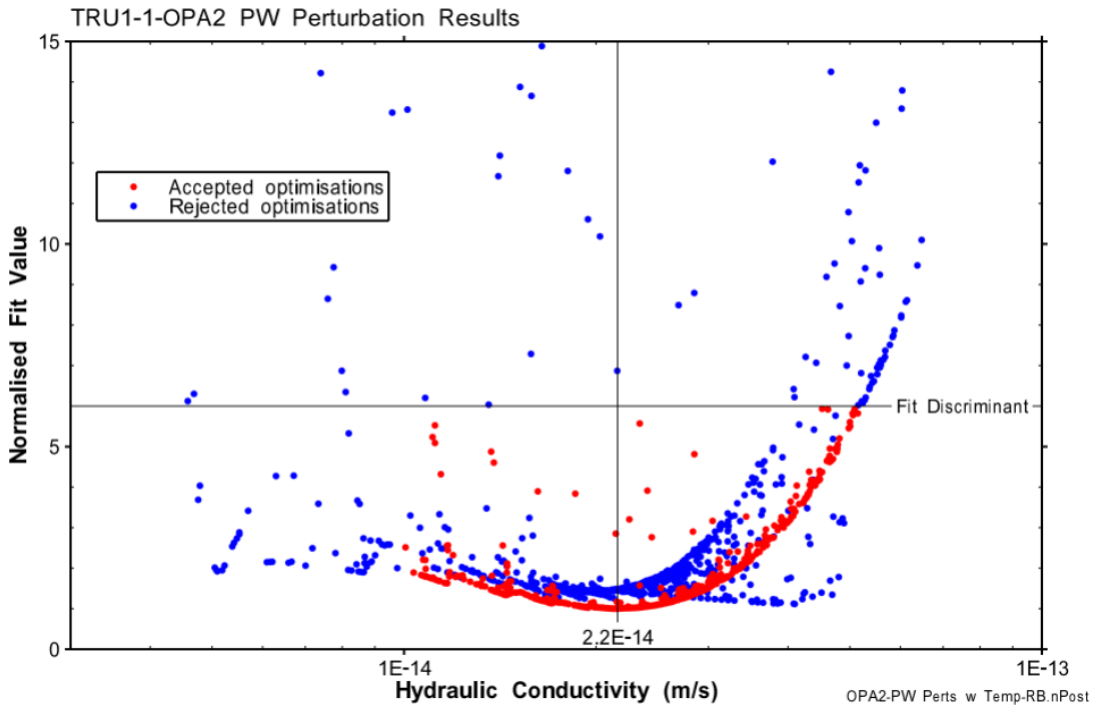

Fig. B-5: Hydraulic test TRU1-1-OPA2: Mapping of the parameter space to the hydraulic conductivity of the formation for the PW perturbation results

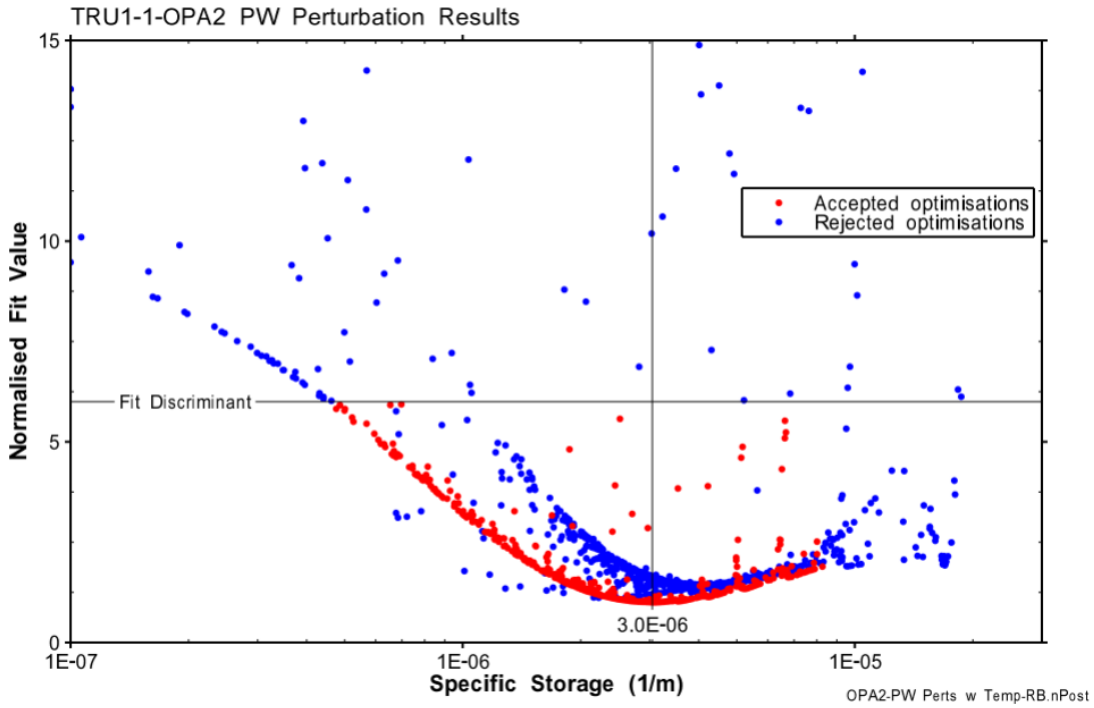

Fig. B-6: Hydraulic test TRU1-1-OPA2: Mapping of the parameter space to the specific storage of the formation for the PW perturbation results

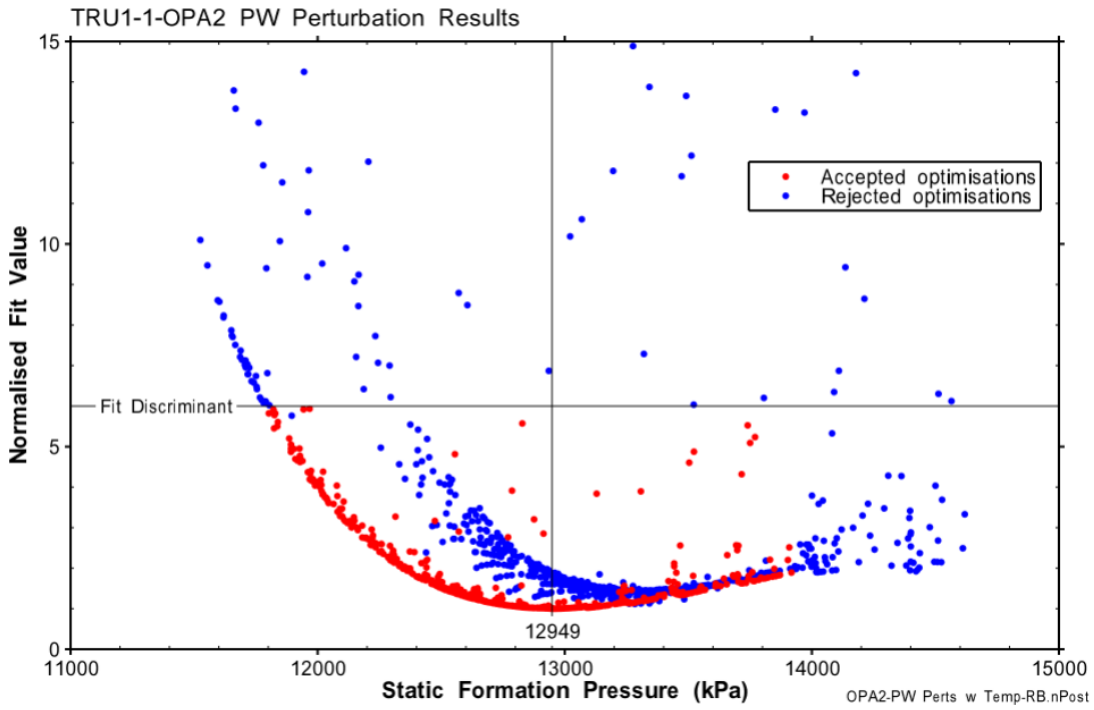

Fig. B-7: Hydraulic test TRU1-1-OPA2: Mapping of the parameter space to the static formation pressure for the PW perturbation results

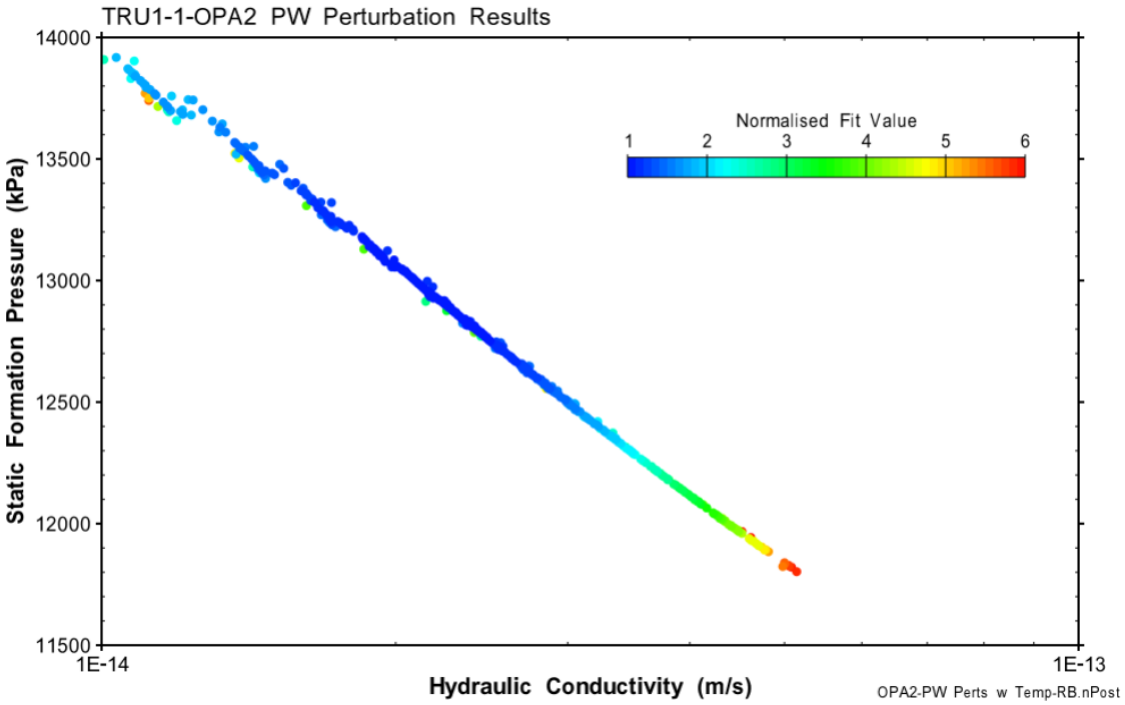

Fig. B-8: Hydraulic test TRU1-1-OPA2: Hydraulic conductivity – static formation pressure correlation for PW

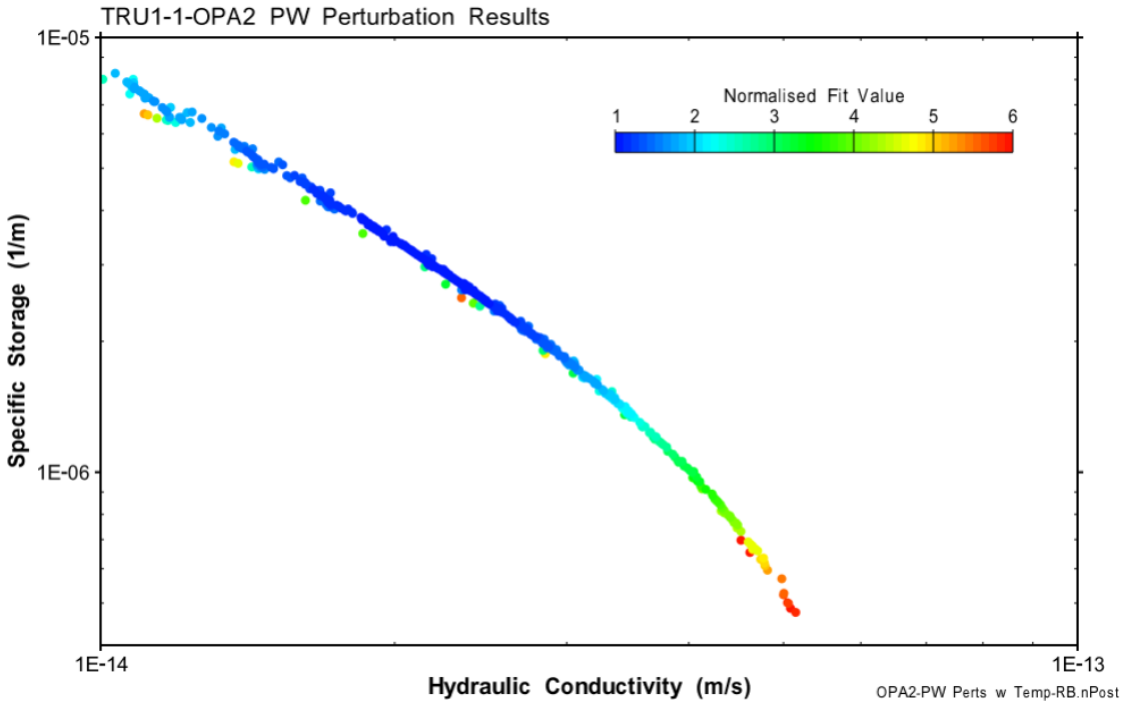

Fig. B-9: Hydraulic test TRU1-1-OPA2: Hydraulic conductivity – specific storage correlation for PW

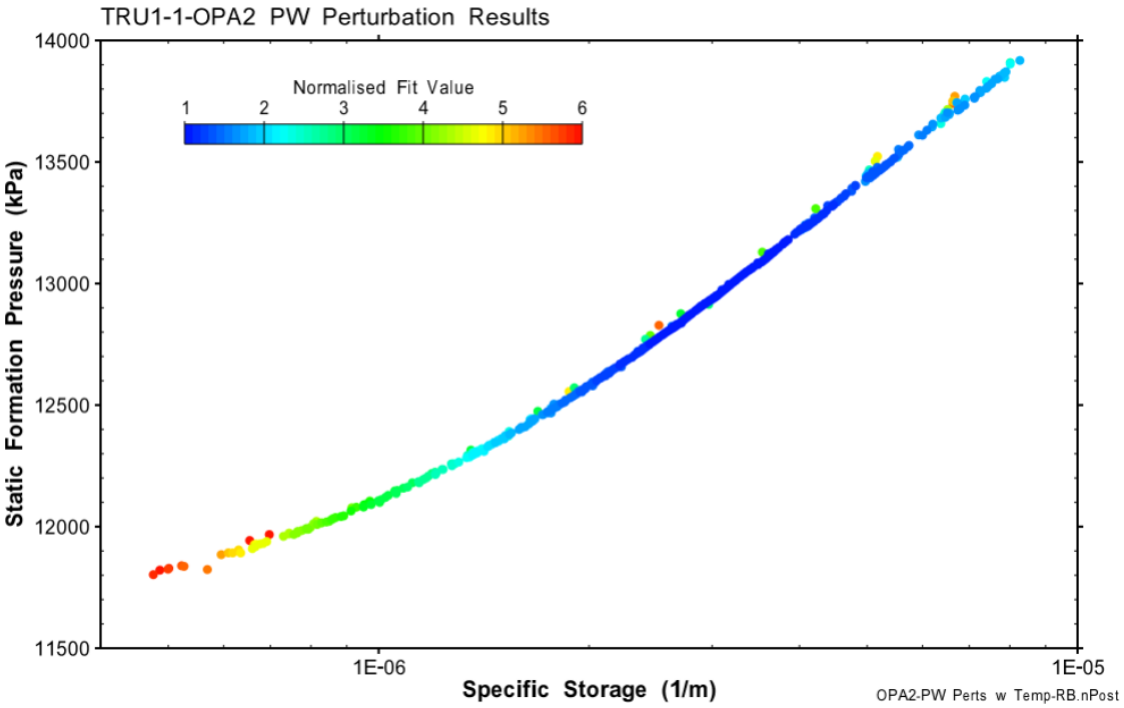

Fig. B-10: Hydraulic test TRU1-1-OPA2: Static formation pressure – specific storage correlation for PW

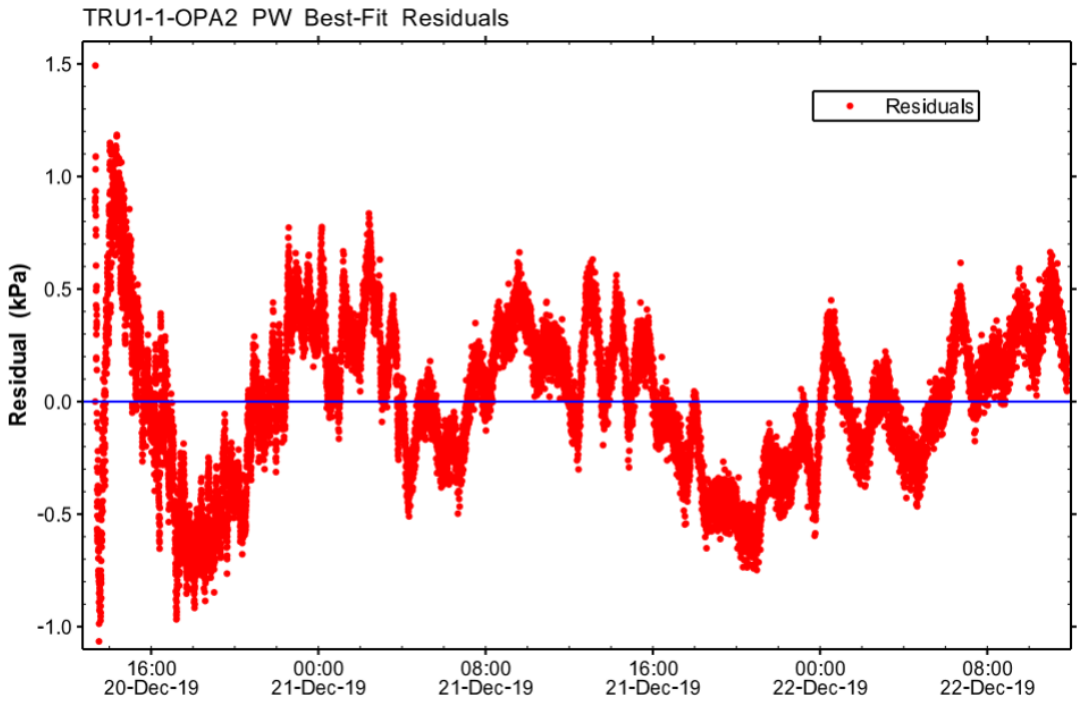

Fig. B-11: Hydraulic test TRU1-1-OPA2: Residuals from best fit to PW data measured by P2

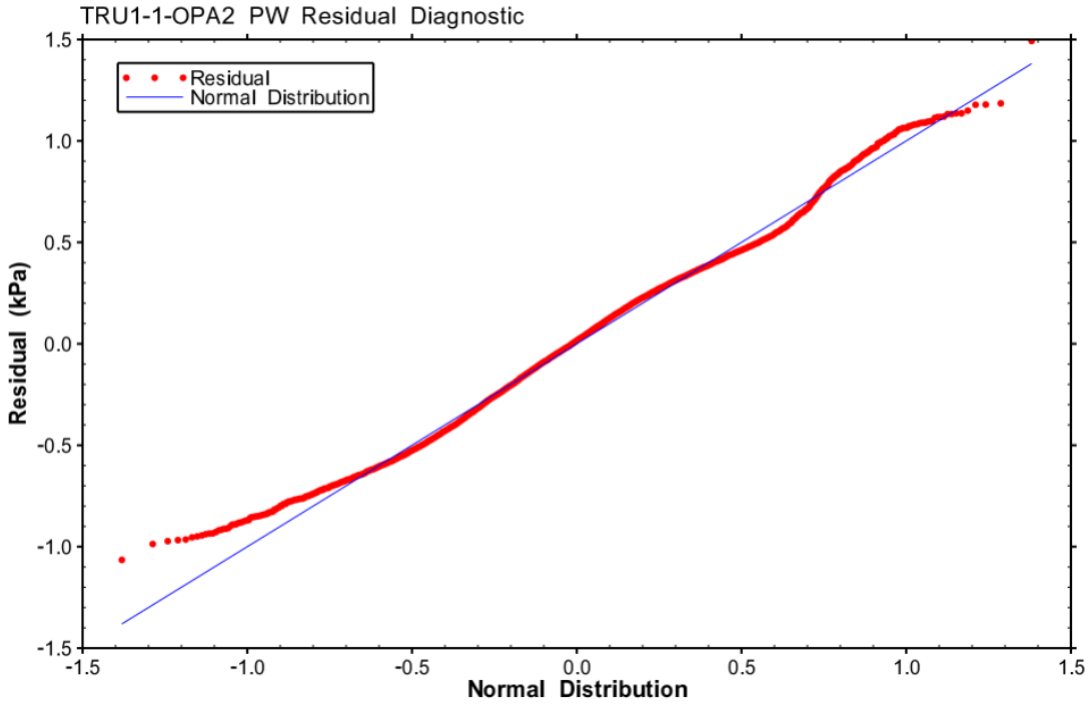

Fig. B-12: Hydraulic test TRU1-1-OPA2: Quantile-normal plot for PW residuals

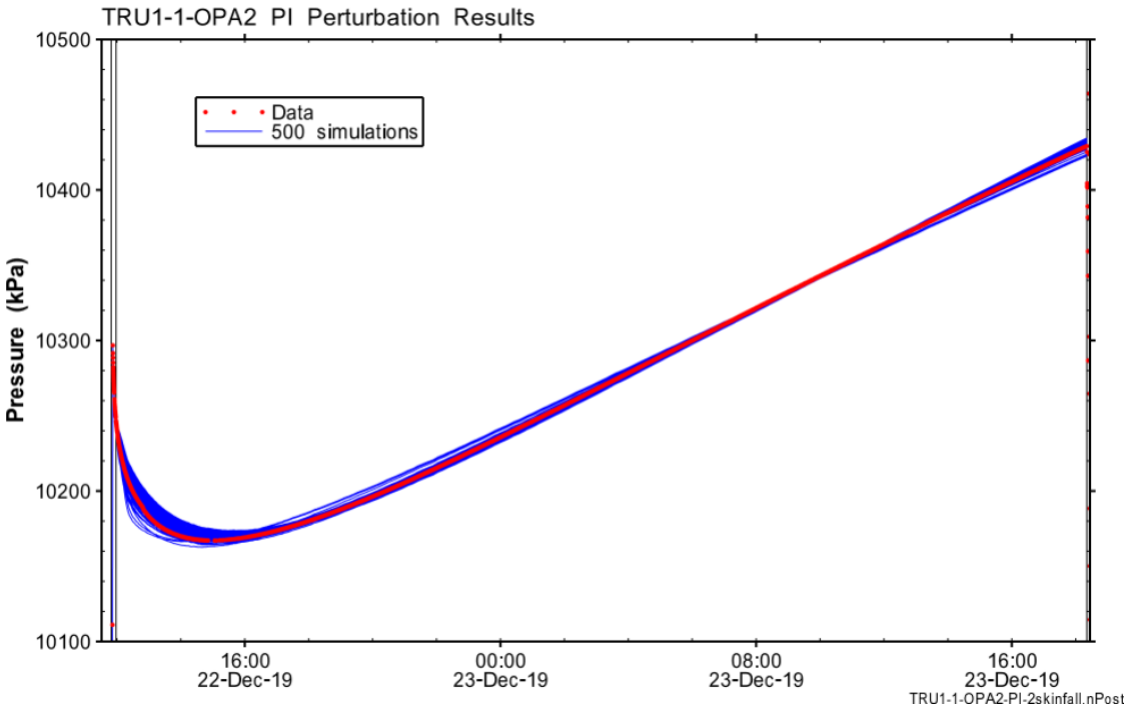

Fig. B-13: Hydraulic test TRU1-1-OPA2: Cartesian horsetail plot showing 500 simulations of PI attributed to optimisation results of the perturbation

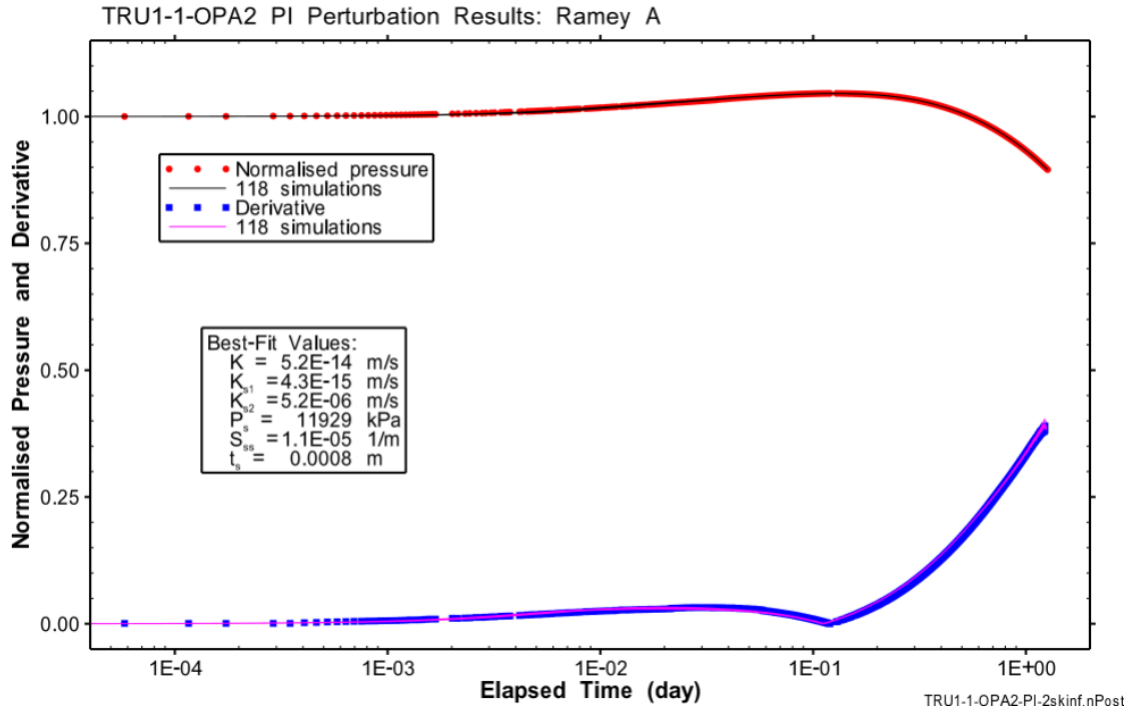

Fig. B-14: Hydraulic test TRU1-1-OPA2: Ramey A horsetail plot showing the 118 simulations of PW attributed to the selected optimisation results of the perturbation

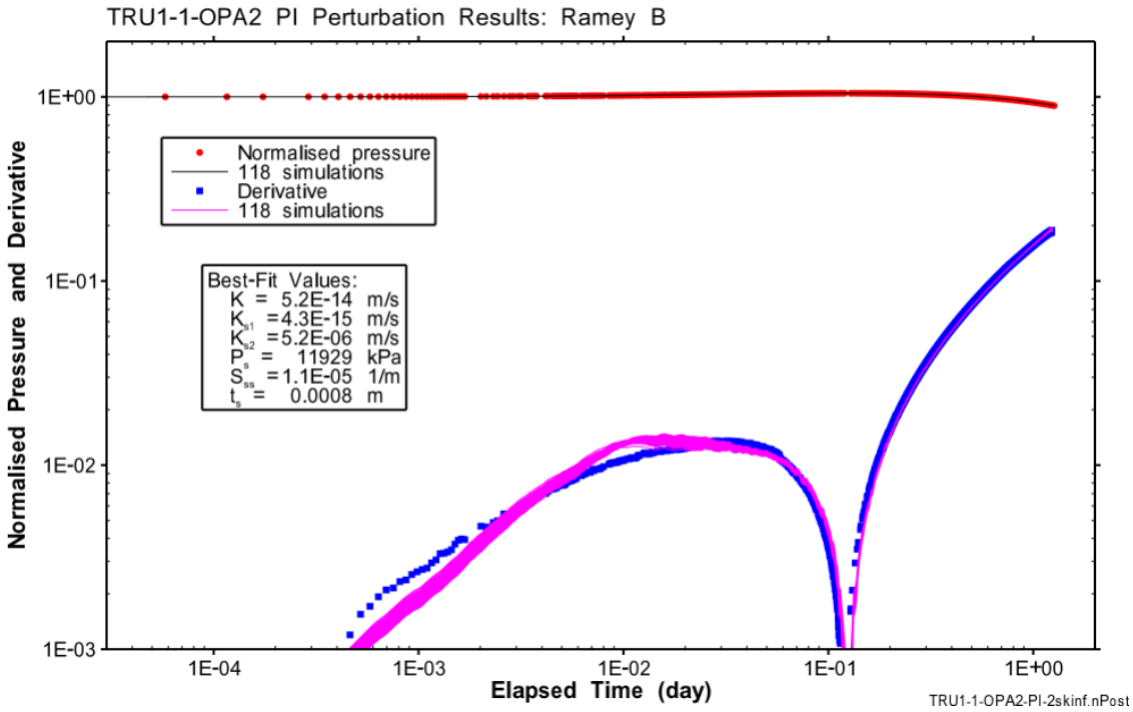

Fig. B-15: Hydraulic test TRU1-1-OPA2: Ramey B horsetail plot showing the 118 simulations of PI attributed to the selected optimisation results of the perturbation

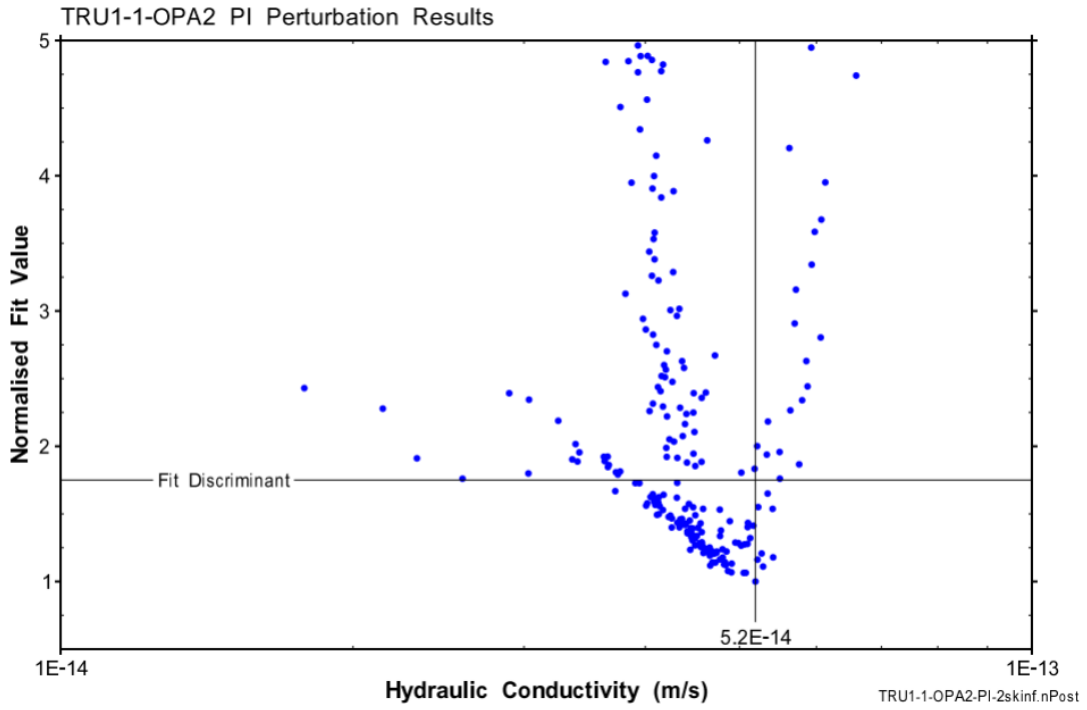

Fig. B-16: Hydraulic test TRU1-1-OPA2: Mapping of the parameter space to the hydraulic conductivity of the formation for the PI perturbation results

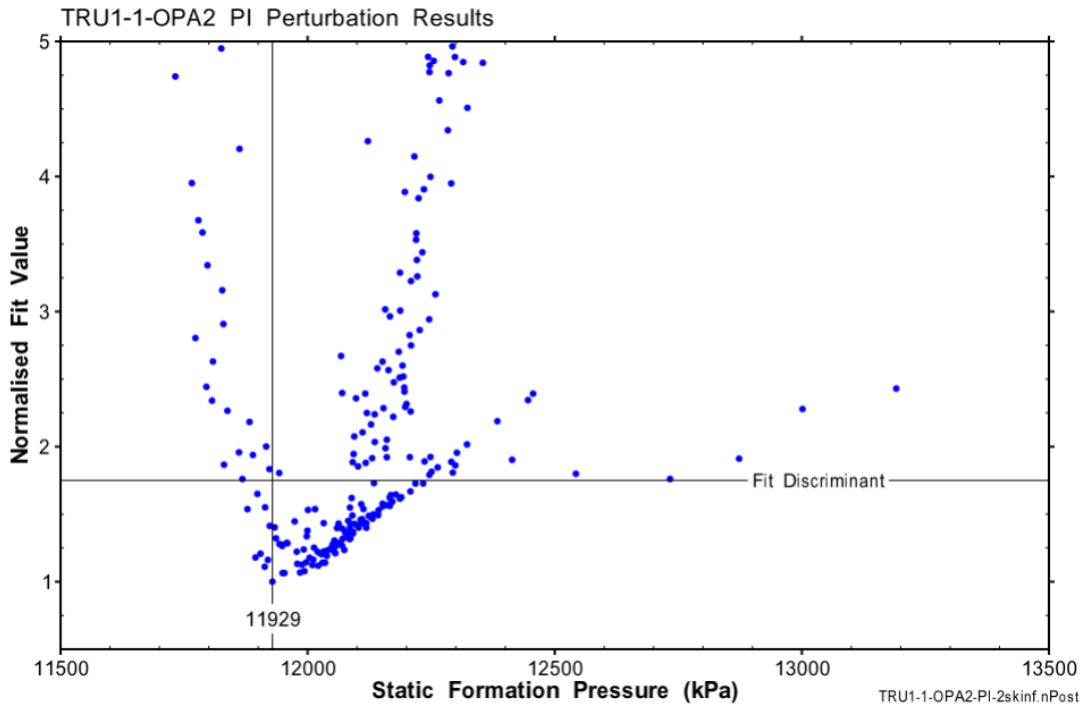

Fig. B-17: Hydraulic test TRU1-1-OPA2: Mapping of the parameter space to the static formation pressure for the PI perturbation results

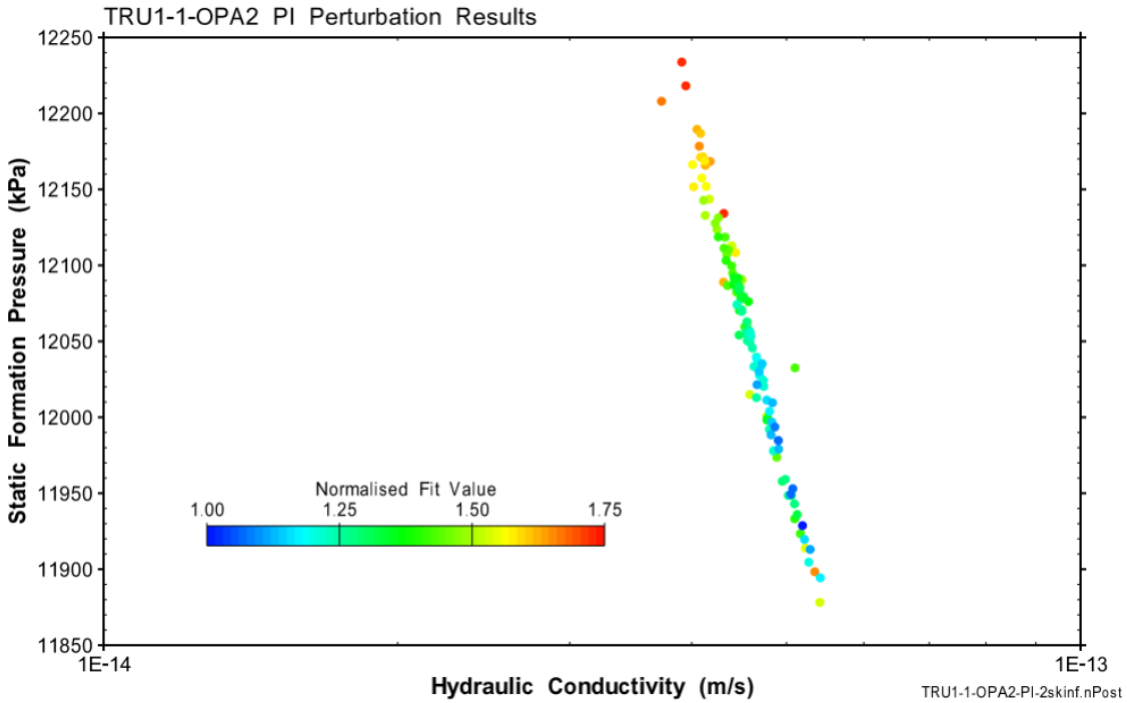

Fig. B-18: Hydraulic test TRU1-1-OPA2: Hydraulic conductivity – static formation pressure correlation for PI

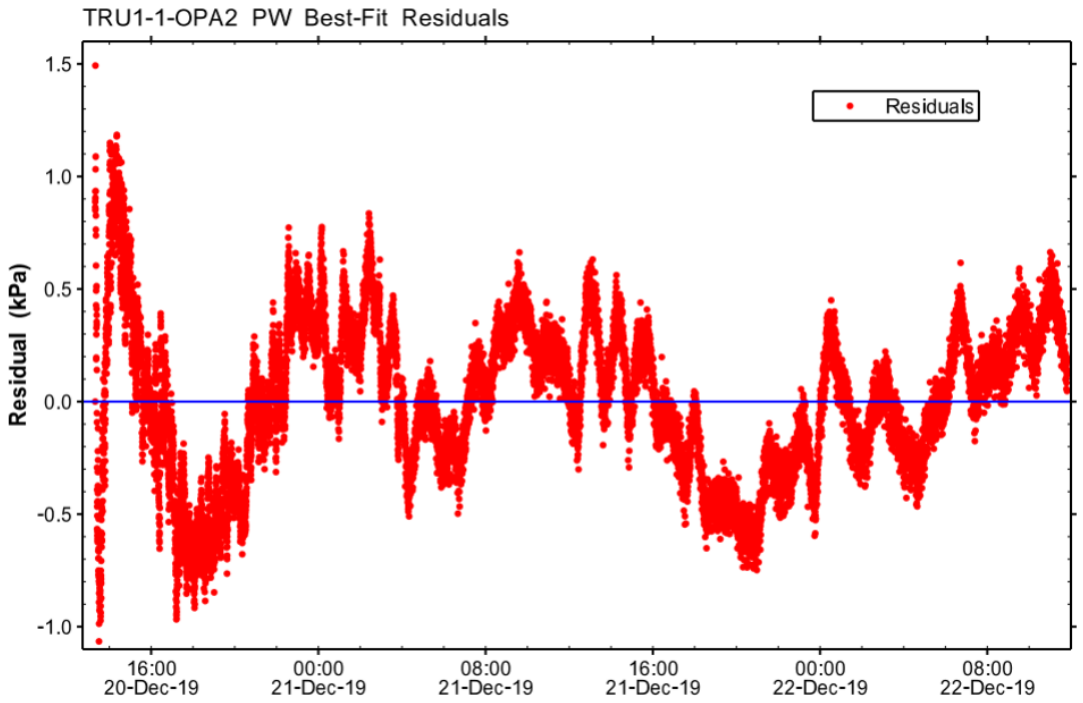

Fig. B-19: Hydraulic test TRU1-1-OPA2: Residuals from best fit to PI data measured by P2

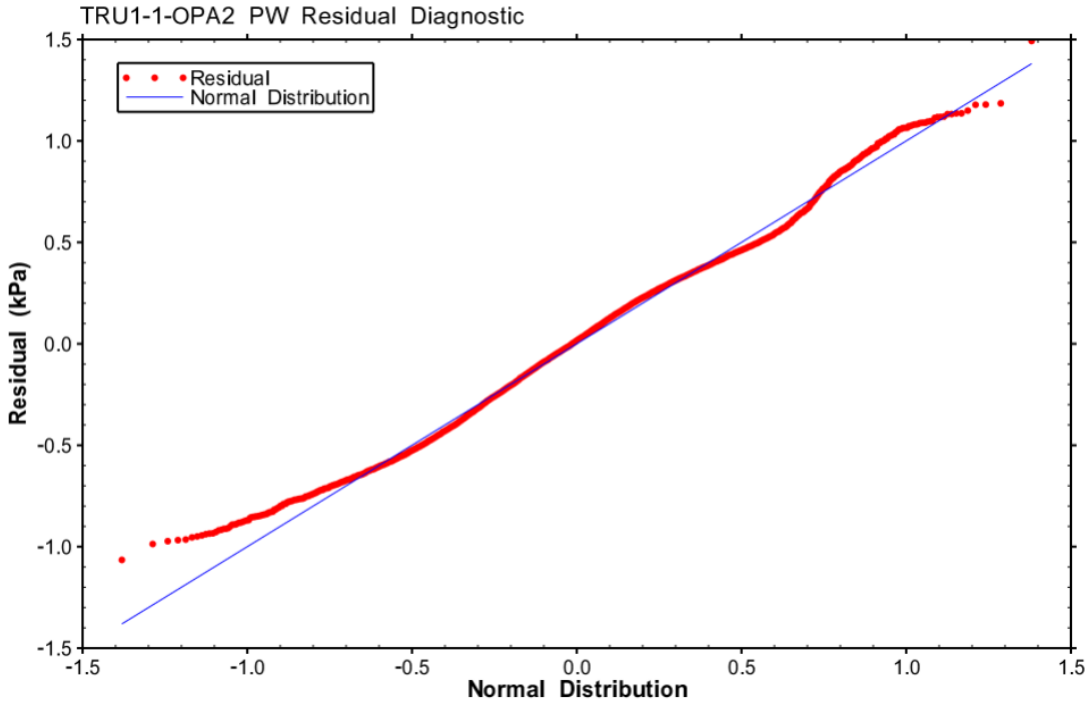

Fig. B-20: Hydraulic test TRU1-1-OPA2: Quantile-normal plot for PI residuals

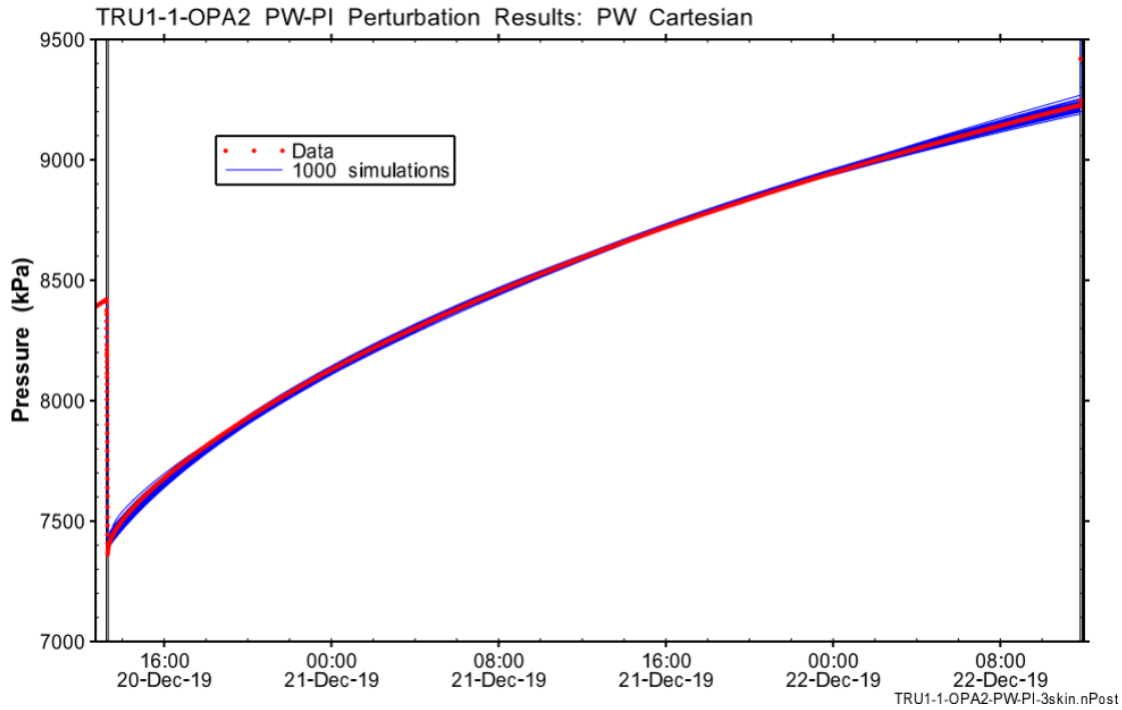

Fig. B-21: Hydraulic test TRU1-1-OPA2: Cartesian horsetail plot showing 1'000 simulations of PW attributed to optimisation results of the perturbation for the sequence PW-PI

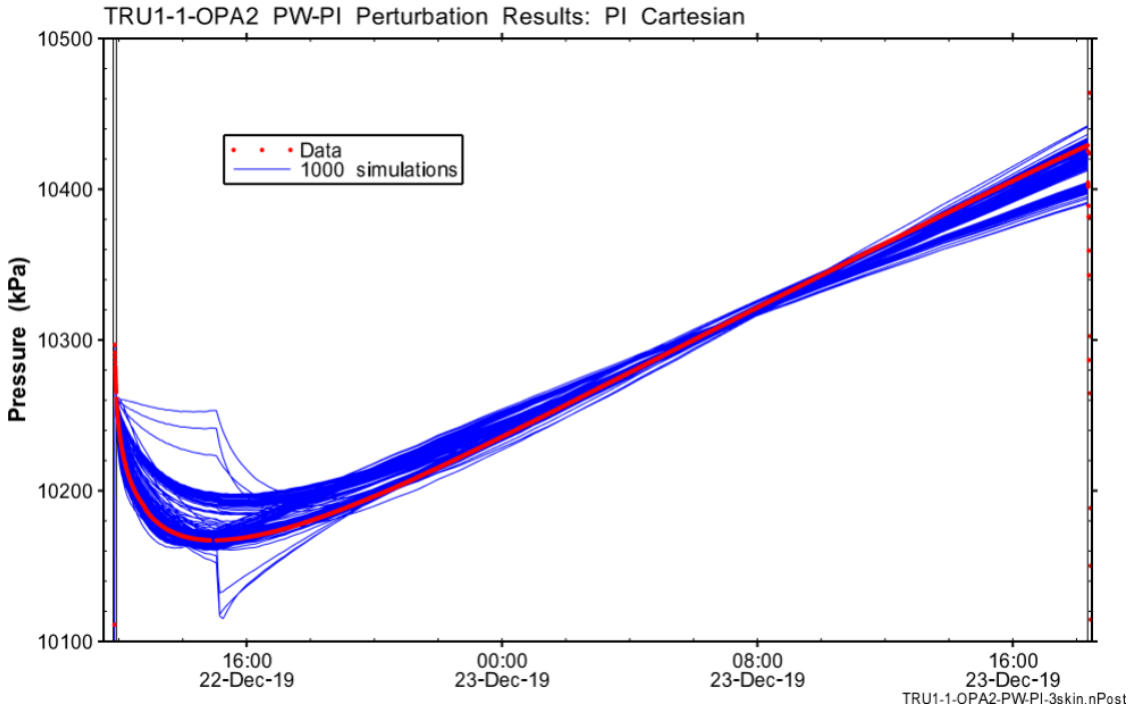

Fig. B-22: Hydraulic test TRU1-1-OPA2: Cartesian horsetail plot showing 1'000 simulations of PI attributed to optimisation results of the perturbation for the sequence PW-PI

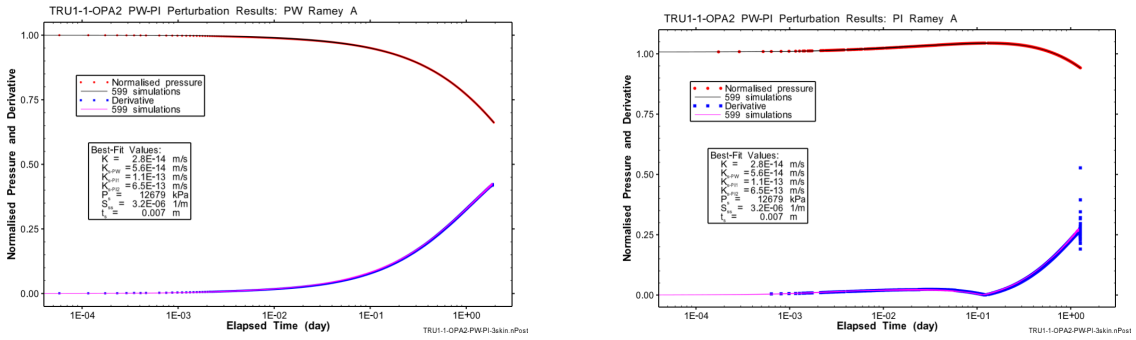

Fig. B-23: Hydraulic test TRU1-1-OPA2: Ramey A horsetail plot showing the 599 simulations of PW attributed to the selected optimisation results of the perturbation (left for PW, right for PI phase)

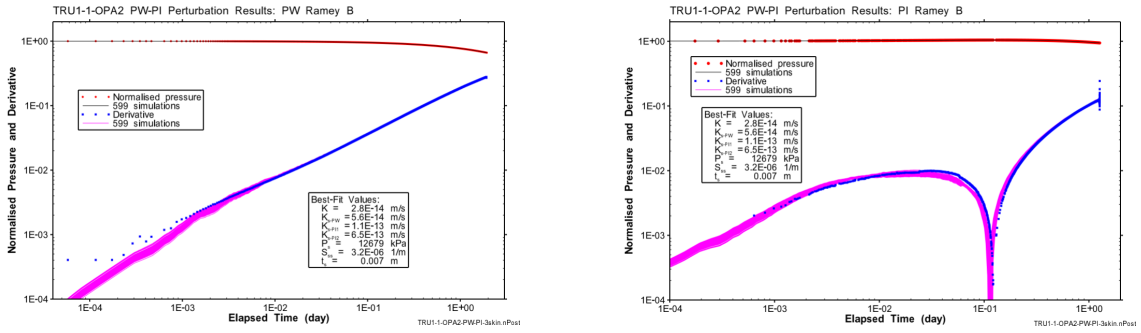

Fig. B-24: Hydraulic test TRU1-1-OPA2: Ramey B horsetail plot showing the 118 simulations of PI attributed to the selected optimisation results of the perturbation (left for PW, right for PI phase)

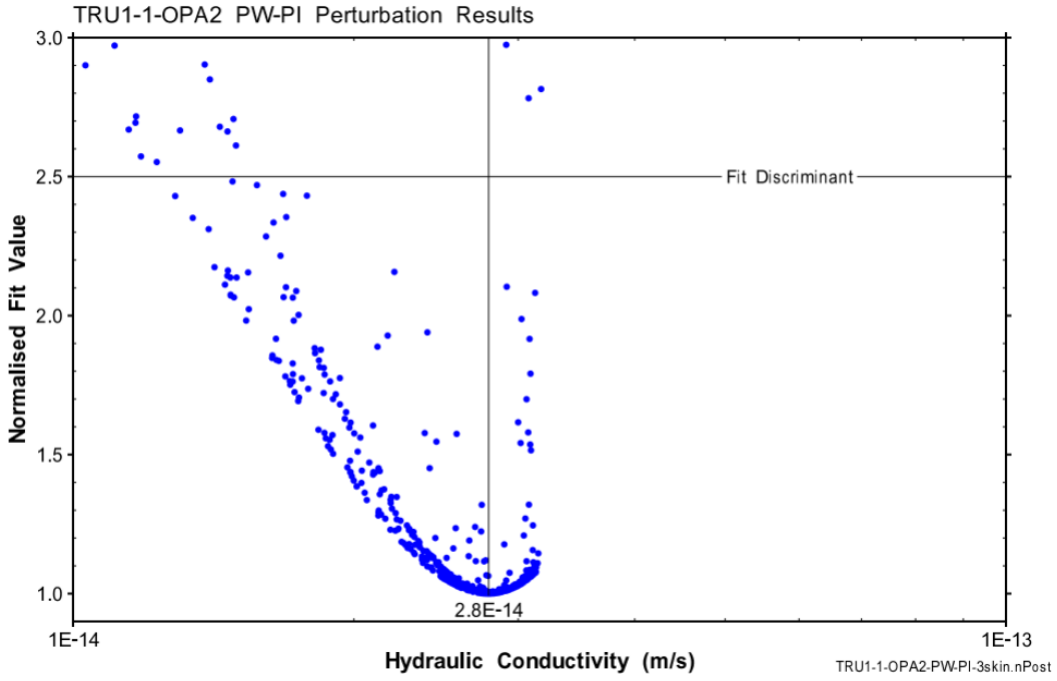

Fig. B-25: Hydraulic test TRU1-1-OPA2: Mapping of the parameter space to the hydraulic conductivity of the formation for the PW-PI perturbation results

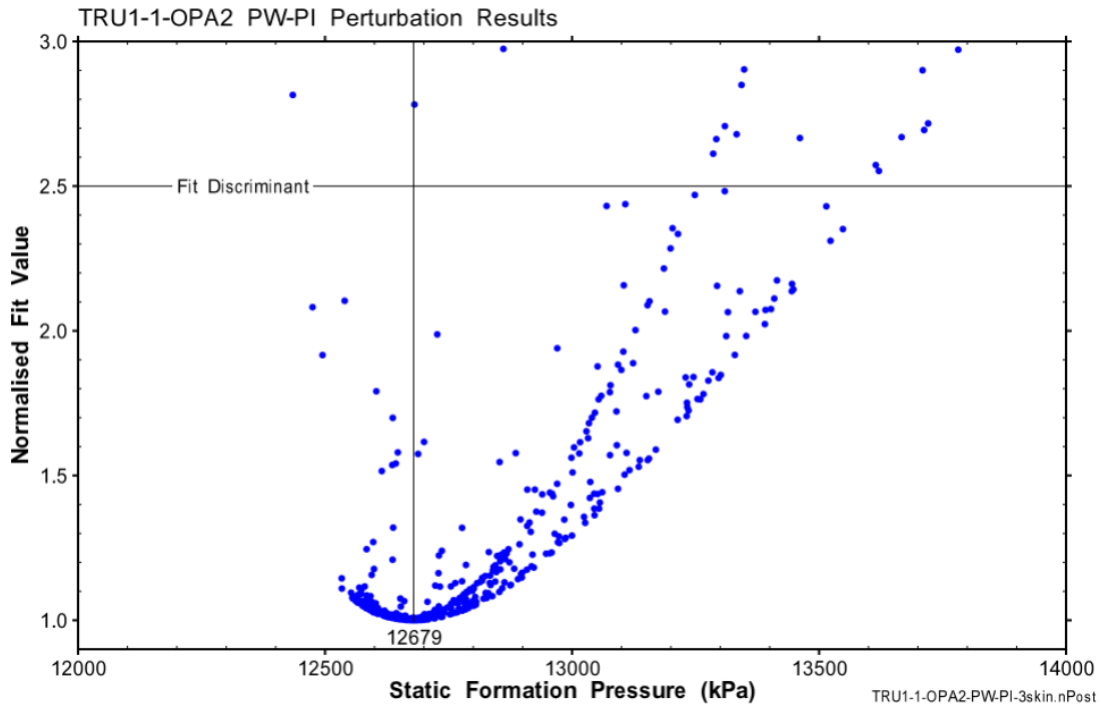

Fig. B-26: Hydraulic test TRU1-1-OPA2: Mapping of the parameter space to the static formation pressure for the PW – PI perturbation results

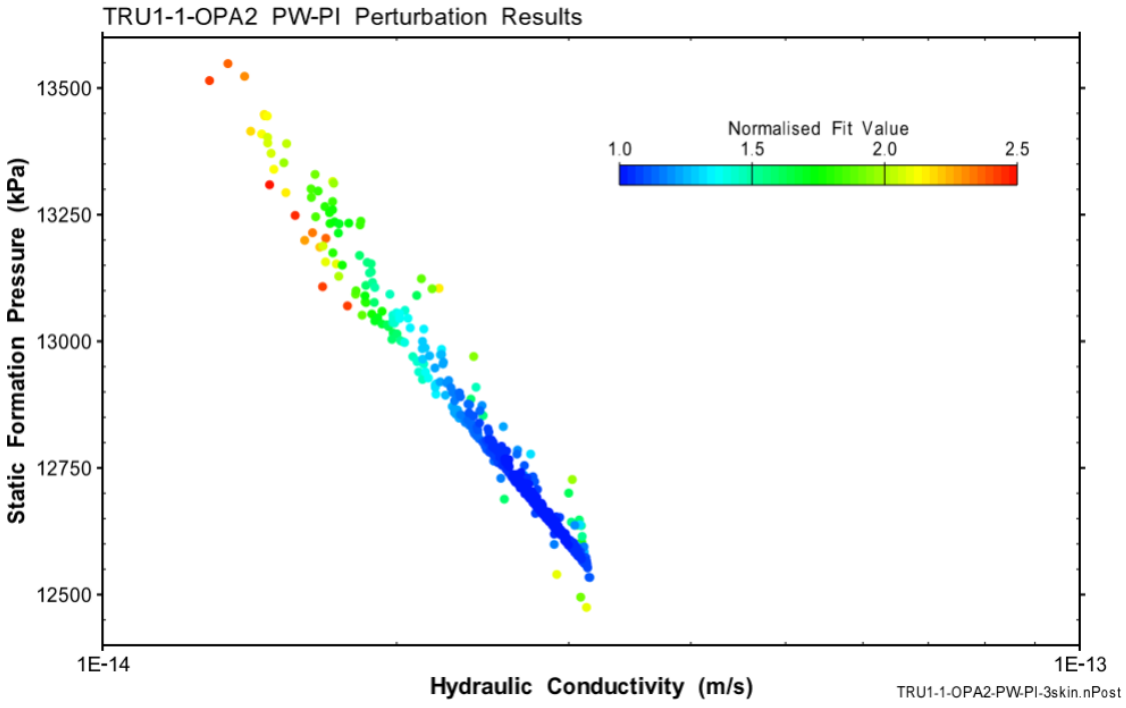

Fig. B-27: Hydraulic test TRU1-1-OPA2: Hydraulic conductivity – static formation pressure correlation for PW-PI

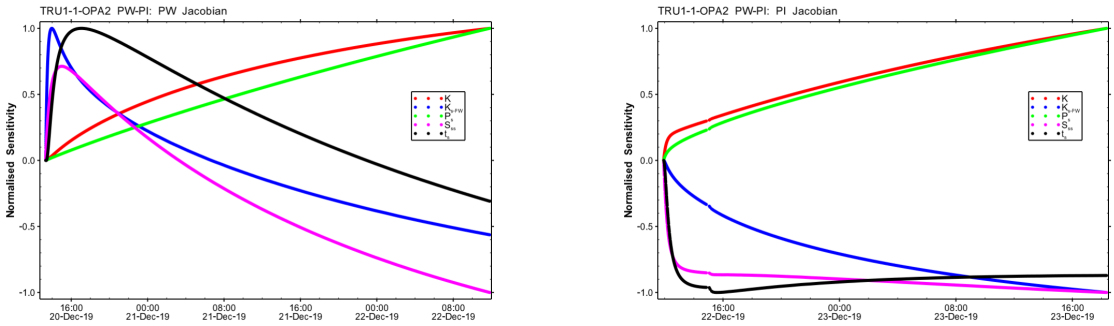

Fig. B-28: Hydraulic test TRU1-1-OPA2: Jacobian plot of parameter sensitivity during PW (left) and PI (right)

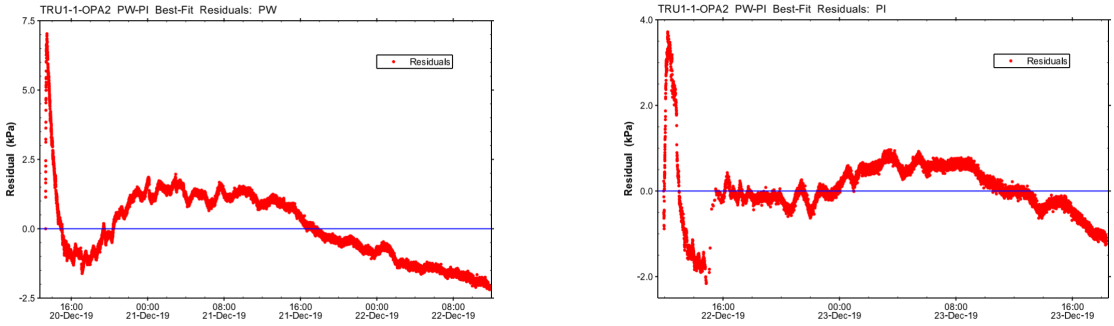

Fig. B-29: Hydraulic test TRU1-1-OPA2: Residuals from best fit to PW-PI data measured by P2 (left for PW, right for PI).

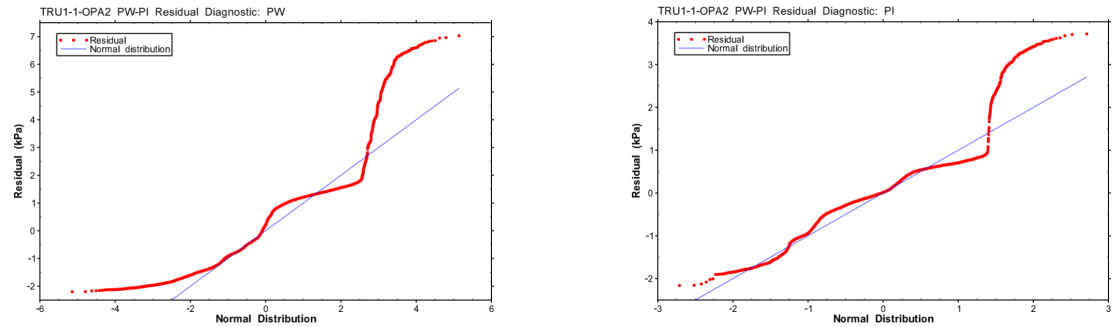

Fig. B-30: Hydraulic test TRU1-1-OPA2: Quantile-normal plot for PW-PI residuals (left for PW, right for PI)

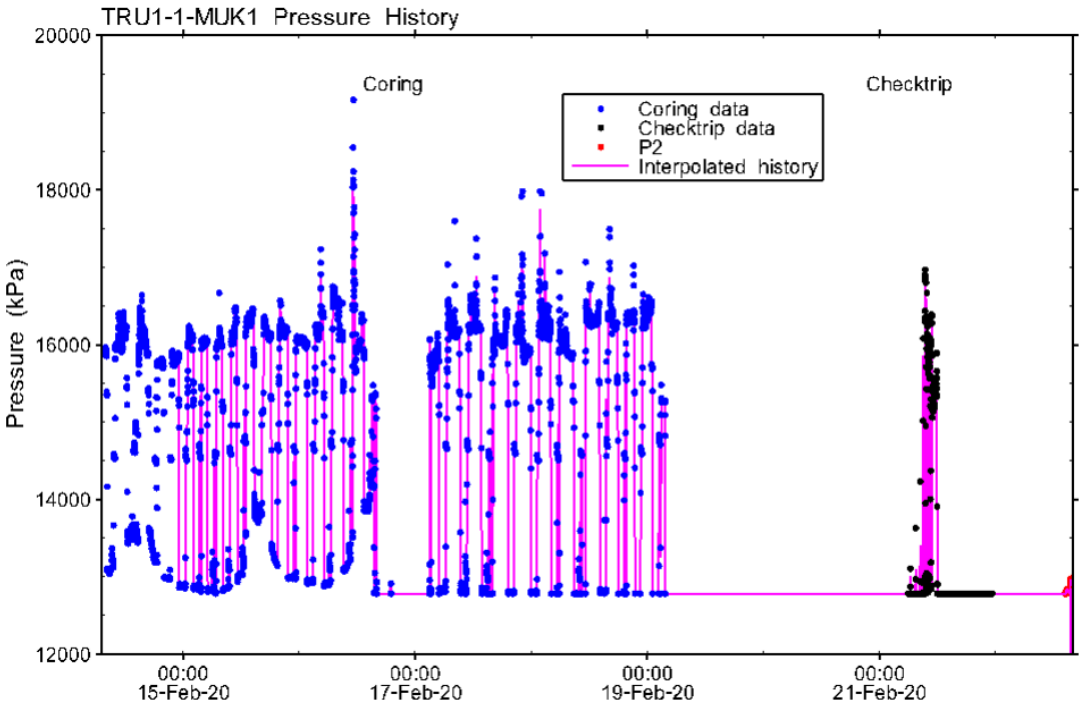

Fig. B-31: Hydraulic test TRU1-1-MUK1: Entire record of the borehole pressure history used in the analysis

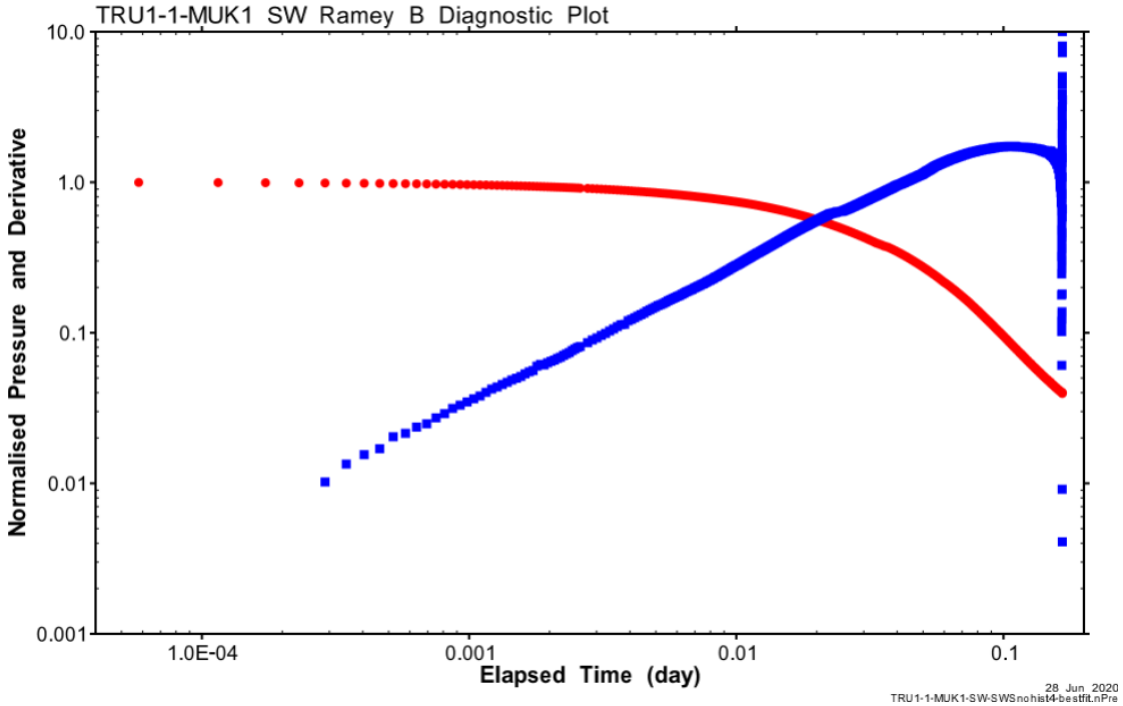

Fig. B-32: Hydraulic test TRU1-1-MUK1: SW Ramey B diagnostic plot

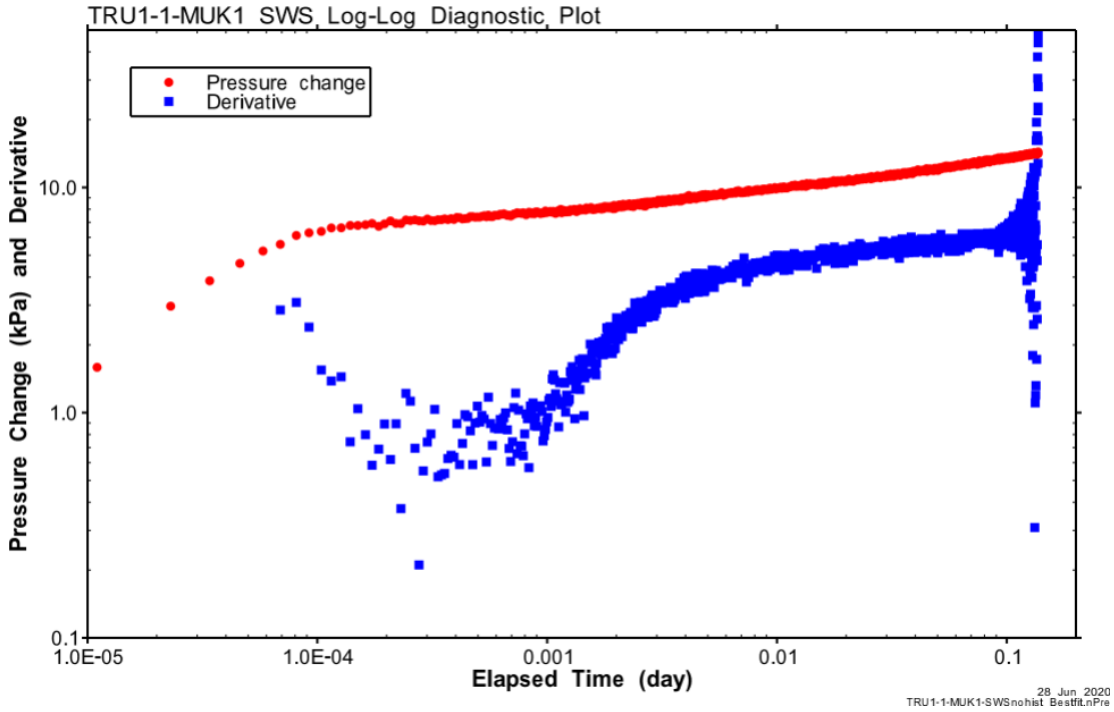

Fig. B-33: Hydraulic test TRU1-1-MUK1: SWS log – log diagnostic plot

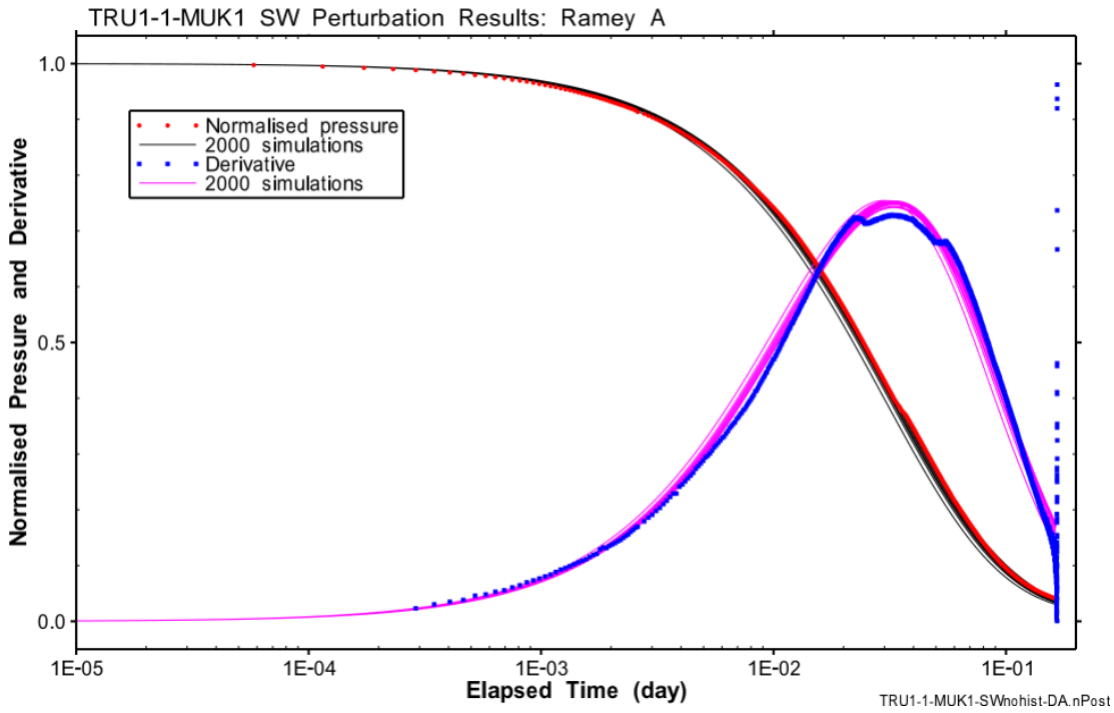

Fig. B-34: Hydraulic test TRU1-1-MUK1: Ramey A horsetail plot of SW data and all 2'000 simulations attributed to the optimisation results of the perturbation

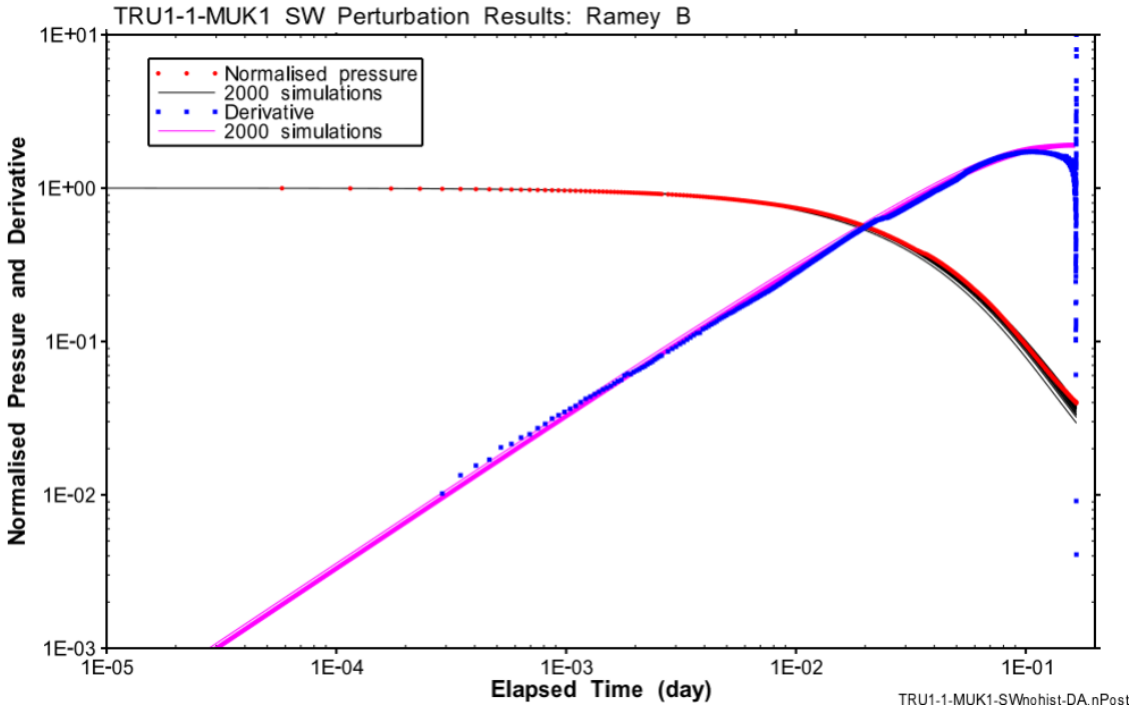

Fig. B-35: Hydraulic test TRU1-1-MUK1: Ramey B horsetail plot of SW data and all 2'000 simulations attributed to the selected optimisation results of the perturbation

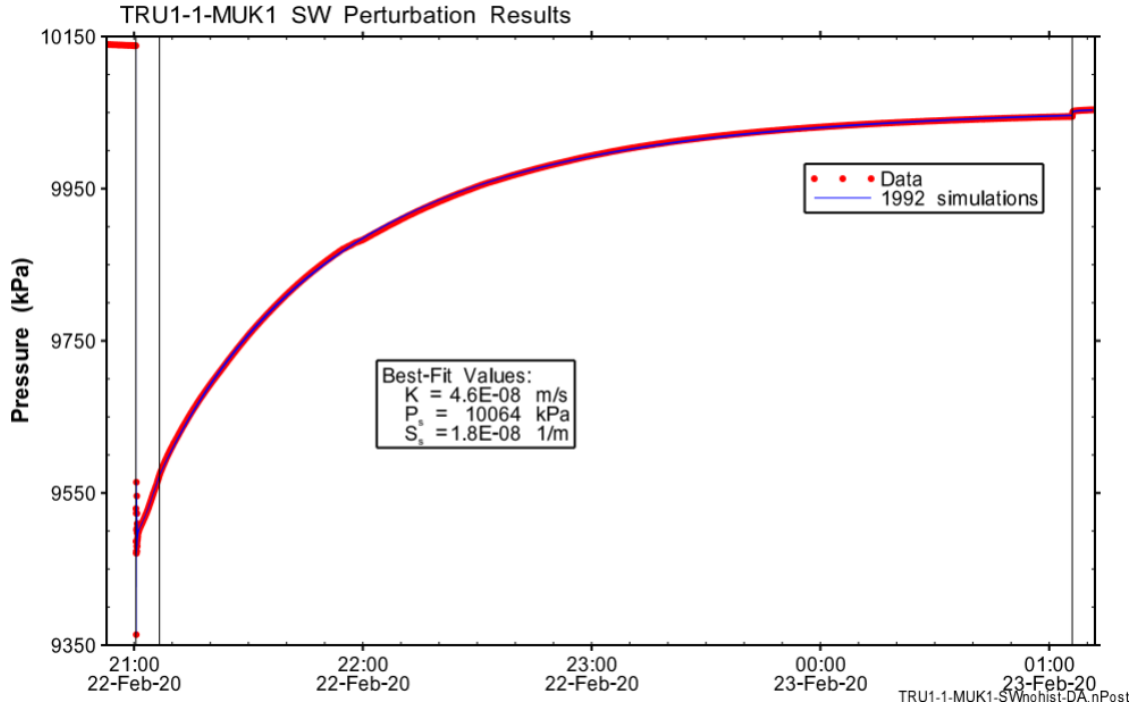

Fig. B-36: Hydraulic test TRU1-1-MUK1: SW Cartesian horsetail plot showing 1'992 accepted simulations attributed to the selected optimisation results of the perturbation

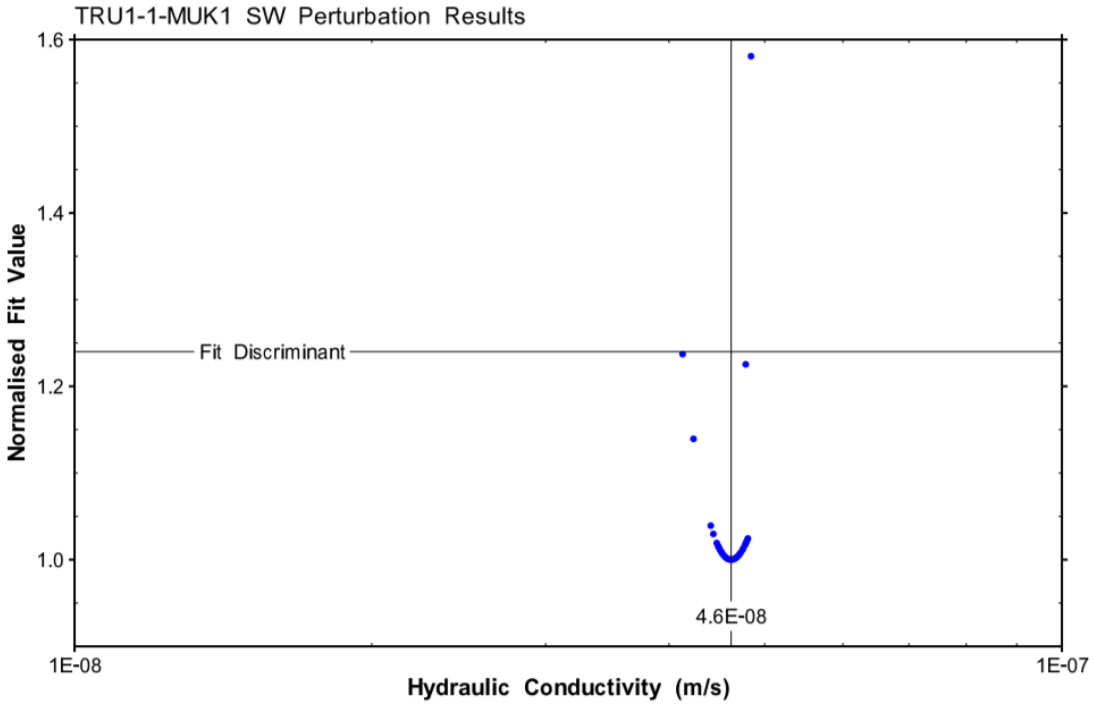

Fig. B-37: Hydraulic test TRU1-1-MUK1: Mapping of the parameter space to the hydraulic conductivity of the formation for the SW perturbation results

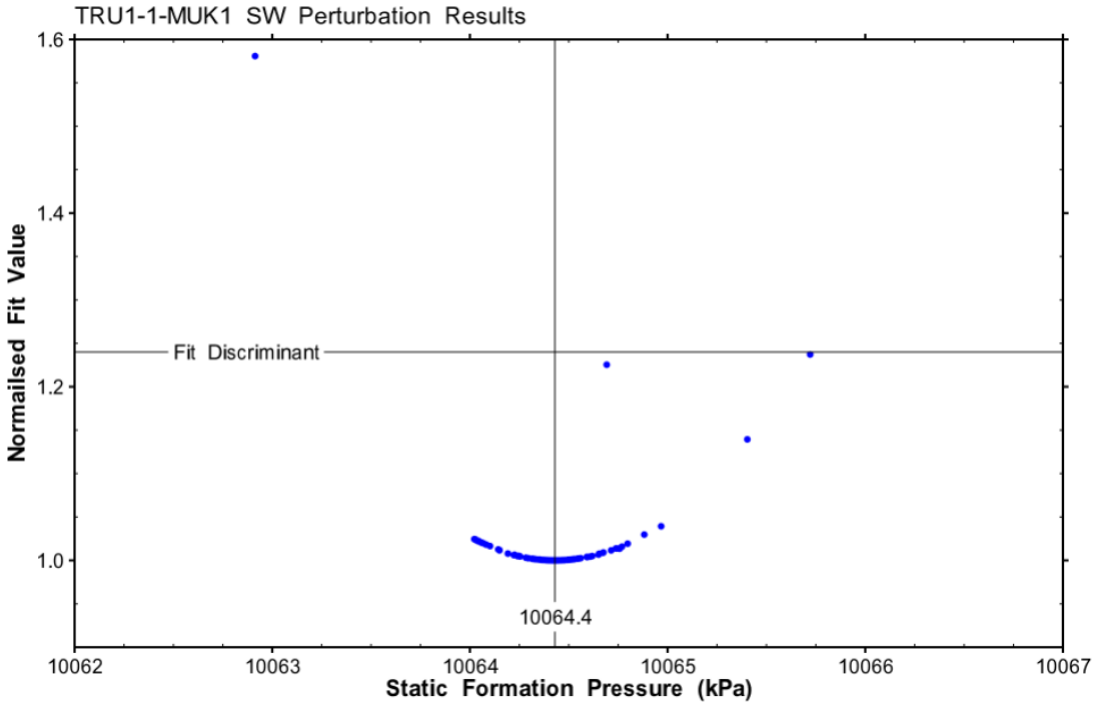

Fig. B-38: Hydraulic test TRU1-1-MUK1: Mapping of the parameter space to the static formation pressure for the SW perturbation results

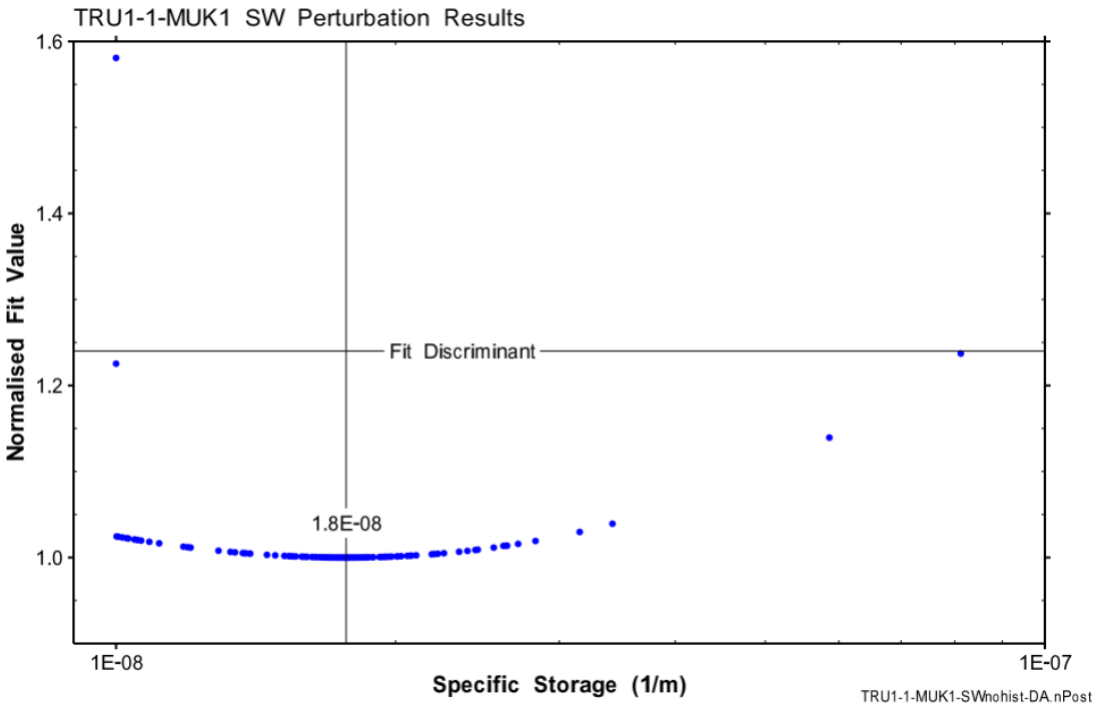

Fig. B-39: Hydraulic test TRU1-1-MUK1: Mapping of the parameter space to the specific storage of the formation for the SW perturbation results

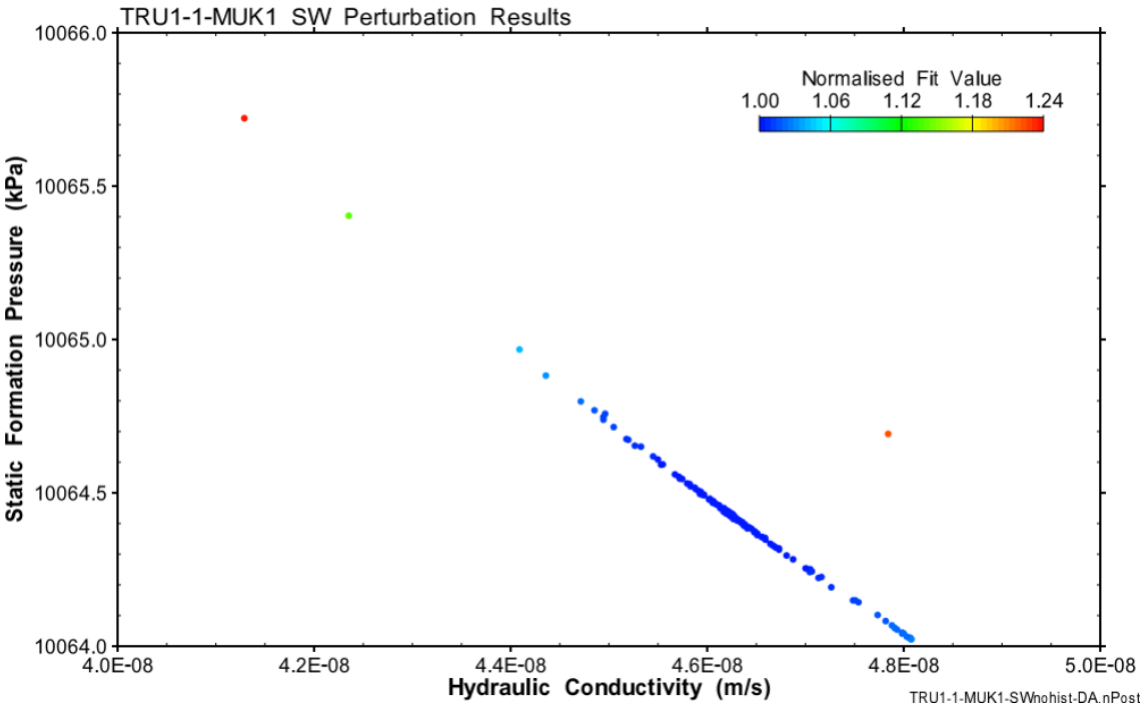

Fig. B-40: Hydraulic test TRU1-1-MUK1: Hydraulic conductivity – static formation pressure correlation for SW

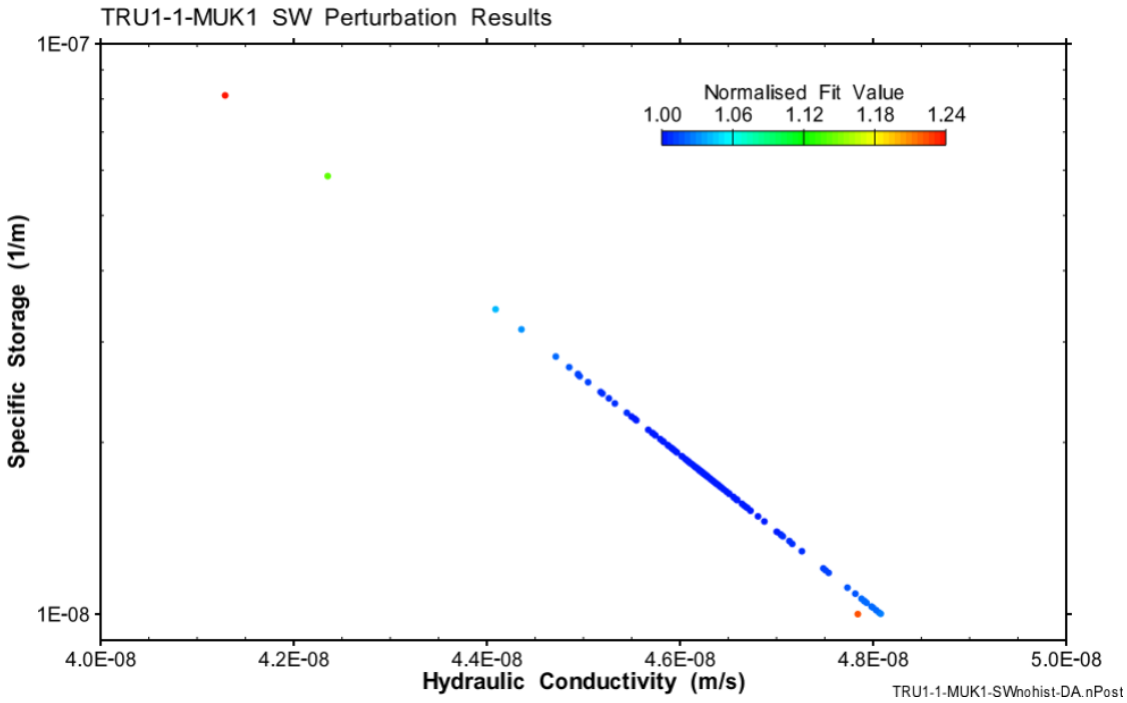

Fig. B-41: Hydraulic test TRU1-1-MUK1: Hydraulic conductivity – specific storage correlation for SW

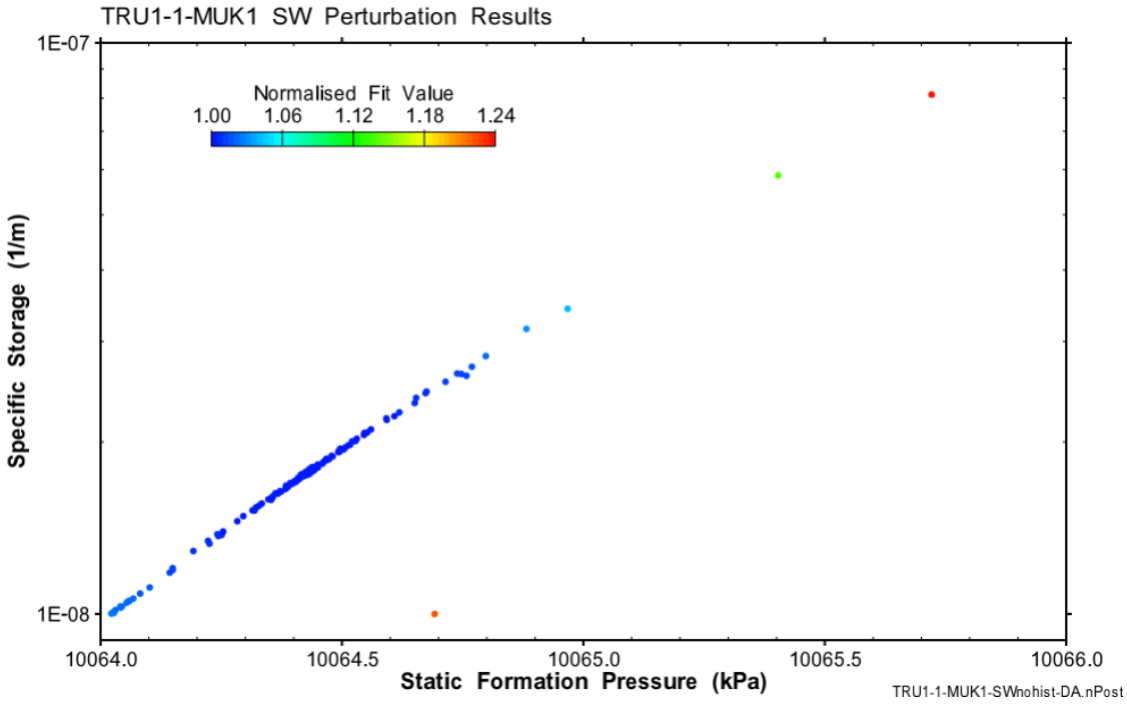

Fig. B-42: Hydraulic test TRU1-1-MUK1: Static formation pressure – specific storage correlation for SW

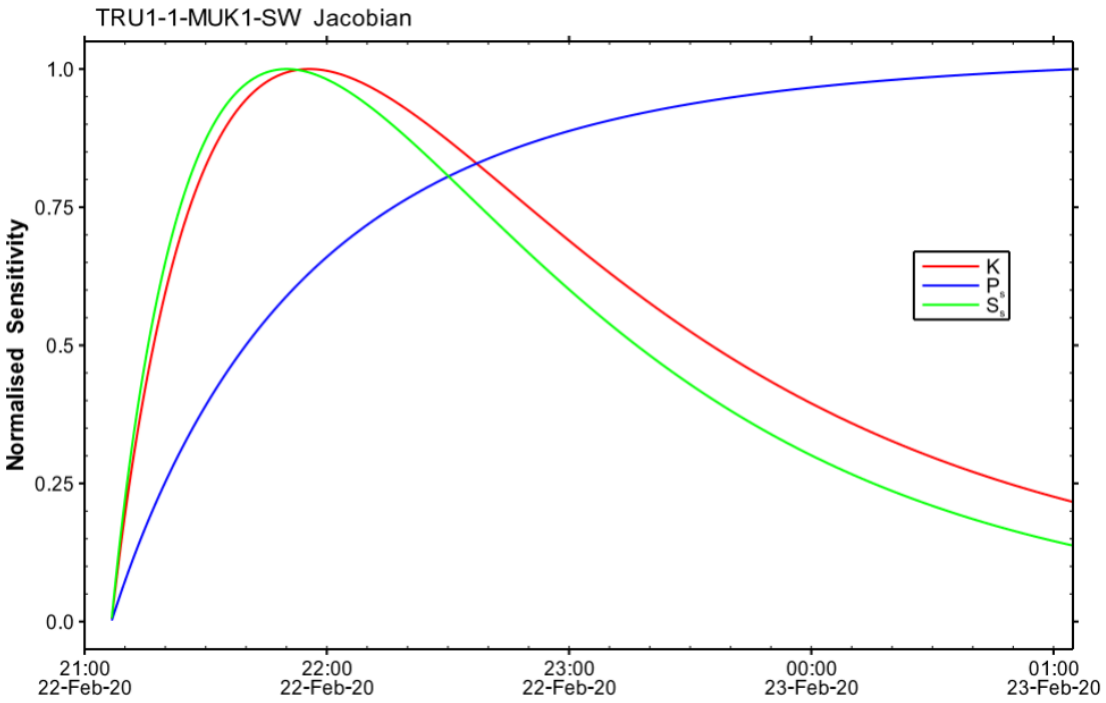

Fig. B-43: Hydraulic test TRU1-1-MUK1: Jacobian plot of parameter sensitivity during SW

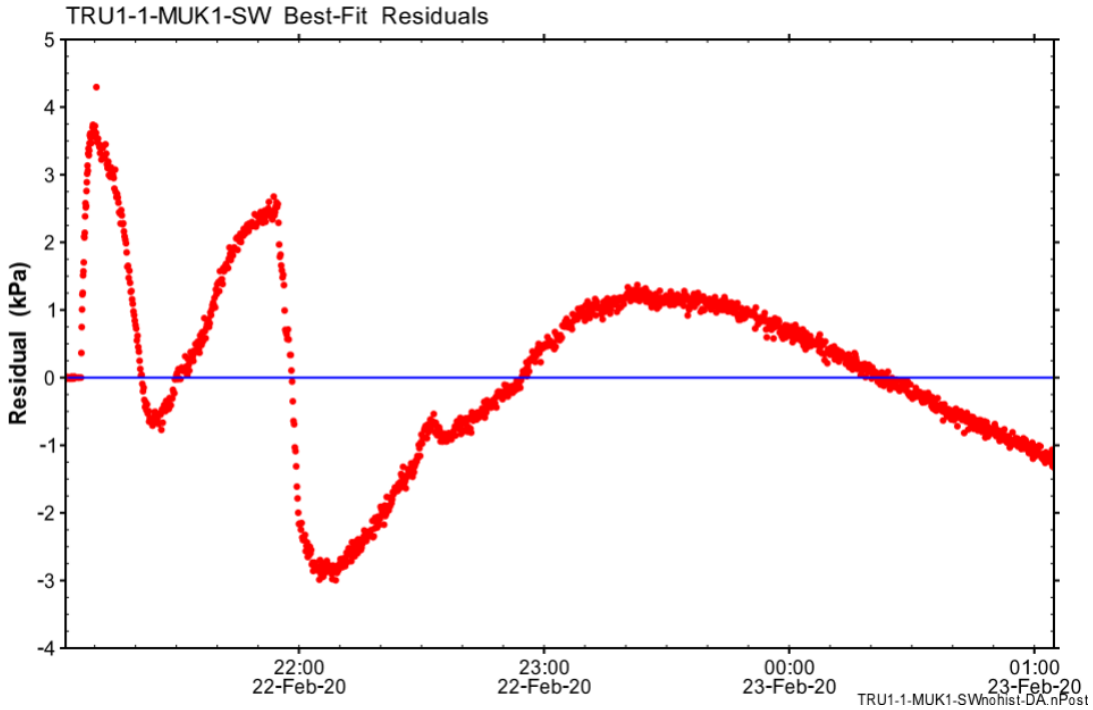

Fig. B-44: Hydraulic test TRU1-1-MUK1: Residuals from best fit simulation to the measurement of the SW phase

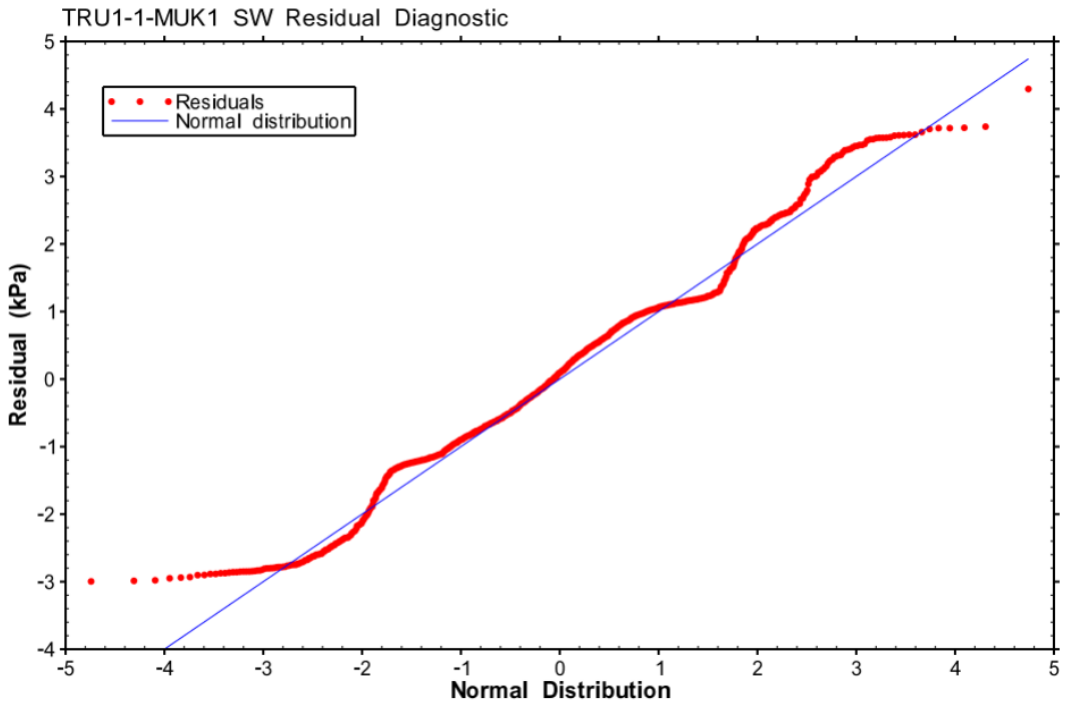

Fig. B-45: Hydraulic test TRU1-1-MUK1: Quantile-normal plot for SW residuals

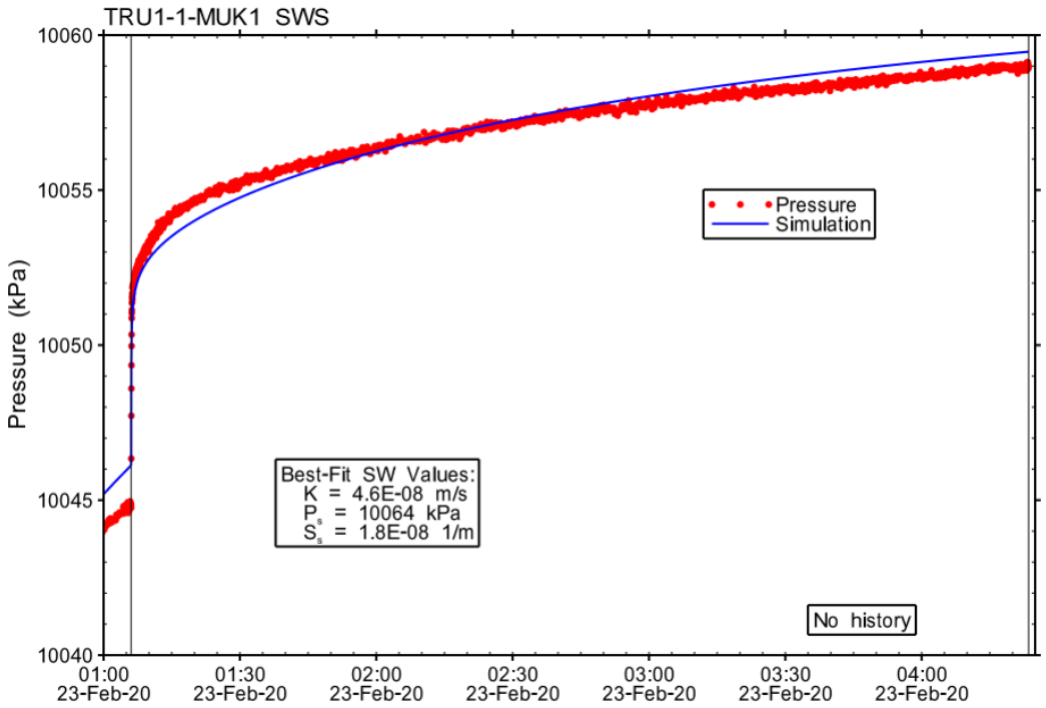

Fig. B-46: Hydraulic test TRU1-1-MUK1: Simulation of TRU1-1-MUK1 SWS using best-fit parameter estimates from SW analysis

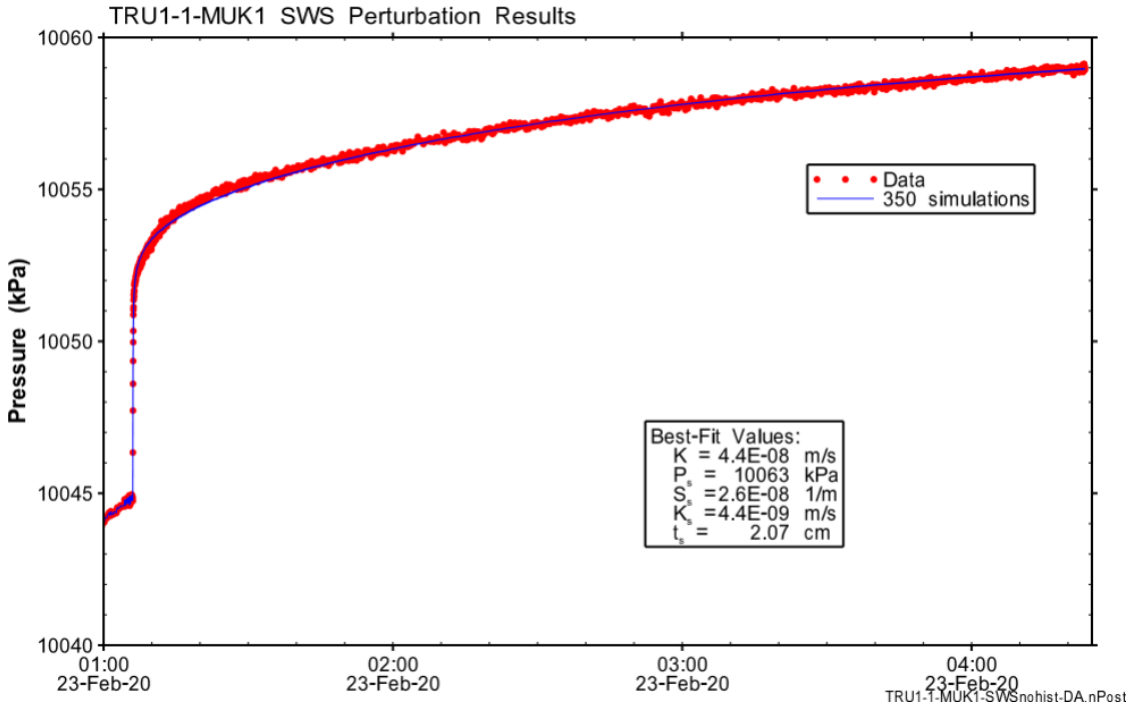

Fig. B-47: Hydraulic test TRU1-1-MUK1: SWS Cartesian horsetail plot showing 350 accepted simulations attributed to the selected optimisation results of the perturbation

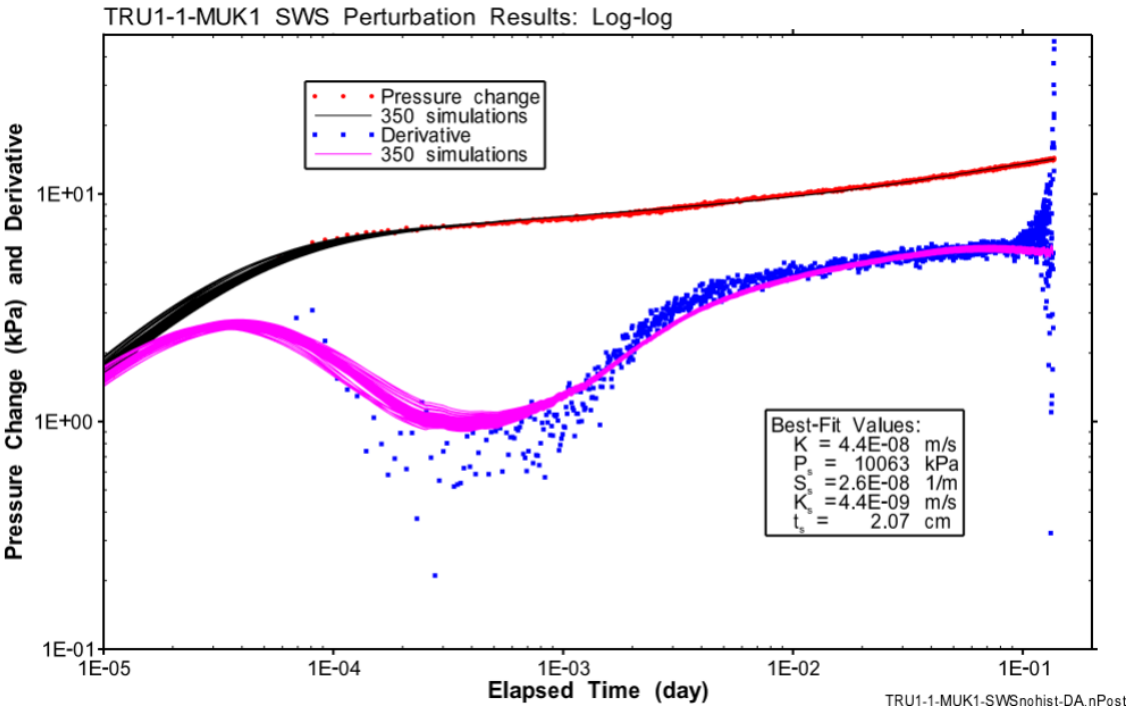

Fig. B-48: Hydraulic test TRU1-1-MUK1: Log – log horsetail plot of SWS data and 350 simulations attributed to the optimisation results of the perturbation

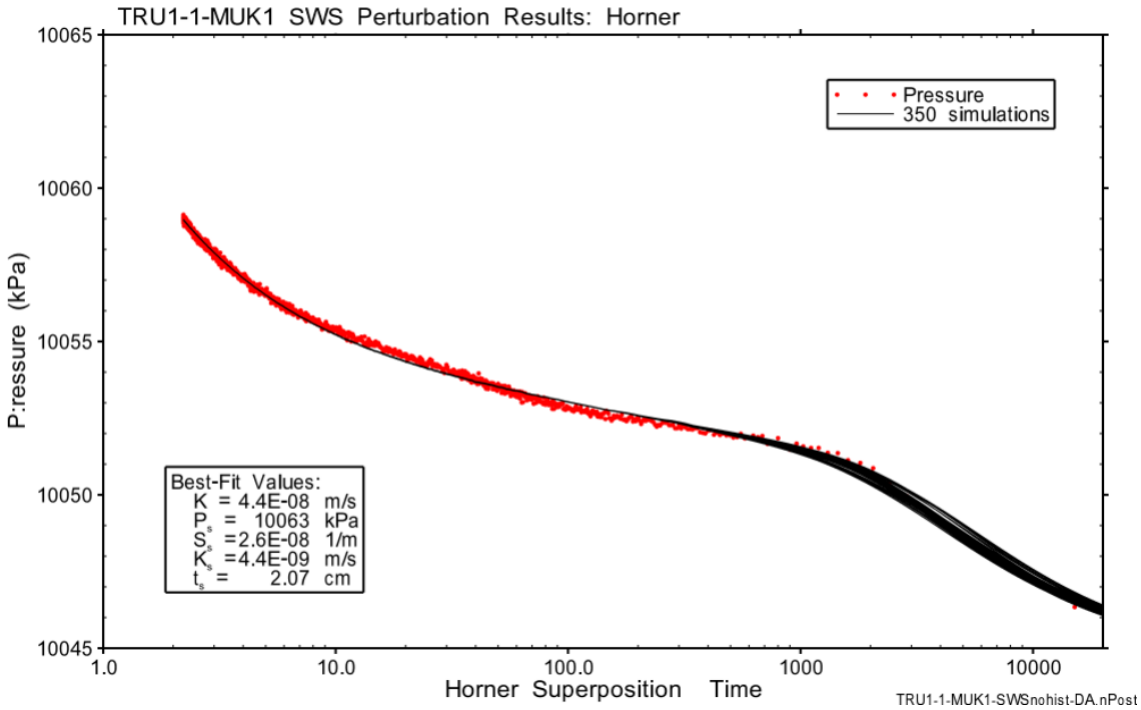

Fig. B-49: Hydraulic test TRU1-1-MUK1: Horner horsetail plot of SWS data and 350 simulations attributed to the selected optimisation results of the perturbation

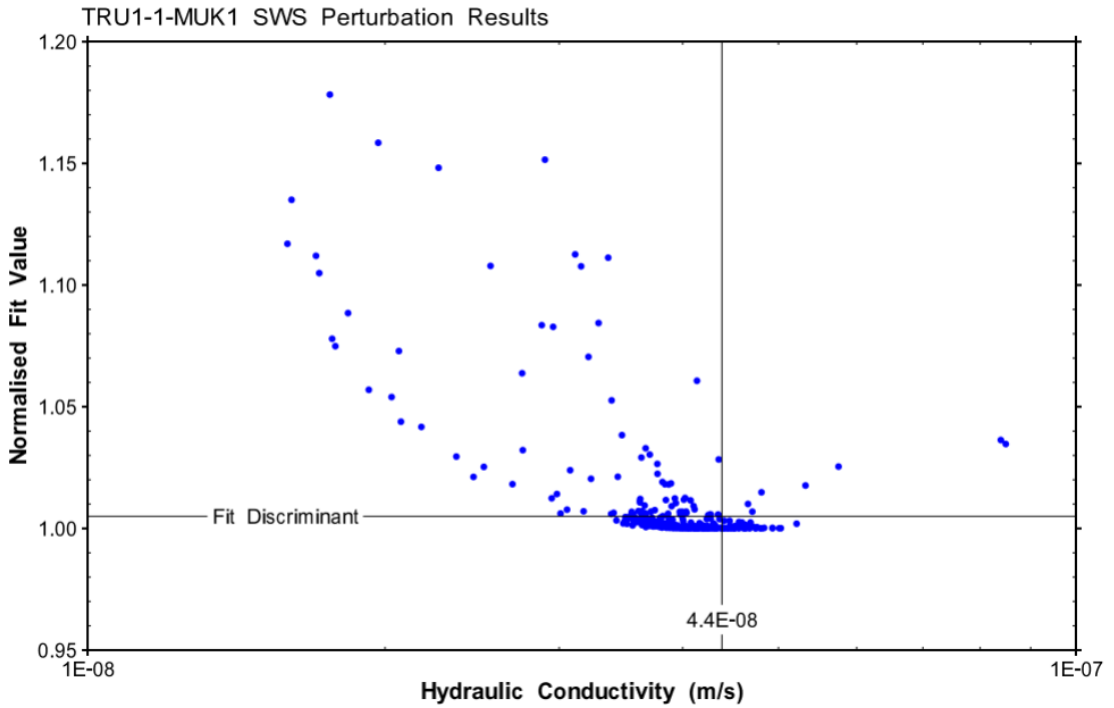

Fig. B-50: Hydraulic test TRU1-1-MUK1: Mapping of the parameter space to the hydraulic conductivity of the formation for the SWS perturbation results

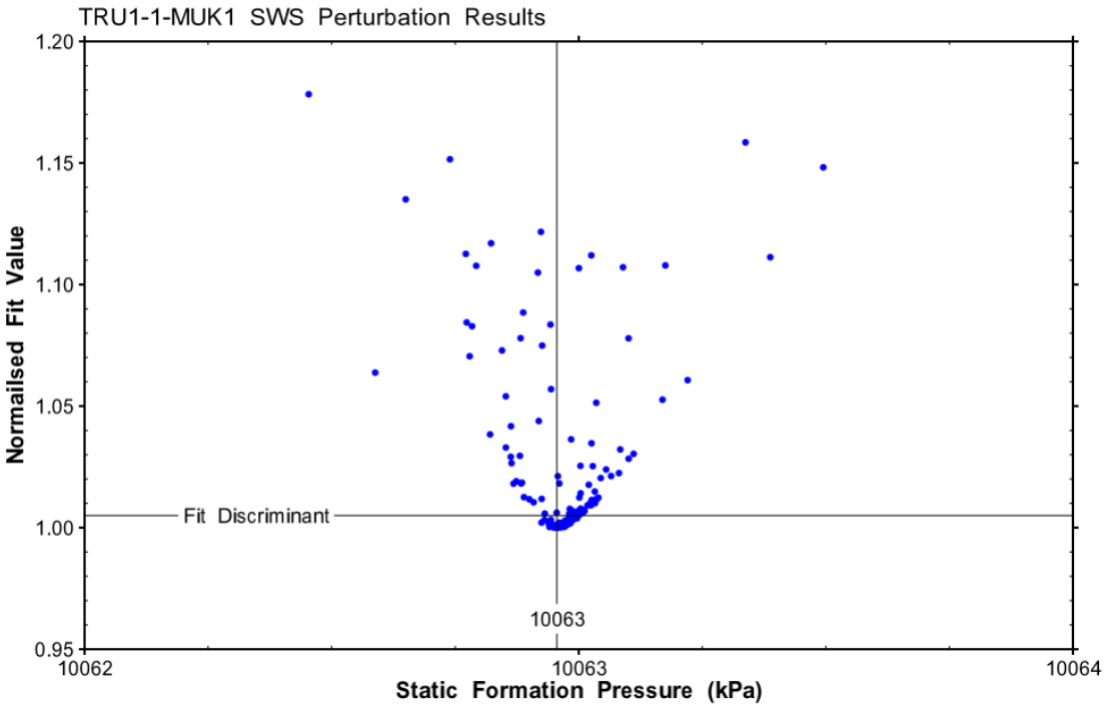

Fig. B-51: Hydraulic test TRU1-1-MUK1: Mapping of the parameter space to the static formation pressure for the SWS perturbation results

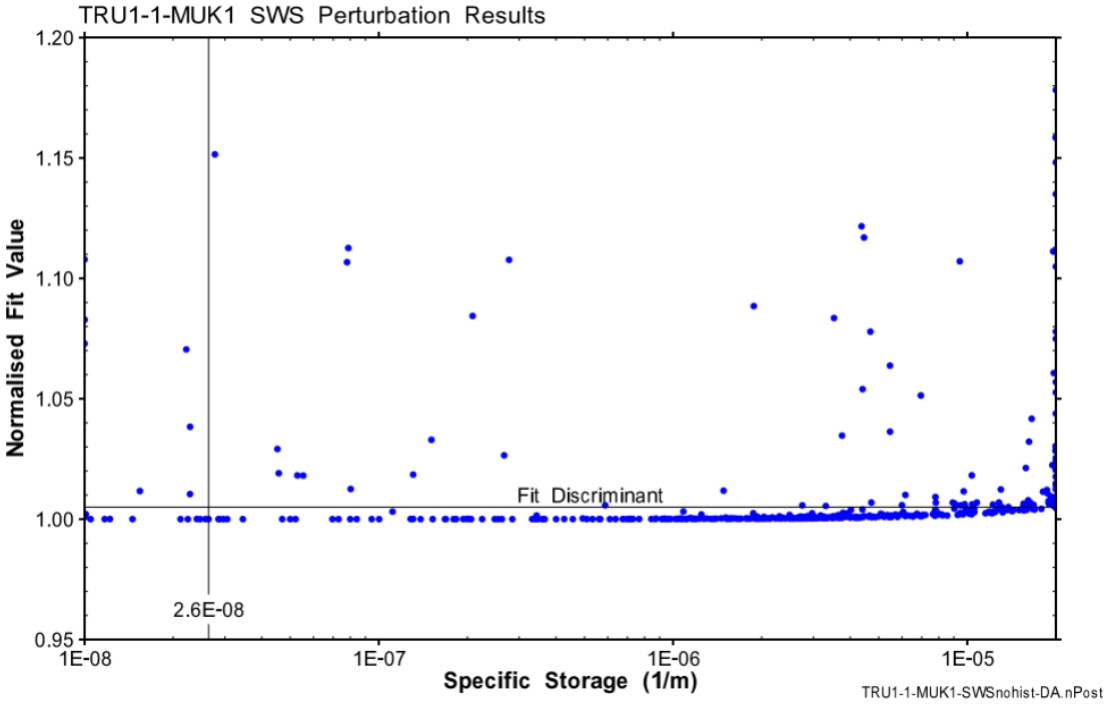

Fig. B-52: Hydraulic test TRU1-1-MUK1: Mapping of the parameter space to the specific storage of the formation for the SWS perturbation results

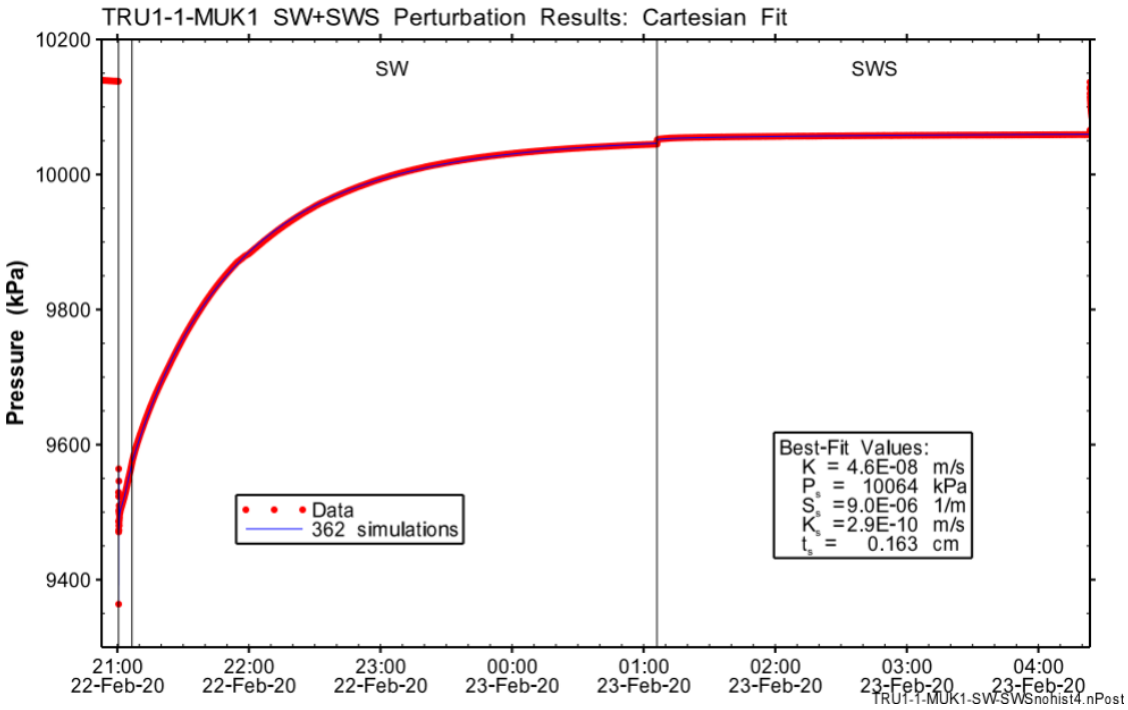

Fig. B-53: Hydraulic test TRU1-1-MUK1: Cartesian horsetail plot of SW and SWS showing 362 accepted simulations attributed to the selected optimisation results of the perturbation

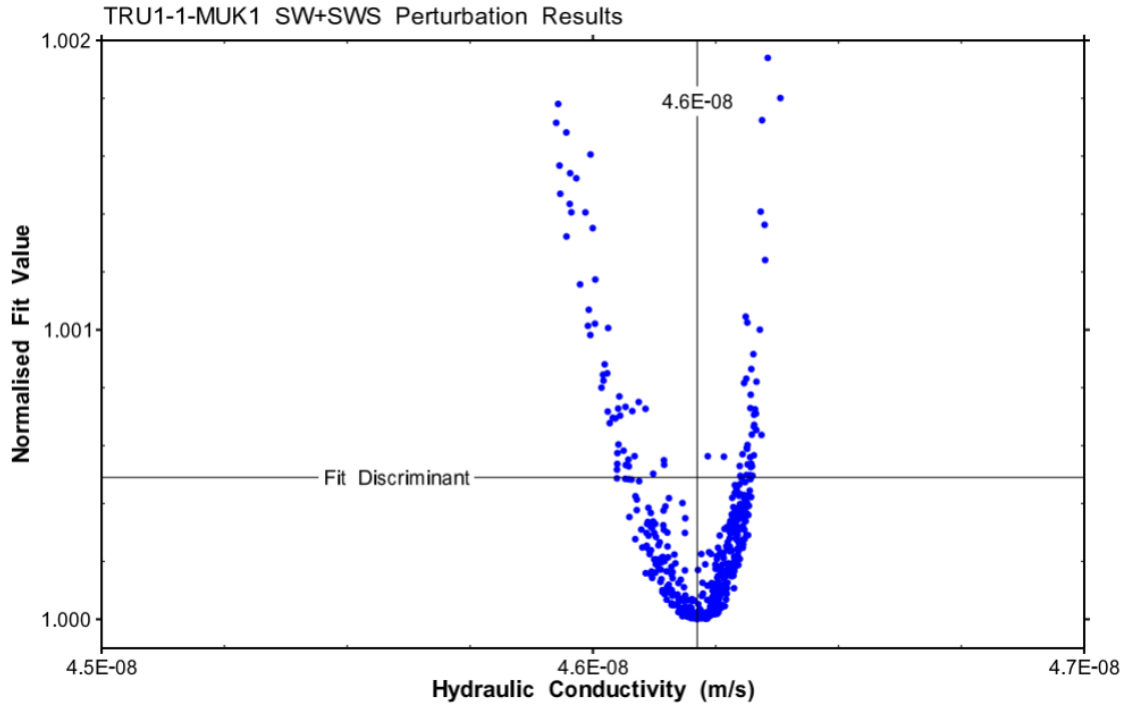

Fig. B-54: Hydraulic test TRU1-1-MUK1: Mapping of the parameter space to the hydraulic conductivity of the formation for the SW-SWS perturbation results

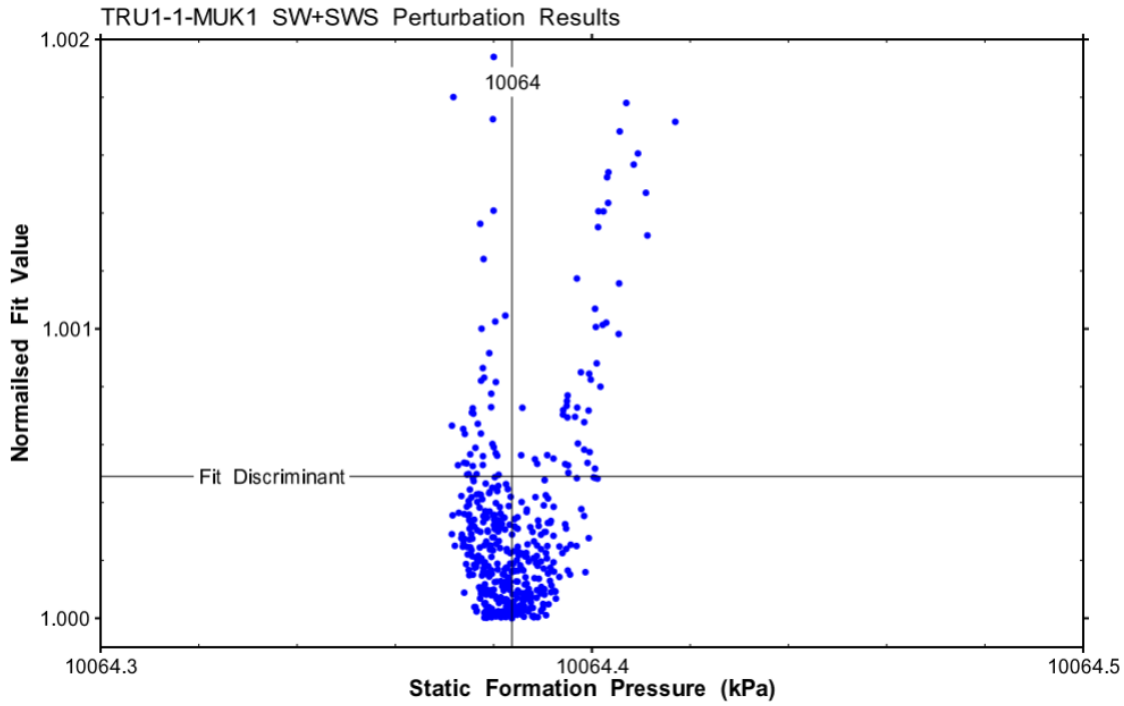

Fig. B-55: Hydraulic test TRU1-1-MUK1: Mapping of the parameter space to the static formation pressure for the SW-SWS perturbation results

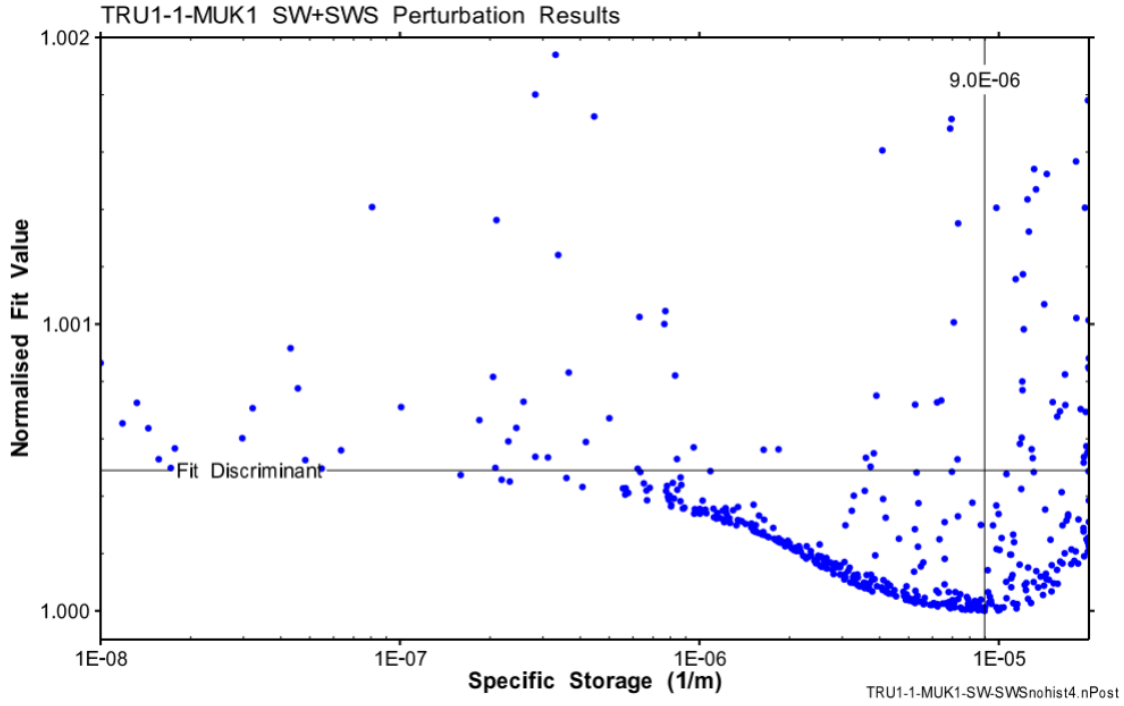

Fig. B-56: Hydraulic test TRU1-1-MUK1: Mapping of the parameter space to the specific storage of the formation for the SW-SWS perturbation results

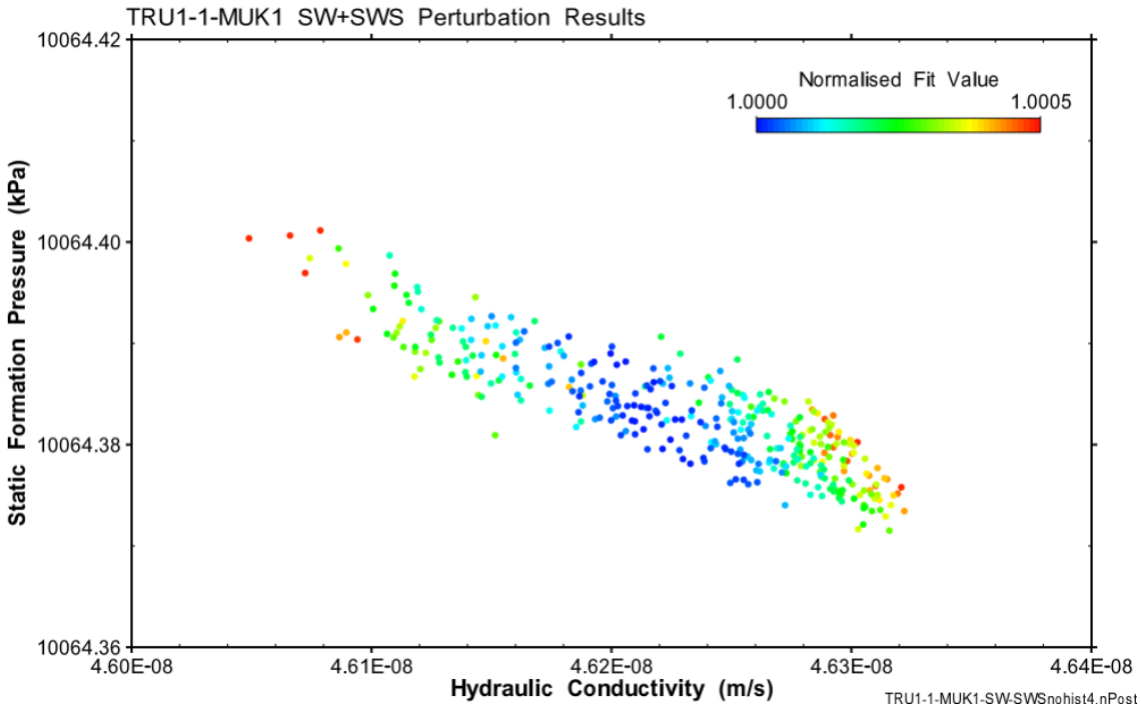

Fig. B-57: Hydraulic test TRU1-1-MUK1: Hydraulic conductivity – static formation pressure correlation for SW-SWS

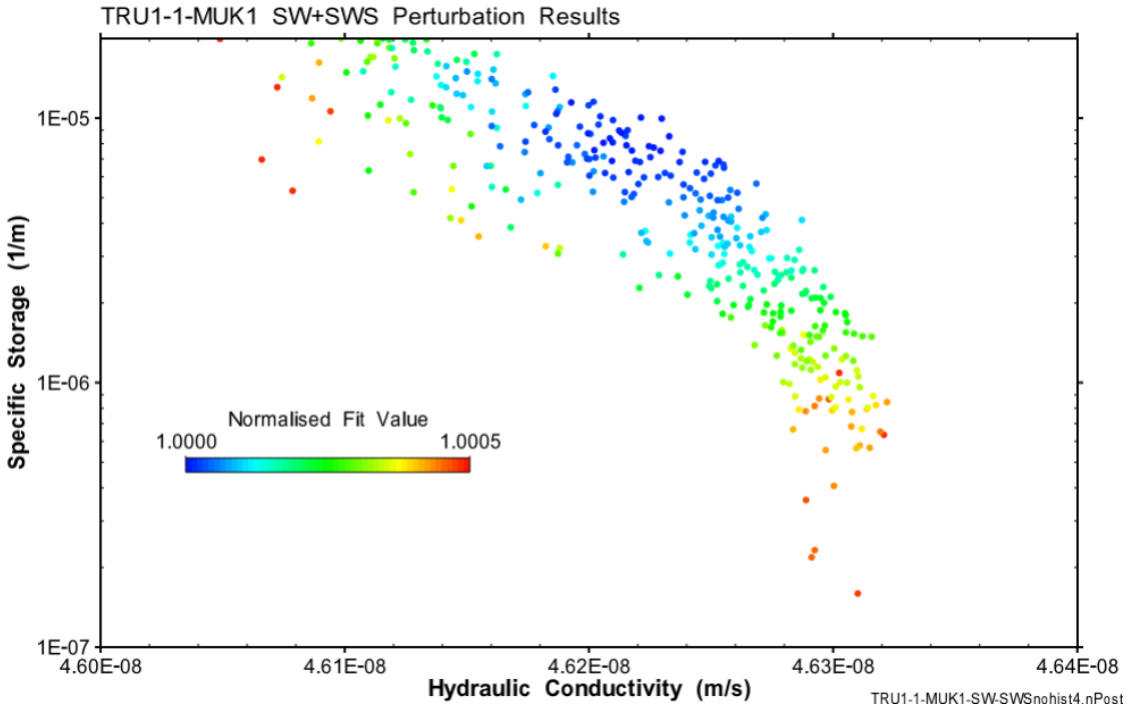

Fig. B-58: Hydraulic test TRU1-1-MUK1: Hydraulic conductivity – specific storage correlation for SW-SWS

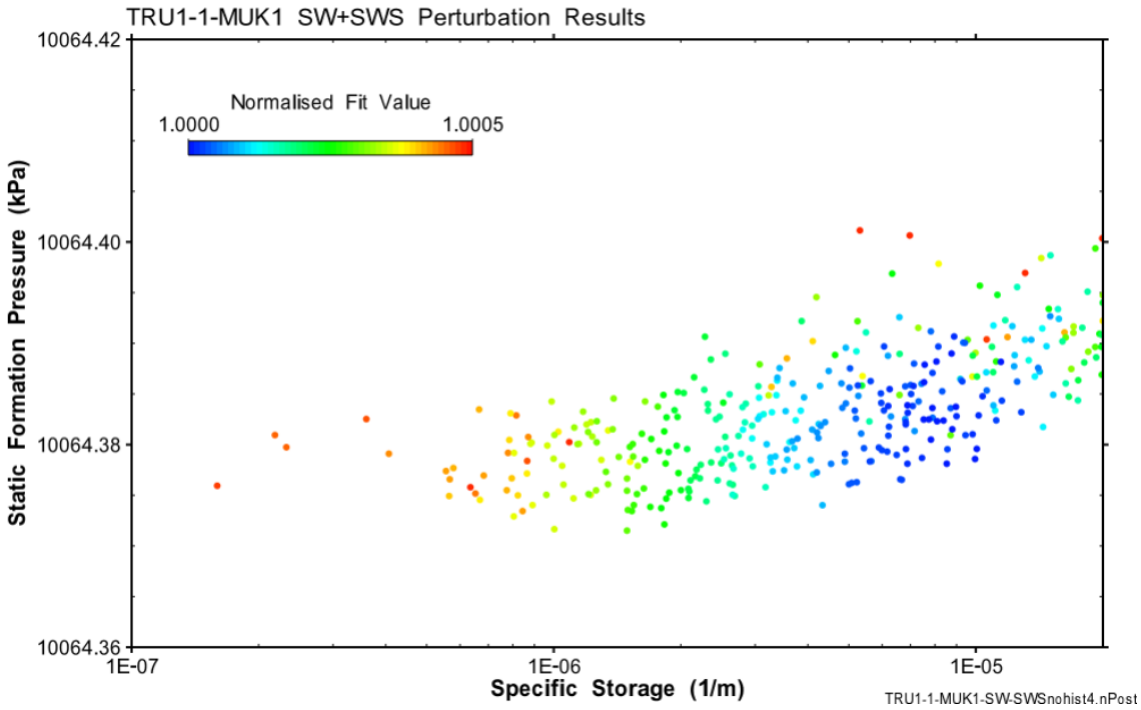

Fig. B-59: Hydraulic test TRU1-1-MUK1: Static formation pressure – specific storage correlation for SW-SWS

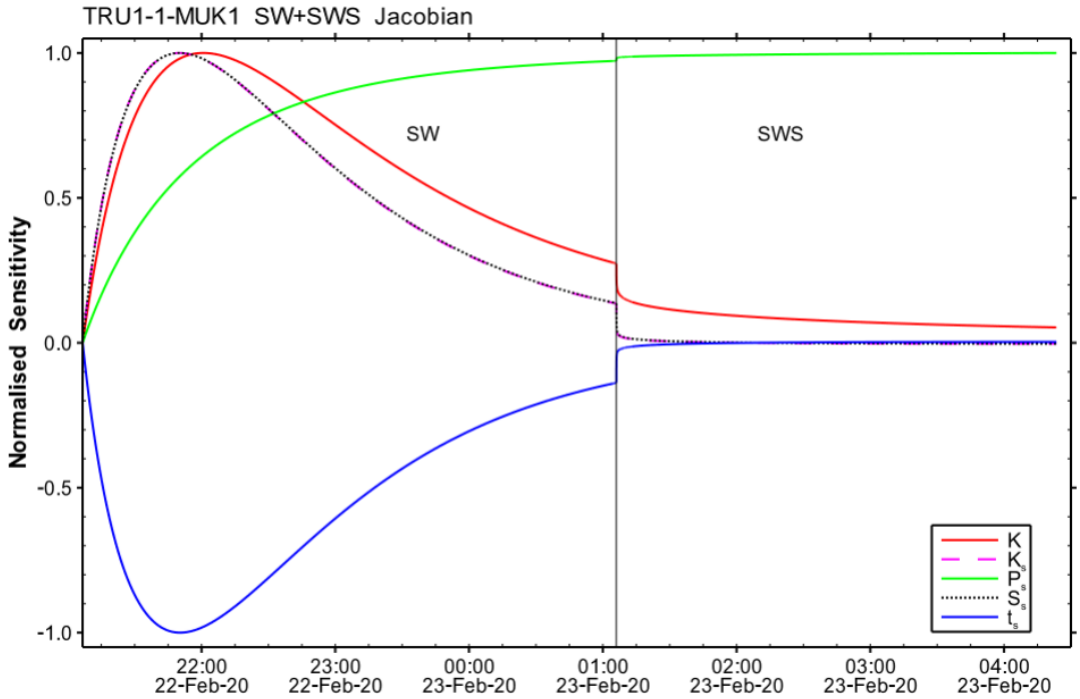

Fig. B-60: Hydraulic test TRU1-1-MUK1: Jacobian plot of parameter sensitivity during SW and SWS from joint SW-SWS best fit

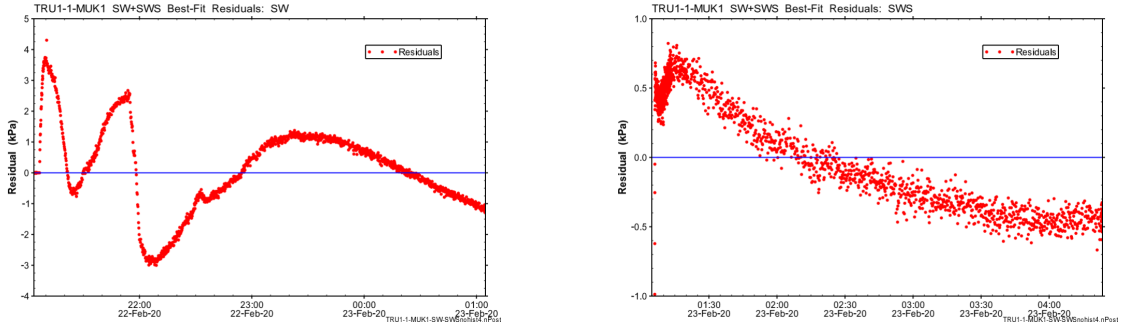

Fig. B-61: Hydraulic test TRU1-1-MUK1: Residuals from best fit to SW-SWS data measured by P2 (left for SW, right for SWS)

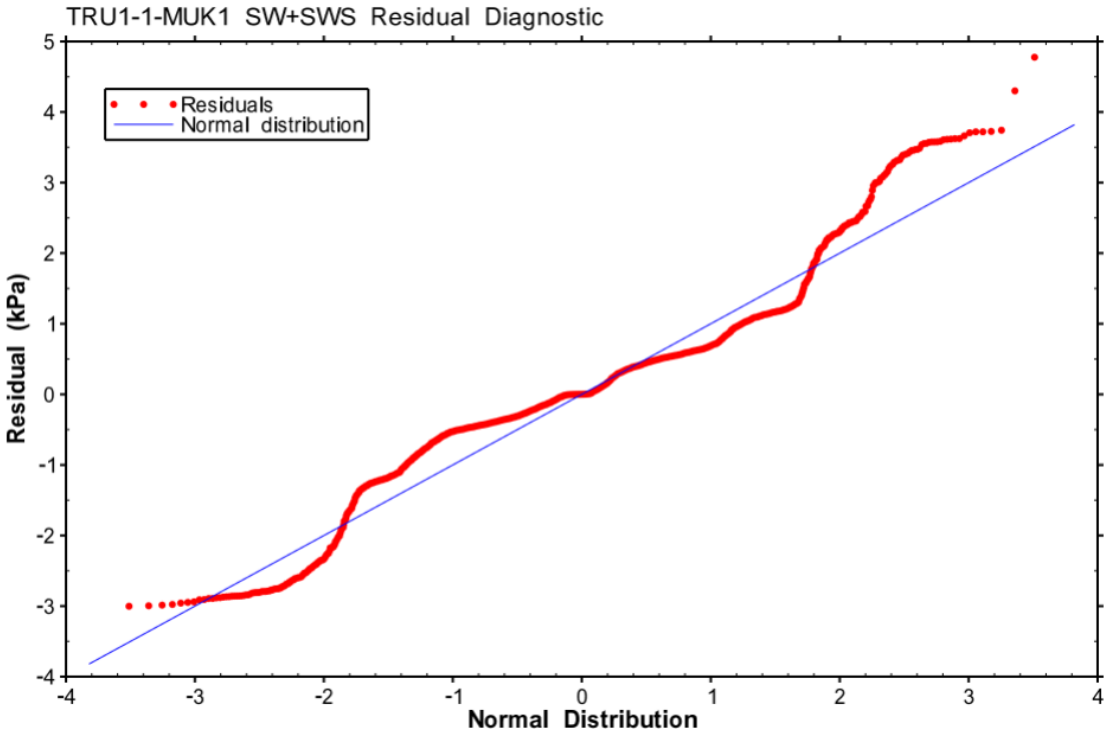

Fig. B-62: Hydraulic test TRU1-1-MUK1: Quantile-normal plot for SW and SWS Cartesian residuals from joint SW-SWS best fit

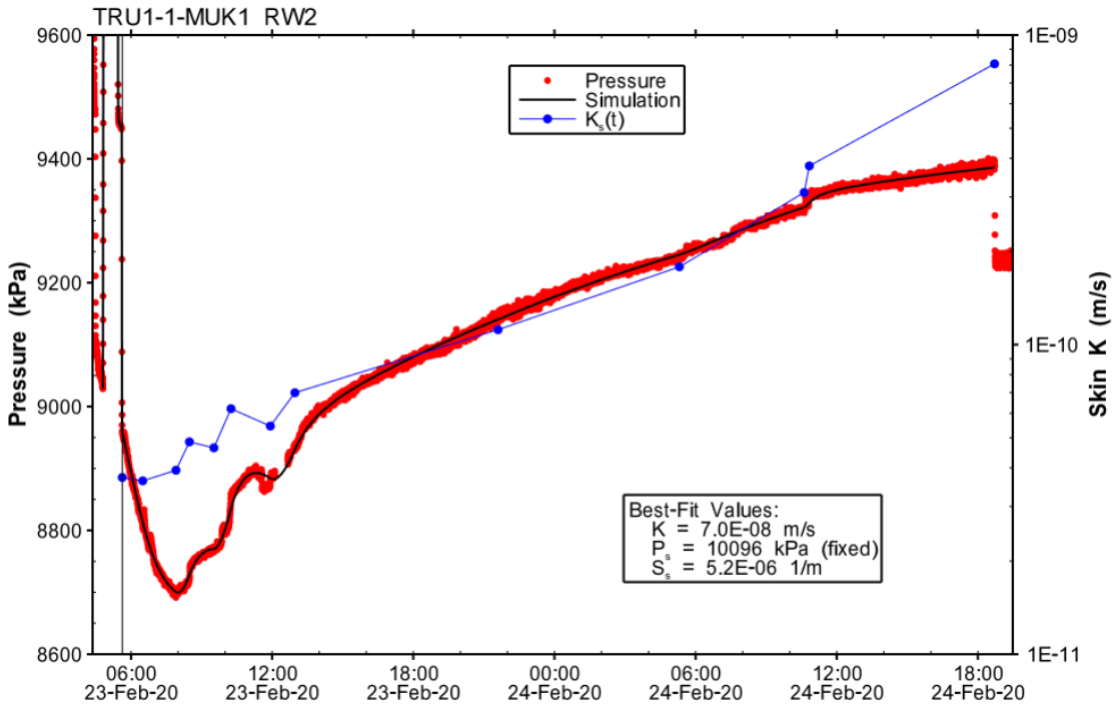

Fig. B-63: Hydraulic test TRU1-1-MUK1: Simulation of the longest production phase (RW2) in relation to hydraulic conductivity of the inner / skin zone